Redox Biochemistry of *Pyrococcus furiosus* Ferredoxin: Fundamentals and Applied Aspects

M.Nahid Hasan

Redox Biochemistry of *Pyrococcus furiosus* Ferredoxin: Fundamentals and Applied Aspects   M. Nahid Hasan

Propositions

accompanying the thesis of M. Nahid Hasan

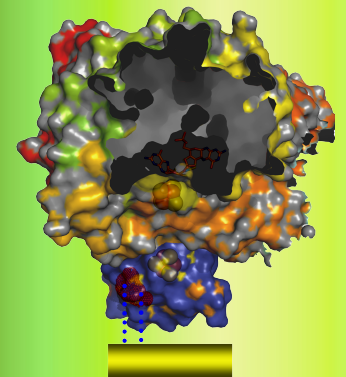## "Redox Biochemistry of *Pyrococcus furiosus* Ferredoxin: fundamental and applied aspects"

1. The origin of life remains unknown.
2. The definition of "Extremophiles" is relative.
3. *Pyrococcus furiosus* Ferredoxin is a mixture of monomeric and dimeric protein in an equilibrium that is far to the dimeric side under physiological ionic strength conditions.
4. The bioinformatics prediction of the frequent occurrence of disulfide bonds in (hyper)thermophiles is not borne out by experimental observation.
5. Aldehyde oxidoreductase from *Pyrococcus furiosus* is the first enzyme of its type, which catalyzes both oxidation of aldehyde and reduction of acid to a significant extent.
6. If enzymes are (or can be made) active on an electrode, then it should be possible to combine the ease of use and versatility of electrochemical methods with the elegance of enzymatic methods. However, slow electron transfer rate (driven by various factors) is the major bottleneck to overcome yet.
7. Recent years have witnessed the severe consequences of global warming mainly in the tropical and poorer countries, adding extra woes to their ailing economies. Support from the developed countries (who are the major contributors to global warming) for disaster management is usually called "kind donation", while it should be called "partial compensation".
8. The iron storage protein ferritin is a wonder ball.
9. Every failure has its own seed of success.

These propositions are considered opposable and defendable and as such have been approved by the supervisor Prof. dr. W. R. Hagen.

Stellingen

behorende bij het proefschrift van M. Nahid Hasan

"Redox Biochemistry of *Pyrococcus furiosus* Ferredoxin:

Fundamental and Applied Aspects."

1. De oorsprong van het leven is nog onbekend.

2. De definitie van "extremofiel" is relatief.

3. *Pyrococcus furiosus* ferredoxine is een mengsel van monomeer en dimeer eiwit in een evenwicht dat ver naar de dimere kant ligt onder fysiologische ionensterkte condities.

4. De bioinformatica-voorspelling dat disulfidebindingen frequent zouden voorkomen in (hyper)thermofielen, wordt niet bevestigd door experimentele waarneming.

5. Aldehyde oxidoreductase van *Pyrococcus furiosus* is het eerste enzym in zijn soort dat zowel de oxidatie van aldehyde als de reductie van zuur in significante mate katalyseert.

6. Als enzymen op een electrode actief zouden zijn (of kunnen worden gemaakt), dan zou het mogelijk moeten zijn om het gebruikersgemak en de veelzijdigheid van electrochemische methoden te kombineren met de elegantie van enzymatische methoden. Echter, trage electronenoverdrachtsnelheid (bepaald door verscheidene factoren) is de belangrijkste beperking die nog moet worden overwonnen.

7. De afgelopen jaren hebben de zware gevolgen van globale opwarming vooral in de tropische en armere landen laten zien met extra ellende voor hun zwakke ekonomieen. Hulp van de ontwikkelde landen (de belangrijkste veroorzakers van globale opwarming) voor rampenbestrijding wordt meestal aangeduid als "gift", terwijl het eigenlijk "gedeeltelijke compensatie" moet worden genoemd.

8. Het ijzeropslageiwit ferritine is een toverbal.

9. Iedere mislukking draagt zijn eigen zaadje tot succes.

Deze stellingen worden opponeerbaar en verdedigbaar geacht en zijn als zodanig goedgekeurd door de promotor Prof. dr. W. R. Hagen.

Redox Biochemistry of *Pyrococcus furiosus* Ferredoxin:

Fundamental and Applied Aspects

Redox Biochemistry of *Pyrococcus furiosus* Ferredoxin:

Fundamental and Applied Aspects

Proefschrift

ter verkrijging van de graad van doctor

aan de Technische Universiteit Delft,

op gezag van de Rector Magnificus prof.dr. ir. J.T. Fokkema,

voorzitter van het college voor promoties,

in het openbaar te verdedigen op maandag 21 januari 2008 om 15.00 uur

door

Muhammad Nahidul HASAN

Master of Science in Medical Molecular Biology

geboren te Lakshmipur, Bangladesh

Dit proefschrijft is goedgekeurd door promotor:

Prof. dr. W.R. Hagen

Samenstelling promotiecommissie:

Rector Magnificus	Voorzitter
Prof. dr. W.R. Hagen	Technische Universiteit Delft, promotor
Prof. dr. S. de Vries	Technische Universiteit Delft
Prof. dr. M.C.M. van Loosdrecht	Technische Universiteit Delft
Prof. dr. I. W.C.E. Arends	Technische Universiteit Delft
Prof. dr. J.W. Hofstraat	Philips Biosciences Eindhoven
	en Technische Universiteit Eindhoven
dr. ir. J. A. Jongejan	Technische Universiteit Delft
dr. Ir. H. A. Heering	Universiteit Leiden

Contents

List of abbreviations:

3-PG	3-phosphoglycerate
AOR	Aldehyde:ferredoxin oxidoreductase
CSA	Chicken serum albumin.
DTT	Dithiothreitol
Fd	Ferredoxin
GAP	Glyceraldehyde-3-phosphate
GAPOR	Glyceraldehyde-3-phosphate oxidoreductase
HEPES	N-(2-hydroxyethyl) piperazine-N-(2- ethanesulfonate)
IPTG	Isopropyl β-D- thiogalactopyranoside
L-BAPNA	N-benzoyl-L-arginine-p-nitroanilide
MES	2-Morpholinoethanesulfonic acid
MOPS	3-Morpholinopropanesulfonic acid
Na-DT	Sodium dithionite
Pfu	*Pyrococcus furiosus*
Purpald	4-amino-3-hydrazino-5-mercapto-1,2,4-trizole
PMSF	Phenylmethylsulfonyl fluoride
RWT	Recombinant wild-type
TCEP	Tris[2-carboxyethyl] phosphine

Chapter one

General introduction

EXTREMOPHILES

Extremophiles are organisms that live under extreme environmental conditions which are harsh and hostile to us. Biologically, an extreme condition can be defined as the state of physicochemical parameters beyond which life can not occur. The convenient conditions for life found in most ecosystems, terrestrial as well as marine, are temperature of 10-40°C, a neutral pH, close to one atmosphere pressure, plentiful water availability, low salt concentration, and low levels of harmful radiation. However, some bacterial species require a temperature as low as 0°C (1) for their survival while some archaea only grow optimally at a temperature as high as 120°C. Extremophiles can be classified according to the extreme condition(s) under which they thrive: high temperature (thermophiles and hyperthermophiles), low temperature (psychrophiles), low pH (acidophiles), high pH (alkaliphiles), high salt concentrations (halophiles), dry conditions (xerophiles), and high pressure (barophiles or piezophiles) (1).

The striking feature of extremophiles is that they not only tolerate the extreme condition(s) but they also exploit these conditions to their advantage, i.e. they require such condition(s) to survive. The interesting question then arises as to how these organisms survive under such extreme condition(s). Based on the available knowledge two mechanisms for the survival of these organisms have been proposed (1); "to keep the environment out" or "to adjust with the environment". In the earlier case the organism living under extreme condition establishes firm barriers between the hostile outside world and the cell's cytoplasm. Therefore, the intra-cellular components / organelles do not require adaptation to the extreme condition(s). In contrast, in the latter case the intra-cellular components of the organisms need to adapt to the external extreme condition. In fact, the defensive or adaptive mechanisms are driven by the extreme parameter to some extent. For example, an acidophile (lives at ~pH 0) and an

alkaliphile (lives at ~pH 10) maintain their intracellular pH close to neutral pH. Acidophiles achieve this pH level via the low permeability of the membrane for protons and by an efficient outward proton pump, while an alkaliphiles appear to solve this problem by membrane potentials (negative inside) and often also by using sodium ions rather than protons to couple bioenergetic transformations. On the other hand, in some cases reaching such an intra-cellular homeostasis state is not possible, and the cell needs to adjust to the extra-cellular conditions. For example, an unicellular psychrophilic or (hyper)thermophilic organism can not protect the cytoplasm from external low or high temperature. In that case the intracellular proteins and organelles become adaptive to low or high temperature mainly via the rearrangement of the structural elements.

The discovery of the extremophiles dates back to 1880 when Farlow isolated the first halophilic species from a salty fish (2). However, the pioneering works by Eleazari Volcani started in 1936 when he isolated several microbial strains living at a salt concentration of 30 to 34% (weight / volume) from the Dead Sea (3). Before 1970, isolation and pure culturing, followed by morphological description of the microorganism was the classical approach to study microbial diversity, which is not sufficient to define its relativity with other species. However, over the last thirty years the approach to study microbial diversity has been improved by the use of molecular techniques for identifying an organism and to group it with other relative species. In 1970 Woose *et al* first chose to use the small ribosomal subunit (16S / 18S rRNA) due to its universality and reasonable conservation (4, 5) among the microbial community. Based on the sequence comparison of these rRNAs from different organism, life on the Earth is divided into three domains: archaea, bacteria and eukarya. Since then, 16S / 18S rRNA has been the most widely used molecular marker in the development of the phylogenic tree of life. In fact the identification of archaea was achieved via the application of molecular techniques. The research on extremophiles was significantly increased when most of these organisms were described to

from the third order of life, archaea (6). From the beginning of their identification, extremophiles attracted attention from different fields of science including molecular biology, biotechnology, evolution and phylogeny, and exobiology.

THERMOPHILES AND HYPERTHERMOPHILES

Thermophiles and hyperthermophiles growing optimally above 60 or 80°C, respectively were started to be isolated during the decade from 1970 to 1980 (6). *Thermus aquaticus,* a thermophilic bacterium living at 60–80°C was isolated from a hot spring at Yellowstone National Park in the US by Thomas Brock in 1969 (7). The first isolated hyperthermophilic archaeon, *Sulfolobus acidocaldarius* which is able to grow at temperatures up to 85°C and at low pH (1–5) was isolated a year later (8). Most of the hyperthermophiles reported until now are members of the domain of archaea, which can be further divided into the two branches of crenarchaeota and euryarchaeota. Crenarchaeotes characterized until now exclusively consist of thermophilic and hyperthermophilic orders, while the euryarchaeota include the orders of methanogens and extreme halophiles in addition to thermophilic and hyperthermophilic orders. A deep branch of euryarchaeota is an order called "Thermococcales" which is represented by three genera: *Pyrococcus* (9), *Thermococcus* (10) and the more recently described *Paleococcus* (11). Of the thirty eight species reported for *Thermococcales*, six species belong to the *Pyrococcus* genus, and the complete sequences are known for the genomes of three of them: *P. abyssi*, *P. furiosus,* and *P. horikoshii* (12).

Pyrococcus furiosus. In 1986 Fiala and Stetter isolated *Pyrococcus furiosus* from the geothermally heated marine sediments off the beach of Porto di Levante, Vulcano, Italy (9). The members of the genus *Pyrococcus* seem to be found only in marine environments and belong to a particular niche (13). Usually, species of *Pyrococcus* are hyperthermophilic (growth at 95-100 °C), heterotrophic and strictly anaerobic, and all utilize peptide as main

carbon source and elemental sulfur is essential for their growth. However, *P. furiosus* and a few other members of this genus are also capable of using carbohydrate as carbon and energy source in the presence of trace amounts of vitamins. Furthermore, they are also capable of growing independently of elemental sulfur, producing H_2, CO_2 and acetate as the main metabolic products, while in the presence of S^0 H_2S is produced instead of H_2. A small electron transfer protein, ferredoxin in association with several redox enzymes plays an important role in various metabolic pathways of *P.furiosus*.

FERREDOXIN

D.C. Wharton first introduced the term "Ferredoxin" for a nonheme "iron-protein" isolated from *Clostridium pasteurianum,* a non-photosynthetic and anaerobic bacterium (14). Ferredoxins (Fd) are small electron-transfer proteins, that contain an (or more) iron-sulfur cluster as the redox active group usually with rather low reduction potential. It is now established that Fds are ubiquitous in biological systems and play important roles in various electron-transfer processes, including respiration, photosynthesis, and fermentation.

For a long time Fds were classified according to their sources from two phyologenetically distinct families: the [3/4Fe-4S] cluster containing bacterial-type, and the [2Fe-2S] containing plant and algal type ferredoxin. However, the existence of a third family, thioredoxin-like [2Fe-2S] low-potential Fds, was initially suggested by Meyer *et al,* based on the primary structure of a [2Fe-2S] protein from *Clostridium pasturianum* (15, 16). Latter this was confirmed by the analysis of the crystal structure of a homologous protein from *Aquifex aeolicus* (17).

Plant and alga-type ferredoxin. Plant-type [2Fe-2S] ferredoxins can be divided into two major classes: oxygenic photosynthetic Fds and Fds involved in other processes than photosynthesis (18). Studies on [2Fe-2S] Fds have been reviewed elsewhere (18, 19). This

PhD research involves *P. furiosus* Fd, a bacterial-type ferredoxin, and therefore, we will focus on this type of ferredoxin only.
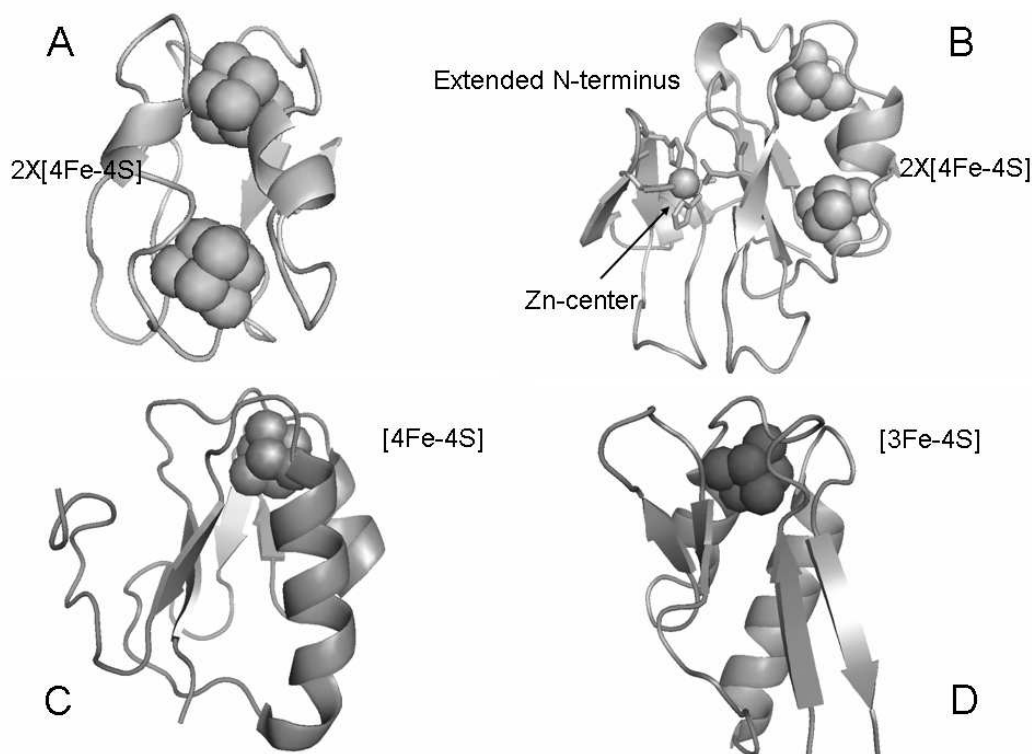
Figure 2: Protein folds for the major types of bacterial ferredoxins. A. di-cluster type, 2[4Fe-4S] Fd from *Clostridium acidurici* (PDB entry 2FDN, 20); B. Zn-center containing di-cluster Fd from *Sulfolobus* species strain 7 (PDB entry 1XER, 21); C. mono-cluster type, [4Fe-4S] Fd from *Bacillus thermoproteolyticus* (PDB entry 1IQZ, 22); and D. mono-cluster type, [3Fe-4S] Fd from *Pyrococcus furiosus* Fd (PDB entry 1SJ1, 23).

Bacterial-type ferredoxin. Bacterial-type Fds can be divided into two major classes: mono-cluster and di-cluster type. The mono-cluster type can be sub-divided into [4Fe-4S] and [3Fe-4S] cluster containing ferredoxins. The di-cluster type can be sub-divided as 2[4Fe-4S], [3Fe-4S] plus [4Fe-4S] cluster containing, and Zn containing di-cluster type ferredoxins (24).

Figure 2: Structural alignment of mono and di-cluster type Fds. Left: Alignment of [3Fe-4S] D.*gigas* FdII (PDB ID 1FXD, 25) in black and [3Fe-4S] *P.furiosus* Fd (PDB ID 1SJ1, 23) in gray, showing high structural homology between the two Fds from prokaryotic and archaeal domain. Right: Alignment of [7Fe-8S] *A. vinelandii* FdI (PDB ID 1FDD, 26) in black and [3Fe-4S] *P.furiosus* Fd (PDB ID 1SJ1, 23) in gray, showing the conservation of the minimal cluster containing unit across different types of Fds from different domains of life.
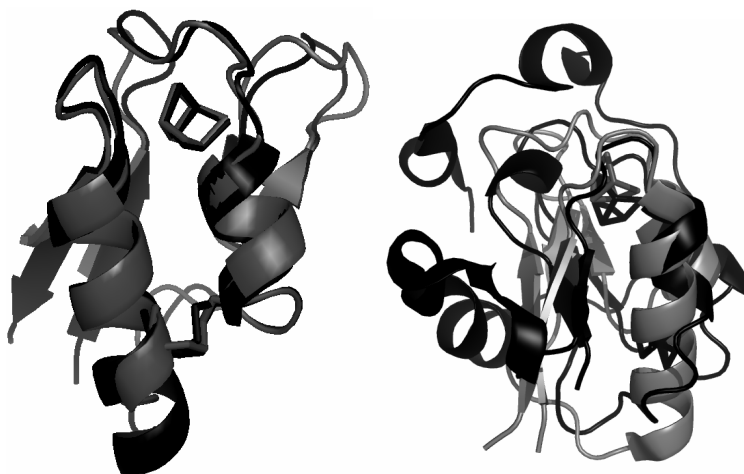
The folding pattern of the bacterial type ferredoxin is presented in figure 1, showing that the basic unit for the formation of the cluster is conserved in all the Fd varieties, across different domains of life. The iron sulfur cluster in this type of Fd is usually coordinated by a consensus sequence motif: Cys-X-X-Cys-X-X-Cys-$(X)_n$-Cys-Pro (n is variable; ≥ 35). But in di-cluster type Fds two types of consensus motifs are reported. The "*clostridial*-type" ferredoxins have two Cys-X-X-Cys-X-X-Cys-X-X-X-Cys-Pro motifs (*Azotobacter vinelandii* FdIII). The "*Chromatium*-type" ferredoxins have one motif of that type and one more unusual Cys-X-X-Cys-X(7-9)-Cys-X-X-X-Cys-Pro motif (*Chromatium vinosum Fd*). Bacterial-type ferredoxins have been purified from various organisms of the bacterial and archaeal domains including psychrophiles, mesophiles, thermophiles and hyperthermophiles, halophiles, acidophiles, methanogenic etc. These ferredoxins are involved in various processes like bacterial nitrate reduction, sulfite reduction, CO_2 reduction and pyruvate oxidation and in some steps of glycolytic pathways of archaea (27). In certain archaea (e.g. *P. furiosus*) Fd

replaces NAD for carrying reducing equivalent to an oxidative phosphorylation machinary. The size and oligomeric states of these Fds also vary from organism to organism and also within the same organism, most probably due to the stability and / or functional requirements. For example *D. gigas* [4Fe-4S] FdI exist as a trimer (28) while [3Fe-4S] FdII from the same organism exists in a tetrameric state (29). *P. furiosus* ferredoxin has been suggested to be a functional dimer (30). Some ferredoxins are composed of 55-60 amino acids (60 residues for *T. maritima*) while some di-cluster ferredoxins are composed of 120-110 amino acids (106 for *A.vinelandii* FdI). However, the conserved sequence composed of ~55 residues as suggested by Otaka and OOi (31), containing the consensus sequences motif for [Fe-S] cluster in addition to some connector residues are present in all varieties (Fig 2). A detailed evolutionary model for the bacterial ferredoxin has been elaborated in two previous reviews (19, 22) and will not be discussed here.
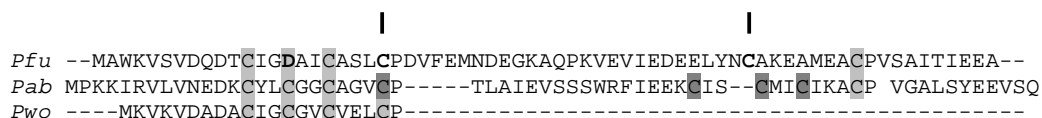
Archaeal ferredoxins. Archaeal ferredoxins are also bacterial-type ferredoxins which posses some unique features in addition to the ones observed in other bacterial-type Fds e.g., resistance to high and low temperature, high salt concentration, high or low pH. Interestingly, the archaeal Fds reflect the differences in the growth conditions of the respective species, rather than their phylogenetic relationships based on the sequences of 16 S rRNA (24). In fact, ferredoxins from hyperthermophiles, methanogens and thermoacidophiles are clustered together in a separated group as the monocluster type, di-cluster type and the Zn- containing di-cluster type, respectively.

Zn-containing Arachael Fds. This class of strictly di-cluster type ferredoxins is exclusively found in thermoacidophilic archaea. Ferredoxins of this type have been purified from *Sulfolobus acidocaldarious* (32, 33), *Desulfurolobus ambivalens* (34), *Thermoplasma acidophilum* (35), and *Sulfolobus* sp.strain 7 (21). This particular type of Fd is mainly confined to fast growing organisms (like *Sulfolobus* and *Themoplasma* species) (36),

indicating an important role of Fd in the metabolism of the respective organism. Fuji *et al* solved the crystal structure of the Fd from *Sulfolobus* sp. Strain 7, the first structure of this type. Unlike the regular bacterial ferredoxins (mono and di-cluster type) the primary structure of this type of archaeal Fds contains a central loop region (residues 37-103) which binds two iron-sulfur clusters, and an N-terminal extension (residues 1-36) (Figure 1b), composed of three β-strands and one α-helix (24). There are seven cysteine residues in this Fd, and structural analysis revealed that these cysteines are coordinating one [3Fe-4S] cluster (site I) and one [4Fe-4S] cluster (site II), forming an iron-sulfur core. In addition, four residues (His^{16}, His^{19}, His^{34}, Asp^{76}) in the extended region serve as the ligands to a tetragonally coordinated, novel zinc center (21). The Zn-center is isolated and buried within the molecule and connects the two [Fe-S] clusters cores and the N-terminal extension region.

Mono-cluster type P. furiosus Fd. *Pfu* Fd is one of the most intensively studied ferredoxins until now. It is a mono-cluster type small Fd, composed of 66 amino acid. *Pfu* Fd is one of the most thermostable ferredoxins, exhibiting minimal degradation for several days at 95ºC (37 and chapter 3). In 1989 Aono *et al* (38) first isolated *Pfu* Fd and reported the remarkable thermostability of the protein and also an unusual EPR signal from the [4Fe-4S]. Since then numerous studies have been carried out for the elucidation of structural-functional relationships and of other features of the protein. One of the distinguishing features of *Pfu* Fd is the coordination of its single [4Fe-4S] cluster by three, rather than four, cysteinyl residues and an aspartate residue. The sequence coordinating the cluster is CxxDxxC….CP, similar to the consensus sequence CxxCxxC…CP (*Clostridial type*). This sequence motif is not conserved even within the *Pyrococcus* genus (Figure 4). The oxo-ligand from the aspartate is not as stable as the s-ligand from cysteines which results in the partial conversion of the [4Fe-4S] cluster to [3Fe-4S] form and a mixture of [4Fe-4S] and [3Fe-4S] forms are obtained when

the protein is purified under aerobic condition. However, the physiological relevance of such conversion (if any) is not clear yet.

```
                                 |                        |
Pfu  --MAWKVSVDQDTCIGDAICASLCPDVFEMNDEGKAQPKVEVIEDEELYNCAKEAMEACPVSAITIEEA--
Pab  MPKKIRVLVNEDKCYLCGGCAGVCP-----TLAIEVSSSWRFIEEKCIS--CMICIKACP VGALSYEEVSQ
Pwo  ----MKVKVDADACIGCGVCVELCP--------------------------------------------
```

Figure 4: Amino acid sequence alignment of [4Fe-4S]-type ferredoxins from *Pyrococcus* genus to show the consensus sequence motif for the cluster. The cluster binding cysteinyl residues are indicated in gray shade and the aspartate is in bold. In case of *P.woosei Fd* only the N-terminus sequence has been aligned. The vertical lines indicate the cysteine residues that *in vitro* can form a disulfide bridge in *Pfu*Fd. The cysteine residues shaded in dark gray in the putative *P. abyssi* ferredoxin gene show the sequence motif for a second [4Fe-4S] cluster. The abbreviations are *Pfu, Pyrococcus furiosus*; *Pab, Pyrococcus abyssi*; *Pwo, Pyrococcus woosei*. Alignment has been performed with Clustal W.

In addition to the cluster-coordinating cysteines, two surface cysteines are present at position 21 and 48. Both the solution NMR molecular model for the oxidized [4Fe-4S] form (39) and the X-ray crystallographic structure of the aerobic [3Fe-4S] form of the protein (23) demonstrated the presence of an intra-molecular disulfide bond between the two non-ligand cysteines. However, it must be noted here that in both cases *Pfu* Fd has been exposed to air for days and so the formation of a disulfide bond is very likely in both cases. Extensive studies have been reported on the native, recombinant wild type and on several mutant varieties of *Pfu*Fd (mainly altering the cluster coordinating amino acids) detailing the effect of temperature and pH on the redox states of the protein and their structural and functional relevance (37, 40-43). *In vitro* disulfide bond formation was also shown, and a possible role of the disulfide bridge as a redox centre was discussed (41), assuming the existence of four formal redox states of *Pfu* Fd, where the cluster is either reduced (Fd_{red}) or oxidized (Fd_{ox})

and Cys 21 and Cys 48 are either in the disulfide form (A) and in the free thiol form (B) (37). However, purification of the *Pfu*Fd under anaerobic condition resulted in a ferredoxin preparation with intact [4Fe-4S] cluster and with no disulfide bond (cf chapter 3 and ref. 37). The physiological relevance of the formation of the disulfide bridge between Cys21 and Cys48 after long (hours) exposure to air in a strict anaerobic organism is unclear. We will address this problem in chapter 3.

Metabolic role of P. furiosus Fd. Ferredoxin plays an important role in the metabolism of *P. furiosus* which can be summarized as in figure 5. It acts as the electron acceptor for two glycolytic enzyme glyceraldehyde-3-phospahte oxidoreductase and pyruvate oxidoreductase and for the enzymes involved in the CoA derivative formation, indol pyruvate oxidoreductase and 2-ketoisovalerate oxidoreductase (VOR). A similar role of ferredoxin for few other oxidoreductases like, aldehyde oxidoreductase, formaldehyde oxidoreductase and WOR5 has been reported. However, the physiological role of these oxidoreductases is unknown (though some are suggested to be involved in the amino acid metabolism). The reduced ferredoxin thus produced acts as the electron donor for the membrane-bound hydrogenase which is involved in proton respiration. The reduced ferredoxin also acts an electron donor for ferredoxin: NAD(P)$^+$ oxidoreductase (FNOR) enabling the production of NAD(P)H, which is presumably used in biosynthetic pathways of the organism. In chapter five we also demonstrate that ferredoxin is capable of mediating reversible oxidation of aldehyde to acid and vice versa *in vitro*.

What molecualr properties confer thermostability to a protein? This is an interesting question, which is still under investigation by many groups. Among the range of factors hypothesized to be involved in the thermal stability of hyperthermophilic proteins are: cumulative or individual contribution of electrostatic interactions, compactness and quarternary structure [44], greater hydrophobicity, better atom packing, deletion or shortening

of loops (45), smaller and fewer cavities, an increased surface area buried upon oligomerization (46, 47), residue substitution within and outside the secondary structures (44, 48), increased occurrence of proline residues in loops (49, 50), decreased occurrence of thermolabile residues (44, 51), increased helical content, increased polar surface area, more hydrogen bonds, and increased salt bridge formation (51-54). It must be emphasized that until now studies predicting the factors contributing to the thermal
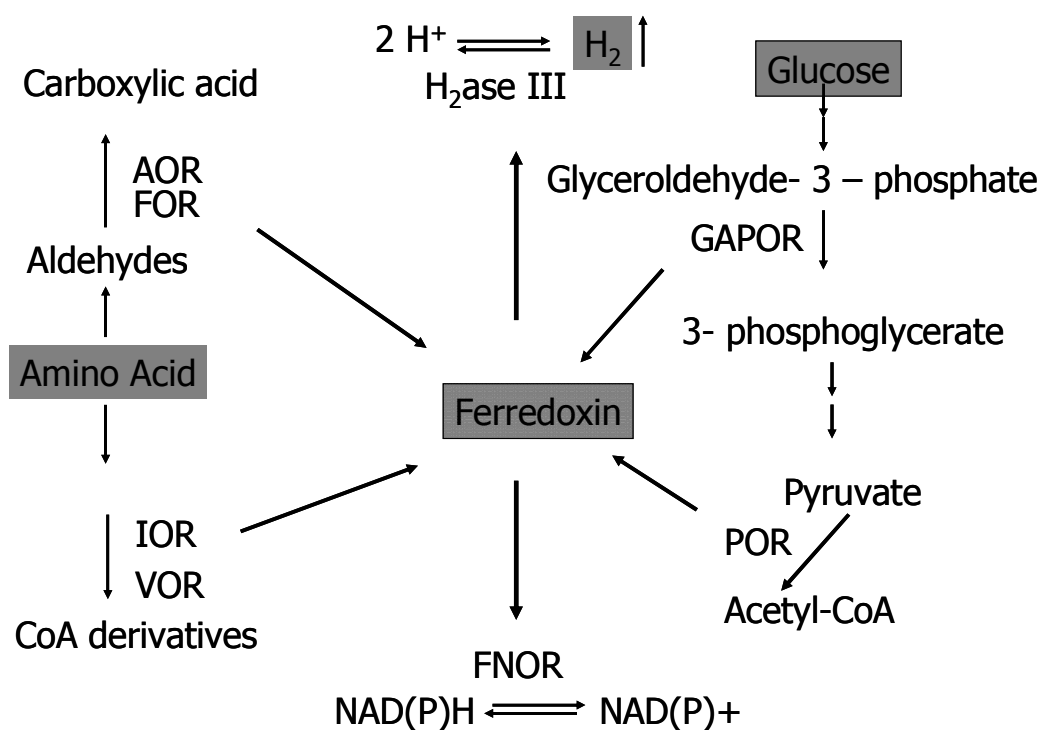
Figure 5: Schematic representation of the different roles of the ferredoxin in the metabolism of *P. furiosus*: in amino acid metabolism, glycolysis, reduction of pyridine dinucleotide, and hydrogen metabolism.

stability of proteins suffer from limitations in some ways. Poor understanding of the relation between the protein sequence and structure,analysis of small sets of samples, bundling up proteins from different domains of life to increase the size of the sample data set, comparison of predicted and resolved structures of proteins, are a few of the notable limiting factors. Therefore, no general rule can be drawn as to how the (hyper)thermophilic proteins attain

their stability. In-depth analysis of specific proteins (or protein families) would perhaps provide better insight into mechanisms governing protein stability, and the well characterized *Pfu*Fd could be a suitable candidate for these studies.

OUTLINE OF THE THESIS.

Chapter two. *Pfu* Fd was initially isolated as a dimeric protein with a molecular mass of 12-13 kDa (38). However, in a series of subsequent publications it has been taken to be a monomeric protein of 7.5 kDa without any experimental evidence. In chapter 2 we demonstrate that *Pfu* Fd as isolated is a (presumably functional) dimer under physiological condition.

Chapter three. In addition to the cluster-coordinating cysteines, *Pfu* Fd posses two additional cysteines at position 21 and 48. It has previously been proposed that these cysteines form a disulfide bridge, which participates in the redox cycle of the protein and also contributes to its stability. However, the formation of the disulfide bond under the strongly reducing intracellular condition in an anaerobic organism like *P. furiosus* is quite unusual. In chapter 3, we demonstrate that under physiology-mimicing condition no disulfide bond is formed, and that these cysteines do not participate in the redox cycle of the protein. In addition, a role of the cysteine residue at position 21 in the hyperthermostability of the protein is proposed.

Chapter four. Protein-film voltammatry is a useful technique to study redox proteins. It is a powerful tool to probe the potential dependence of enzymatic activity and the role of cofactors in relaying electrons for controlled enzymatic reactions. Although *Pfu*Fd has been subjected to solution voltammetric studies by different groups, no electrochemisty on this protein adsorbed on the electrode has been reported previously. Furthermore, absorption voltammetry for other small redox proteins (e.g. cytochrome *c*) has been reported, however, with modification of the electrode surface for tethering the protein molecule on the electrode. In this chapter we demonstrate that *Pfu*Fd can be directly immobilized on a polycrystalline gold electrode without surface modification, and that it retains its structure-functional integrity. A transition between the dimeric and monomeric form was observed in an atomic

force microscopic study. A detailed X-ray photoelectron spectroscopy (XPS) analysis on the immobilized *Pfu*Fd is reported, and this is the first study to distinguish among the sulfurs in different cysteines in immobilized protein: surface-bound, cluster-ligating, and free ones.

Chapter five. This chapter is an extension of the work initiated in chapter four. The application of the *Pfu*F modified gold electrode for the study of the associated redox enzymes from *P.furiosus* is reported in this chapter. Both non-turnover and catalytic voltammograms for two redox enzymes (aldehyde oxidoreductase and glyceraldehyde-3p-oxidoreductase) from *P. furiosus* have been observed on the *Pfu*Fd modified gold electrode. The formation of complexes between the redox enzymes and ferredoxin, and reversible oxidation of crotonaldehyde (aldehyde to acid and acid to aldehyde) is also described in this chapter.

REFERENCES

1. Seckbach J. (ed.) (2006), *Life as We Know It,* Springer 3-20.

2. Farlow WG (1880). U.S. Commission of Fish and Fisheries, 969–974.

3. Wilansky B (1936). Nature 138, 467.

4. Woese CR (1987). Microbiol. Rev. 51, 221–271.

5. Woese CR and Fox GE (1977). Proc. Natl. Acad. Sci. USA 74, 5088–5090.

6. Gargaud M (Ed.) (2005) Lectures in Atrobiology, Vol. I, 657–679.

7. Brock TD and Freeze H. (1969) J. Bacteriol. 98, 289–297.

8. Brock TD, Brock KM, Belly RT and Weiss RL (1972) Arch Mikrobiol. 84, 54–68.

9. Gerhard F and Karl OS (1986) Arch Microbiol 145: 56- 61

10. Achenbach-Richter L, Gupta R, Zillig W and Woese C R (1998) Syst. Appl. Microbiol. 10, 231-240

11. Takai K, Sugai A, Itoh T, and Horikoshi K (2000) Int. J. Syst. Evol. Microbiology. 50, 489-500.

12. Holden J.F and Adams M.W.W. (2003) *Encyclopedia of Life Support System.* Eolss Publishers

13. Morikawa M, Izawa Y, Rashid N, Hoaki T and Imanaka T (1994) Appl. Environ Microbiol. 60(12): 4559-4566

14. Mortensen LE, Valentine RC, Carnahan JE Biochem. Biophys. Res. Commun. (1962) 7:448-52.

15. Meyer J, Bruschi MH, Bonicel JJ and Bovier-Lapierre GE (1986) Biochemsitry 25, 6054-6061

16. Meyer J (1988) Trends Ecol. Evol. 3, 222-226

17. Yeh AP, Chatelet C, Soltis SM, Kuhn P, Meyer J and Res DC (2000) J. Mol. Biol. 300, 5787-595

18. Sticht H and Rosch P (1988) Prog. Biophys. and Mol. Biol. 70, 95-136

19. Matsubara H and Saeki K (1992) Ad. Inorg. Chem. 38, 223-280

20. Dauter Z, Wilson KS, Seeker LC, Meyer J and Moulis JM (1997) Biochemistry 36, 16065-16073.

21. Fujii T, Hata Y, Wakagi T, Tanaka N, and Oshima T (1996)   Nat. Struct. Biol. 3, 834-837.

22. Fukuyama K, Okada T, Kakuta Y, and Takahashi Y (2002) J. Mol. Biol. 315 pp. 1155-1166,

23. Nielsen MS, Harris P, Ooi BL, Christensen HEM (2004) Biochemistry 43, 5188-5194,

24. Iwasaki T, Suzuki T, Kon T, Imai T, Urushiyama A, Ohmori D and Oshima T (1996) J. Biol. Chem. 272(6), 3453-3458

25. Kissinger CR, Sieker LC, Adman ET and Jensen LH (1991) J.Mol.Biol, 219 693-715,

26. Shen B, Martin LL, Butt JN, Armstrong FA, Stout CD, Jensen GM, Stephens PJ, La Mar GN, Gorst CM, Burgess BK (1993) J. Biol. Chem. 268, 25928-39.

27. Corné HV, Kegen SWM, Judith ET, Gerrit JS, Adams MWW, de Vos WM and van der Oost J (2003) Biochem. J. 375, 231-246

28. Bruschi M (1979) Biochem Biophys Res Commun 91:623-628

29. Bruschi M and Guerlesquin F (1988) FEMS Microb. Lett. 54 (2) 154-175.

30. Hasan MN, Hagedoorn PL and Hagen WR (2001) FEBS Lett 531, 335-338

31. Otaka E and Ooi T (1989) J Mol Evol 29:246-254

32. Minami Y, Wakabayashi S, Wada K, Matsubara H, Kerscher L, and Oesterhelt D (1985) J. Biochem. (Tokyo) 97, 745–753

33. Breton JL, Duff JLC, Butt, JN, Armstrong FA, George SJ, Pe´tillot Y, Forest E, Schafer G, and Thomson AJ (1995) Eur. J. Biochem. 233, 937–946

34. Teixeira M, Batista R, Campos AP, Gomes C, Mendes J, Pacheco I, Anemu IS and Hagen W R (1995) Eur. J. Biochem. 227, 322–327

35. Wakabayashi S, Fujimoto N, Wada K, Matsubara H, Kerscher L, and Oesterhelt D (1983) FEBS Lett. 162, 21–24

36. Stetter, K. O. (1995) ASM News 61, 285–290

37. Kim CH, Brereton PS, Verhagen MFJM and Adams MWW (2001) Meths. Enzymol. 334, 30-40

38. Aono S, Bryant FO and Adams MWW (1989) J. Bacteriol. 171, 3433-3439

39. Sham S, Luigi C, Wang PL, Bren K, Haarklau H, Brereton PS, Adams MWW and La Mar GN (2002) Biochemistry 41, 12498-12508

40. Gorst CM, Yeh YH, Teng Q, Calzolai L, Zhou ZH, Adams MWW and La Mar G (1995) Biochemistry 34: 600-611

41. Gorst CM, Zhou ZH, Ma K, Teng Q, Howard JB, Adams MWW and La Mar G (1995). Biochemistry 34: 8788-8795

42. Telser J, Smith ET, Adams MWW, Conover RC, Johnson MK and Hoffman BM (1995) J. Am. Chem. Soc. 117: 5133-5140

43. Hagedoorn P-L, Driessen MCPF, van den Bosch M, Landa I and Hagen WR (1998) FEBS Lett. 440, 311-314

44. Robinson-Rechavi M, Alibes A and Godzik A (2006) J. Mol. Biol. 356, 547–557

45. Russell RJM, Ferguson JMC, Haugh DW, Danson MJ and Taylor, GL (1997) Biochemistry 36, 9983-9994

46. Salminen T, Teplyakov A, Kankare J, Cooperman BS, Lahti R and Goldman A (1996) Prot. Sci. 5,1014-1025

47. Karshikoff A and Landestien R (1998) Prot. Eng. 11, 867-872

48. Zuber H. (1998) Biophys. Chem. 29,171-179

49. Haney P, Konisky J, Koretke KK, Luthey-Schulten Z. and Wolynes PG (1997) Proteins 28, 117-130

50. Watanabe K, Hata Y, Kizaki H, Katsube Y and Suzuki Y (1997) J. Mol. Biol. 269, 142-153

51. Kumar S, Tsai CJ and Nushinov R (2000) Prot. Eng. 3, 179-191

52. Querol E, Perezs-Pons JA and Mozon-Villarias A (1996) Protein Eng. 9:256-271

53. Vogt G, Woell S and Argos P (1997) P J Mol Biol 269, 631-643

54. Szilagyi A and Zavodszky P (2000) Structure 8, 493-504

Pyrococcus furiosus ferredoxin is a functional dimer.

ABSTRACT

Pyrococcus furiosus ferredoxin is subject to a monomer / dimer equilibrium as a function of ionic strength. At physiological ionic strength, approximately 0.35 M NaCl, the protein is very predominantly homodimer. The monomeric form exhibits impaired electron transfer on a glassy carbon; it also has a decreased S = 3/2 over S = 1/2 ratio as shown by EPR spectroscopy. Even following sterilization at 121°C the dimer is stable in denaturing gel electrophoresis.

INTRODUCTION

Pyrococus furiosus is a strict anaerobic, hyperthermophilic marine archaeon with an optimal growth temperature of 100° C [1]. *P. furiosus* is a practical model organism, as it grows easily and rapidly, in the absence of elemental sulfur, on cheap substrates in up to several hundred liter batch cultures, and cell-free extract is readily obtained by osmotic shock in water. Furthermore, the complete genome of *P. furiosus* has been determined, as well as that of the related species *P. abyssi* and *P. horikoshii*. The biochemistry has now been studied for 13 years. When grown on carbohydrate, e.g., starch, *P. furiosus* uses a modified Embden-Meyerhoff pathway for glycolysis to the level of acetate [2].

A single ferredoxin has been purified from *P. furiosus* and no putative additional ferredoxins are indicated from our genome inspection. The 7.5 kDa *P. furiosus* ferredoxin, *Pfu* Fd, is extremely thermostable. It contains a single $[4Fe-4S]^{(2+;1+)}$ cubane with Cys, Asp, Cys, Cys coordination [3]. Two additional Cys residues can reversibly form a disulfide bridge [4]. *Pfu* Fd is synthesized in considerable amounts reflecting its key role(s) in mainstream electron transfer. The protein acts as the electron-acceptor for the two glycolytic redox enzymes, glyceraldehyde-3-phosphate oxidoreductase and pyruvate oxidoreductase, and as the electron-donor for a transmembrane multisubunit hydrogenase complex [5]. *Pfu* Fd is also the putative redox partner of several other oxidoreductases involved in oxoacid or aldehyde activation [6]. Structural studies of *Pfu* Fd have presented several difficulties. It has thus far not been possible to obtain crystals suitable for X-ray crystallographic analysis. A crystallized one-to-one complex of the ferredoxin with formaldehyde oxidoreductase afforded a high-resolution structure of the enzyme, however, the ferredoxin was found to be disordered [7]. ^{1}H-NMR studies have shown multiple structural heterogeneity, part of which has been interpreted to initiate at the disulfide bridge, which appears to occur in two mirror orientations [8]. EPR spectroscopy has established a spin mixture of S = 1/2 and S = 3/2 species for the $[4Fe-4S]^{1+}$

cluster. EPR also provided evidence for multiple S = 1/2 heterogeneity in the reduced cluster following aerobic purification [3].

The cumulative manifestations of heterogeneity have incited us to re-visit a long-standing, unsolved problem regarding the oligomeric state of the *Pfu* Fd. In the original paper on the purification of *Pfu* Fd, a molecular mass of 12-13 kDa was reported, and the possibility was raised that the ferredoxin as isolated exists as a dimer [9]; the calculated mass of the gene product (ignoring the prosthetic group) is 7.26 kDa. However, in a subsequent 1990-paper by Conover et al. [3] *Pfu* Fd was re-defined as monomeric with reference to data to be published (E. Eccleston, J.B. Park, M.W.W. Adams, and J.B. Howard, manuscript in preparation). To our knowledge this paper has not been published. In all later literature *Pfu* Fd has been implicitly or explicitly taken to be monomeric with frequent reference to the paper by Conover et al. Also, Smith et al. claimed their MALDI-MS data on dried protein to indicate that *Pfu* Fd is monomeric [10]. During purifications of *Pfu* Fd over the years we noted chromatographic behaviour suggestive of strong dimerization. In the present paper we describe experiments to determine the aggregation state of *Pfu* Fd and its relation to some physico-chemical properties of the protein.

METHOD AND MATERIALS

The cultivation of *P. furiosus* (DSM 3638) was carried out as previously described [11]. Purification of *Pfu* Fd was carried out as stated previously [12] except that lysozyme was omitted. The protein concentration was determined with Micro-Biuret reagents. Gel electrophoresis was carried out with the Phast System (Pharmacia) and NuPAGE (Invitrogen) Bis-Tris electrophoresis system according to the manufacturers' instructions. The Phast system is based on the Laemmli protocol except for tricine in the running buffer. For the NuPAGE system Bis-Tris-HCl buffered (pH 6.4) 4-12% gradient or 10% homogeneous

polyacrylamide gels were used with a running buffer (pH 7.3) comprised of 50 mM MES, 50 mM Tris Base, 1%SDS, 1 mM EDTA, and an antioxidant. In contrast to the traditional Laemmli sample buffer [13], the sample buffer contained lithium dodecyl sulfate (LDS) and 50 mM DTT as denaturant.

Analytical gel filtration was carried out with a HR 10/30 (10 mm x 30 cm, 24 ml) Superdex S-75 column (Pharmacia LKB). All the buffers used contained 50 mM Tris-HCl pH 7.8, 10% (v/v) glycerol, 2 mM DTT, 2 mM sodium dithionite, in addition to variable amounts of NaCl. The column was equilibrated with buffer containing the desired concentration of salt before every run. All the buffers and columns were thoroughly flushed with argon to make them anaerobic and all the experiments were carried out under a small over-pressure of argon to maintain strict anaerobic condition. For molecular weight determination a mixture of 1.5 µl cytochrome c (25 mg/ml), 10 µl *Pfu* Fd (7.5 mg/ml) and 10 µl myoglobin (3 mg/ml) was injected onto the column. In all other salt effect studies a mixture of 2.5 µl *Pfu* Fd (7.5 mg/ml) and 4 µl cytochrome c (2.5 mg/ml) was diluted to a total volume of 25 µl with the running buffer at the desired salt concentration and briefly incubated at room temperature before loading onto the column.Cyclic voltammetry experiments were carried out as described earlier [14]. All the EPR measurements were carried out as described earlier [15]. The conductivity of the cell lysate was measured with a Consort K720 conductivity sensor, calibrated with standard NaCl solutions (0-80 mM).

RESULTS

Size exclusion chromatography. To determine the physiological oligomeric form (monomer/dimer) of *Pfu* Fd size exclusion chromatography experiments were carried out at different salt concentrations from 0.15 M to 3.25 M NaCl. At 0.15 M – 1 M NaCl the retention time for *Pfu* Fd was greater than that of myoglobin (Mw = 17 kDa) and less than

that of cytochrome *c* (Mw = 13.7 kDa) (Fig. 1A), which suggests that at physiological salt concentration (approx. 0.35 M NaCl, see below) it exists as a dimer. With the increase of salt concentration above 1 M NaCl the retention time increased (Fig. 1B), indicating a change in apparent mass, which we attribute to a shift from dimer to monomer. At 3 M NaCl the retention time for *Pfu* Fd became longer than that for cytchrome *c*. To exclude the possibility of hydrophobic interaction between the *Pfu* Fd and the gel matrix, we have also carried out an experiment adding 20% acetonitrile to the buffer at 3M NaCl. No change in the retention time of *Pfu* Fd was observed compared to the run without acetonitrile (not shown).
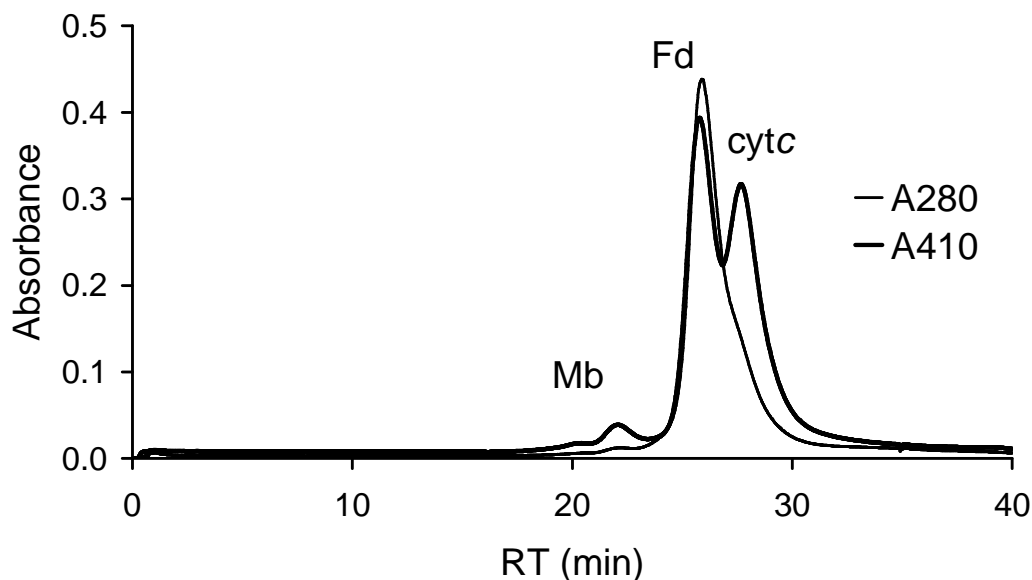
Fig. 1A. Gel filtration of anaerobically purified *Pfu* Fd, horse heart cytochrome *c*, and horse myoglobin on a Superdex-75 column (10 mm x 30 cm). The buffer was 100 mM NaCl, 50 mM Tris-HCl (pH 7.9), 10% glycerol (v/v), 2 mM DTT, 2 mM sodium dithionite. The experiment was carried out with a flow rate of 0.5 ml/min, at room temperature (~20°C) and anaerobic condition. Amounts of proteins loaded were *Pfu* Fd ~75 µg, cytochrome *c* ~40 µg and myoglobin 30 µg.

Gel electrophoresis. *Pfu* Fd as isolated appeared as a 12-13 kDa protein in denaturing polyacrylamide gel electrophoresis (Fig. 2). Several SDS-PAGE experiments were carried out to find conditions to monomerize the *Pfu* Fd. No change in apparent mass has been observed on 4-12% gradient or on 10% homogeneous NuPAGE; nor on 8-25% gradient or on 20% PhastGel (Amersham Biosciences), after heating the protein for one hour at 70°C or 95°C in a denaturing buffer containing 2.5% SDS or LDS, 1 mM EDTA, 5% 2-mercaptoethanol or 5-50 mM DTT (data not shown). We also did not observe any change in the apparent mass after treating the protein for one hour under sterilizing conditions (121°C and ~90 kPa overpressure) either in 100 mM DTT + LDS sample buffer, or in LDS sample buffer, or in Laemmli sample buffer (Fig. 2).
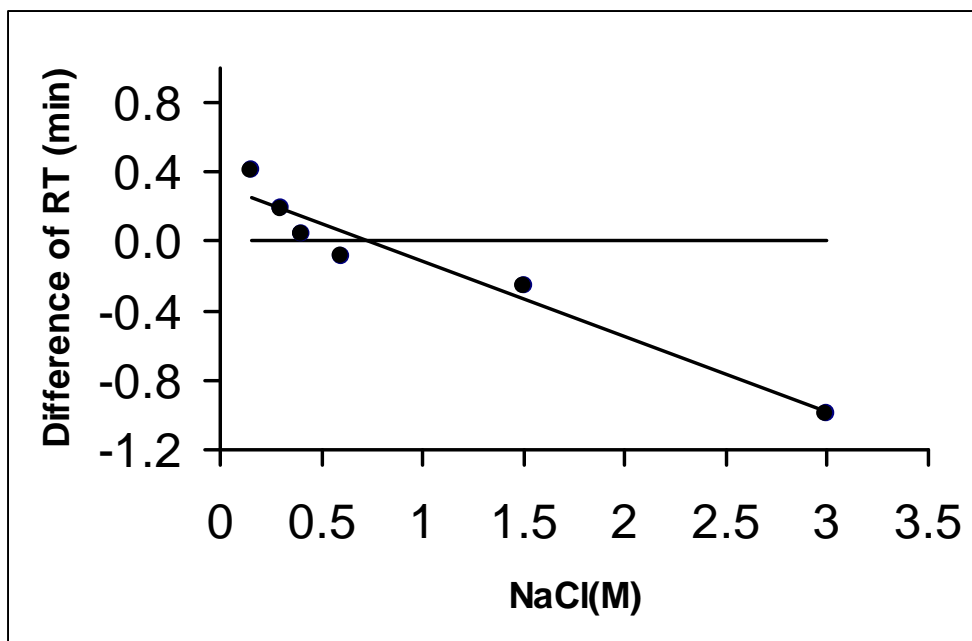

Fig. 1B. Dependence of the retention time (RT) of *Pfu* Fd on the salt concentration. The Y-axis shows the difference of the retention time between cytochrome *c* and *Pfu* Fd, with respect to the RT for cytochrome *c*. The experiments were carried out under the same conditions as in Fig.1A except for a stepwise increment of salt concentration.

Cyclic voltammetry. Direct electrochemistry was carried out with a mixture of *Pfu* rubredoxin (Rb) and *Pfu* Fd at pH 7.2, room temperature (approximately 20°C), and at 0 and 3 M NaCl concentration. Well defined, reversible and reproducible voltammograms were obtained at low potential scan rate of v = 10 mV/s for both *Pfu* Fd and *Pfu* Rb (Fig. 3). The reduction potential for the [4Fe-4S] cluster of the *Pfu* Fd was found to be –365 ± 5 mV, while for *Pfu* Rb it was ~0 mV, similar to the values reported earlier at low salt [16,17]. However, at high salt concentration the voltammogram for *Pfu* Fd broadened considerably, indicating a kinetically impaired heterogeneous electron transfer, while that of *Pfu* Rb was unchanged. Heterogeneous electron transfer rate constants were determined from the apparent cathodic-to-anodic peak potential separation at different potential scan rates, assuming a protein diffusion coefficient of $D = 1 \times 10^{-6}$ cm^2/s, according to the method of Nicholson [18]. From the estimated rate constants, k = 0.92 ± 0.1 cm/s at 0 M NaCl and k = 0.35 ± 0.1 cm/s at 3.25
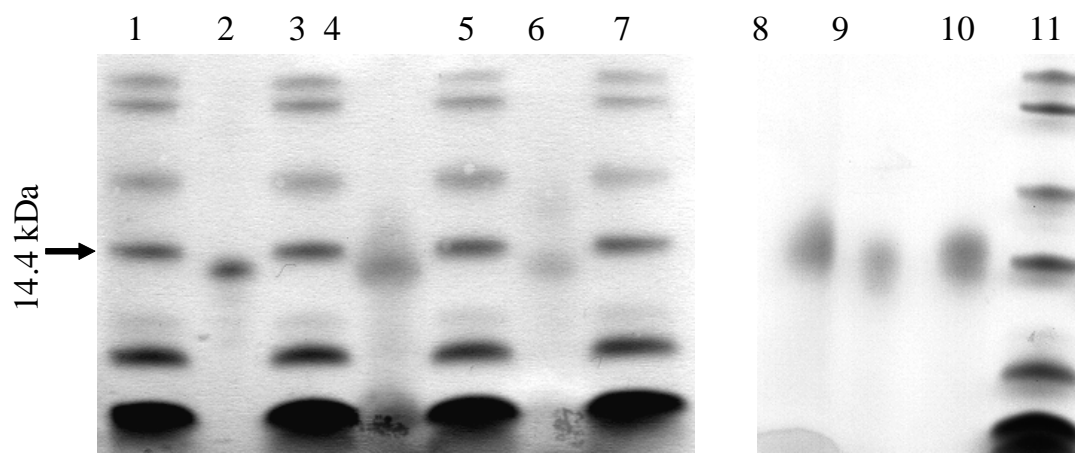
Fig. 2. SDS-PAGE of pure *Pfu* Fd at different conditions, a mixture of *Pfu* Fd plus *Pfu* rubredoxin, and cytchrome *c*. Conditions: Bis-Tris buffered 10% polyacrylamide gel, 50 mM MES running buffer with antioxidant, LDS sample buffer with 50 mM DTT. Lane- 1, 3, 5, 7, 11 - Mark 12 MW standard kit (Invitrogen); sizes are from top to bottom 36.5, 31, 21.5, 14.4, 6, 3.5 kDa; Lane 2- cytochrome *c*; Lane 4- mixture of *Pfu* Fd and *Pfu* rubredoxin; Lane 6- pure *Pfu* Fd; Lane 8- sterilized *Pfu* Fd in LDS sample buffer; Lane 9- sterilized *Pfu* Fd in LDS sample buffer + 100 mM DTT; Lane10- sterilized *Pfu* Fd in Laemmli sample buffer.
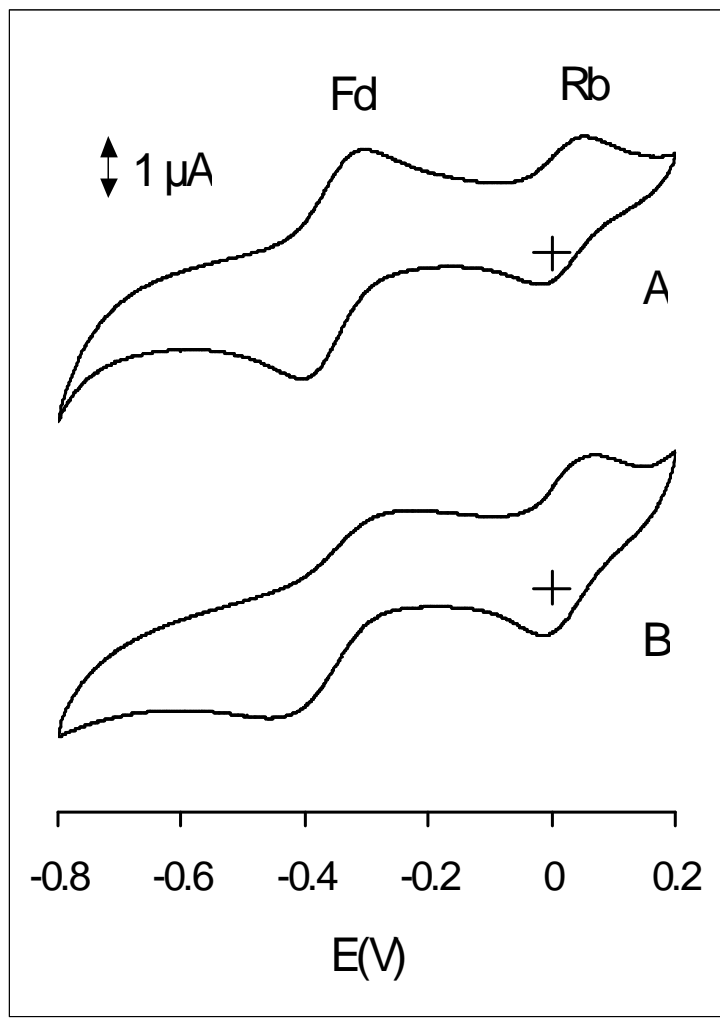
Fig. 3. Cyclic voltammograms of a mixture of *Pfu* Fd and *Pfu* rubredoxin. Experimental conditions: scan rate 10 mV/s, room temperature, hydrophobic carbon electrode surface. Trace A: voltammogram of the mixture in 25 mM MOPS (pH 7.2) with 7 mM neomycin; Trace B: voltammogram of the mixture in 3 M NaCl, 25 mM MOPS (pH 7.2), with 7 mM neomycin.

M NaCl, it was apparent that at high salt the electron transfer rate of *Pfu* Fd was impaired by 70%.

EPR spectroscopy. The EPR spectrum attributed to the [4Fe-4S]$^{1+}$ cubane cluster in reduced *Pfu* Fd is a mixture of a high-spin S = 3/2 signal and an unusually broad S = 1/2 signal [19].

This combination of spin states (sometimes called 'physical spin mixtures' to discriminate it from thermodynamic spin mixtures) is quite commonly found for $[4Fe-4S]^{1+}$ clusters
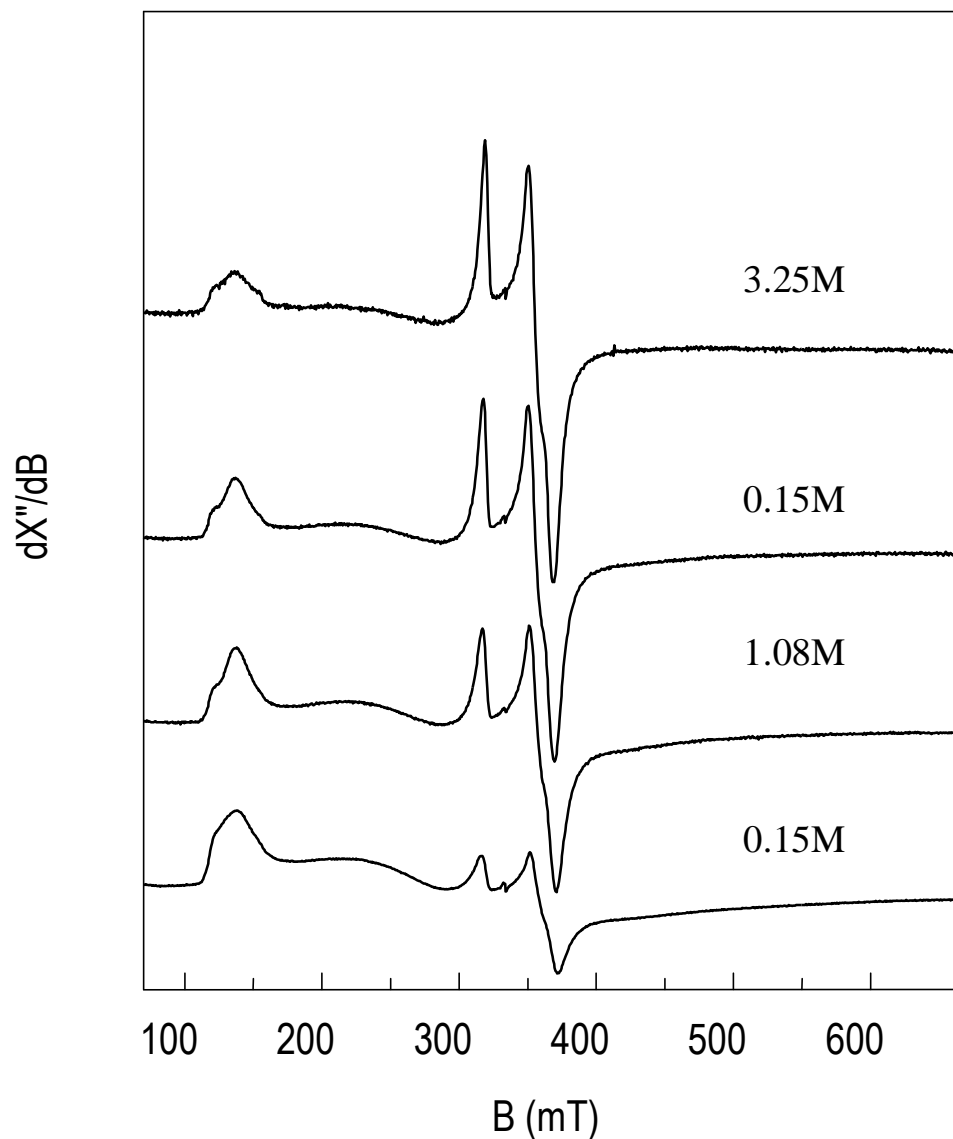
Fig. 4. EPR spectra of anaerobically purified *Pfu* Fd at different ionic strengths. The traces from bottom to top are at 0.15 M, 1.08 M, 2.14 M and 3.25 M NaCl, respectively. The spectral amplitudes have been normalized to that of the bottom trace (7.5 mg/ml protein). EPR conditions: microwave frequency, 9.42 GHz, microwave power, 8 mWatt; modulation frequency, 100 kHz; modulation amplitude, 5 mT; temperature, 8 K.

especially in proteins from anaerobic microorganisms, however, their nature is not understood [20]. In the Fe-protein of nitrogenase, which is paradigmatic for cubane physical spin mixtures, the ratio of S = 3/2 over S = 1/2 can be changed discretely with addition of ethylene glycol or urea [21].

In *Pfu* Fd we found that the S = 3/2 over S = 1/2 ratio can be changed monotonously as a function of the ionic strength (NaCl concentration) as illustrated in Fig. 4. With increasing ionic strength the relative amount of S = 1/2 signal increased. Spectral simulations (following [22]; not shown) indicated that the relative amount of S = 1/2 increased from approximately 2% at 0.15 M NaCl to approximately 20% at 3.25 mM NaCl. For obvious sensitivity reasons the EPR experiments were done with protein concentrations that were several orders-of-magnitude higher than, e.g., those of the gel filtration experiments, and so we would expect an increased tendency towards dimerization under otherwise equal conditions. We therefore tentatively identify the S = 3/2 to S = 1/2 shift with a shift in *Pfu* Fd protein dimer to monomer equilibrium.

Intracellular ionic strength. Frozen cells were thawed and suspended in de-ionized water to make the cells lysate. 5x and 10x diluted cell-lysates were used to estimate the conductivity. With a calibrated conductivity sensor the intracellular salt concentration was determined to be ~350 mM, which is similar to the ionic strength of the media used for cultivating the organism.

DISCUSSION

The 7.5 kDa ferredoxin from *P. furiosus* has been studied intensively for 13 years. The protein has posed significant problems apparently related to conformational inhomogeneities. A 3D structural determination has thus far not been achieved either with X-ray crystallography or with multi-dimensional NMR [8]. Part of these problems may well be

related to modification of the Fe-S cluster upon exposure to oxygen and / or to multiple forms of the putative Cys-Cys disulfide bridge (open / closed and cis / trans) [8]. However, we would like to put forth here the contention that a major determinant of the *Pfu*Fd inhomogeneity problem can be traced back to the question of its oligomeric state.

We find the early claim of Smith et al. that the MALDI-MS experiment indicated monomeric *Pfu*Fd, unconvincing, where they also noted that "proteins consisting of non-covalently bound subunits break during ion formation and only individual subunits are detected". Blamey et al. have more recently reported gel electrophoresis and gel filtration experiments on a ferredoxin from *Pyrococcus woesei*, which indicate a monomer/dimer equilibrium for that protein, however with a cross-over concentration between 0.2 – 0.5. M NaCl [23].

On the basis of gel filtration and gel electrophoresis experiments we propose that the *Pfu*Fd is a mixture of monomeric and dimeric protein, in an equilibrium that is far to the dimeric side under physiological ionic strength conditions. The EPR spectroscopic and electrochemical experiments suggest that there is a significant difference in electronic structure and reactivity between the dimeric and monomeric form, namely, the dimer is very predominantly S = 3/2 (at low temperature) and exhibits fast heterogeneous electron transfer, while the monomer is for a significant part S = 1/2 and is impaired in its electron transfer at least with activated-carbon electrodes. Based on the previous we hypothesize that *Pfu*Fd is a functional dimer *in vivo*, and we note, in addition that all (putative) natural electron-transfer partners of *Pfu*Fd are redox enzymes catalyzing two-electron reactions.

REFERENCES

[1]   Fiala, G., and Stetter, K.O. (1986) Arch. Microbiol. 145, 56-61.

[2]   Kengen, S.W.M., Stams, A.J.M. and de Vos, W.M. (1996) FEMS Microbiol. Rev. 18, 119-138.

[3]   Conover, R.C., Kowal, A. T., Fu, W., Park, J.B., Aono, S., Adams, M. W. W. and Johnson, M. K. (1990) J. Biol. Chem. 265, 8533-8541.

[4]   Grost, C.M., Zhou, Z.H., Ma, K., Teng, Q., Howard, J.B., Adams, M.W.W. and La Mar, G.N. (1995) Biochemistry 34 8788-879.

[5]   Silva, P.J., van den Ban, E.C.D., Wassink, H. Haaker, H., De Castro, B., Robb, F.T. and Hagen, W.R. (2000) Eur. J. Biochem. 267, 6541-6551.

[6]   Adams, M.W.W., Holden, J.F., Menon, A.L. Schut, G.J., Grunden, A.M., Hou, C., Hutchins, A.M., Jenney, Jr., F.E., Kim, C., Ma, K., Pan, G., Roy, R., Sapra, R., Story, S.V. and Verhagen, M.F.J.M (2001) J. Bacteriol. 183, 716-724.

[7]   Hu, Y., Faham, S., Roy, R., Adams, M.W.W. and Rees, D.C. (1999) J. Mol. Biol. 286, 899-914.

[8]   La Mar, G.N.. (2001) Methods Enzymol. 334, 351-389.

[9]   Aono, S., Bryant, F. O. and Adams, M. W. W. (1989) J. Bacteriol. 171, 3433-3439.

[10]   Smith, E.T., Cornett, D. S., Amster, I. J. and Adams, M. W. W. (1993) Anal. Biochem. 209, 379-380.

[11]   Arendsen, A.F., Veenhuizen, P.Th.M. and Hagen, W.R. (1995) FEBS Lett. 368, 117-121.

[12]   Kim, C.H., Brereton, P. S., Verhagen, M. F. J. M. and Adams, M. W. W. (2001) Methods Enzymol. 334, 30-40.

[13]   Laemmli, U.K. (1970) Nature 227, 680-685.

[14]   Hagen, W.R. (1989) Eur. J. Biochem. 182, 523-530.

[15]   Pierik, A.J. and Hagen, W.R., (1991) Eur. J. Biochem. 195, 505-516.

[16]   Hagedoorn, P. L., Driessen, M.C.P.F., van den Bosch, M., Landa , I. and Hagen, W.R. (1998) FEBS Letters 440, 311-314.

[17]   Brereton, P.S., Verhagen, M.F. J. M., Zhou, Z. H. and Adams, M. W. W. (1998) Biochemistry 37, 7351-7362.

[18]   Nicholson, R.S. (1965) Anal. Chem. 37, 135-1355.

[19]   Telser, J., Lee, H.I., Smith, E. T., Huang, H., Brereton, P.S., Adams, M. W. W., Conover, R. C., Johnson, M. K. and Hoffman, B. M. (1998) Appl. Magn. Reson. 14, 305-321.

[20]   Hagen, W.R. (1992) Adv. Inorg. Chem.38, 165-222.

[21]   Hagen, W.R., Eady, R.R., Dunham, W.R. and Haaker, H. (1985) FEBS Lett. 189, 250-254.

[22]   Hagen, W.R., Hearshen, D.O., Sands, R.H. and Dunham, W.R. (1985) J. Magn. Reson. 61 220-232.

[23]   Blamey, J.M., Chiong, M., López, C., and Smith, E.T. (2000) Anaerobe 6, 285-290.

Chapter three

Structural role of non cluster ligating cysteines in *Pyrococcus furiosus* ferredoxin: a study on cysteine to serine single and double mutants.

This chapter is to be submitted.

ABSTRACT

Pyrococcus furiosus ferredoxin (*Pfu*Fd) is a small electron-transfer protein with a single [4Fe-4S] cluster. In addition to the cluster coordinating cysteines, there are two cysteines present at position 21 and 48. They have previously been observed *in vitro* to form a disulfide bridge upon prolonged oxidation, and this has been suggested to be functional *in vivo* in redox chemistry and/or of protein stabilization. Here, a site directed mutagenesis approach altering either one or both of the residues reveals that the molecular structure and oligomeric organisation of wild type and two single mutants are unaltered. UV-Vis spectra, EPR spectra, and cluster reduction potentials of all the varieties are also similar. The double mutant C21S/C48S is of low stability even at ambient temperature. However, EPR and voltametric analysis show incorporation of the FeS cluster in this variety. All the mutants show decreased resistance to thermal denaturation with a stability order of C48S > C21S > C21S/C48S. In a reconstituted electron transfer chain with (croton)aldehyde oxidoreductase the mutant ferredoxins result in slightly decreased overall activity. On a time scale of < 30 minutes disulfide bond formation between these two cysteines is not observed. It is concluded that the disulfide bond has no physiological relevance, and that the non-oxidized cysteine 21 and cysteine 48 contribute individually to overall structure stabilization.

INTRODUCTION

Hyperthermophilic archaea and bacteria are organisms that grow optimally at ≥80ºC. Deep sea vents, submarine hydrothermal areas, continental solfataras, and geothermal power plants are the main sources for these organisms. The discovery of hyperthermophilic microorganisms raised interesting questions as to how these organisms are able to not only tolerate high temperature but also exploit the extreme condition(s) to their advantage. Therefore, detailed studies identifying the contributing factors towards the higher-temperature resistance are essential for a better understanding of protein structure and stability in these organisms, and for rationally engineering more thermostable enzymes [1]. A simple model involving a small protein may offer better opportunity for the study of the contributions of particular amino acid residues to the stability and function than a large and complex protein. For example, thermolabile glyceraldehyde-3-phosphate dehydrogenases from lobster muscle and its thermostable homologue from *Geobacillus stearothermophilus* have similar 3-D structures while the amino acid composition differs at 130 positions out of 330 positions [2]. Apparently, it is difficult to pin down the role of a single or multiple amino acids in attaining the thermostability to this protein. The small electron transfer protein ferredoxin could be a more suitable target to analyze and depict the contributing factors towards the thermostability of the protein. The single cluster type monomeric form of ferredoxin is a small protein of 60 to 70 amino acids. This protein can easily be obtained as ferredoxins are widespread in the three domains of life. Otaka and Ooi [3] and Wächtershauser [4] even considered ferredoxin as the first bioinorganic catalyst. Indeed, ferredoxins from different domains of life [5-10] have been used as a model system to investigate the structural contribution towards the stability of thermophilic proteins. Therefore, *Pyrococcus furiosus* ferredoxin (*Pfu*Fd) may offer a suitable system not only to understand the mechanism of protein thermostability but also to elicit ancestral ways of protein stabilization. *P. furiosus* ferredoxin is a small electron-

transfer protein of 66 amino acids. It is one of the most thermostable ferredoxins, exhibiting minimal degradation for several days at 95ºC (this work and [11]). It contains a cubane type [4Fe-4S] cluster bound by a $CxxDxxCx_nCP$ sequence motif (similar to the $CxxCxxCx_nCP$ consensus). In addition to the cluster-coordinating cysteines, two surface cysteines are present at position 21 and 48. Both the solution NMR molecular model for the oxidized [4Fe-4S] form [12] and the X-ray crystallographic structure of the aerobic [3Fe-4S] form of the protein [13] demonstrated the presence of an intra-molecular disulfide bond between the two non-ligand cysteines. Extensive studies have been reported on the native, recombinant wild type and on several mutant varieties of *Pfu*Fd (mainly altering the cluster coordinating amino acids) detailing the redox states under different conditions, and their structural and functional relevance [11, 14, 16, 17, 18]. *In vitro* disulfide bond formation was also shown, and a possible role of the disulfide bridge as a redox centre was discussed [15]. However, a physiological relevance of the formation of the disulfide bridge between Cys21 and Cys48 after long (hours) exposure to air is unclear in a strict anaerobic organism. Based on a recent database analysis Beeby *et al*. [19] suggested a stabilizing role of a putative disulfide bond in some intracellular proteins in a subset of (hyper)thermophilic organisms, including *P. furiosus,* whose genomes exhibit the highest occurrence of predicted disulfide bonds and contain a specific gene encoding a putative protein disulfide oxidoreductase(PDO). PDO catalyses the formation and breakdown of disulfide bonds in the cytosolic reducing environment, however, *in vivo* redox partners for this enzyme remain elusive. Mayer *et al* reported a decrease in the T_m (by 8ºC) and in the half life (20 fold lower) of mutants varieties (in which cysteine residues involved in disulfide bridge formation were deleted) of a plant-type [2Fe-2S] ferredoxin from an aerobic extremophilic organism, *Aquifex aeolicus* [20]. On the other hand the crystal structure of another plant type [2Fe-2S] ferredoxin from *Mastigoclaudus laminosus* [5] reveals two other structural determinants conferring thermal

stability to the protein: increased salt bridges and a flexible loop that increases the hydrophobic accessible surface area. Disulfide bond formation and its possible role towards the stability of ferredoxin from *Thermatoga maritima,* a thermophilic homologue of *Pfu*Fd, has been described by Sticht *et al* [21]. Later, the contribution of electrostatic interaction, compactness, and the quarternary structure of the same protein towards it stability has been demonstrated by Robinson-Rechavi *et al* [7]. A mesophilic counterpart of *Pfu*Fd, *Desulfovibrio gigas* ferredoxin II also contains additional cysteines, at positions 18 and 42, and was shown to form a disulfide bond in vitro [22]. On the other hand, a thermophilic analogue of *Pfu*Fd, *Bacillus thermoproteolyticus* ferredoxin has only four cysteine residues, all of which are involved in the cluster formation. The thermal stability of this particular protein is not much different than that of its homologues. We therefore decided to explore the possible structure-functional role of the Cys 21 and Cys 48 in *Pfu*Fd.

Here we report the high yield production of recombinant wild type *Pfu*Fd and its C21S and C48S single and double mutant varieties. The purified wild type and mutant proteins are characterised by SDS-PAGE electrophoresis, size exclusion chromatography, UV-visible spectroscopy, cyclic voltammetry and EPR. The mutational effects are studied as functions of thermal denaturation, oligomeric nature and catalytic activity.

MATERIALS AND METHODS

Chemicals, enzymes, vectors and sequence. Oligonucleotides were bought from Thermo Electron Corporation (Germany). *Pfx* polymerase and pENTR Directional TOPO® cloning kit and NuPage (SDS) gels were obtained from Invitrogen. Restriction enzymes and T_4 ligase were purchased from New England Biolabs. Culture media were from Becton, Dickinson and Company (Le Pont de Claix, France). Polymerase chain reactions (PCR) were run on a Biometra T Gradient machine. Plasmid DNA was purified with the Mini prep Kit (Qiagen).

DNA sequencing was performed by Base Clear (Leiden, The Netherlands). Expression vector pET24d was bought from Novogen, while the *E. coli* BL21 (DE3) cells and isopropyl β-D-thiogalactopyranoside (IPTG) were purchased from Stratagene (La Jolla, CA). Tris[2-carboxyethyl] phosphine (TCEP) was bought from Pierce and dithiothreitol (DTT) was from Sigma Aldrich. All other chemicals were bought from Sigma Aldrich.

Cloning and site directed mutagenesis. The putative ferredoxin gene from the *Pfu* cells was amplified by using oligonucleotides 5`-CA<u>CCATGG</u>CGTGGAAGGTTTCTG-3` as the forward primer (*NcoI* site underlined) and 5`-CCAAAGTTC<u>AAGCTT</u>TCAAGCCTCCTC-3` (*HindIII* site underlined) as the reverse primer. After an initial denaturation step of 10 minutes (because of the high GC content of *Pfu* chromosomal DNA) at 94ºC, the reaction mix was incubated for amplification using the following steps: 1 min at 94ºC, 45 sec at 40ºC and 1.5 min at 72ºC for 25 cycles with a final extension step of 10 min at 72ºC. A high fidelity *Pfx* polymerase was used to avoid unexpected mutation(s), which may occur in the course of PCR experiments. Oligonucleotides 5`- GCA<u>AGC</u>CTCAGCCCAGACGTC-3`, as forward and 5`-GTCTGGGCTGAG<u>GCT</u>TGC-3`, as reverse primer were used for the site directed mutagenesis at position 21 (C21S).

A second set of primers 5`-TACAAC<u>AGC</u>GCTAAGGAAGCTATG-3`and 5`-AGCTTCCTTAGC<u>GCT</u>GTTGT-3` was respectively used as forward and reverse primer for introducing mutation at position 48 (C48S). These two sets of primers were further used to raise the double mutant C21S/C48S in sequential PCR steps. Both the single mutants and the double mutant were raised using a sequence overlapping extension (SOE)-PCR protocol. All the PCR reactions gave a band of the expected size (~220 bp) as the sole end product.

The amplified variants of the ferredoxin gene were then inserted into the pENTR™/SD/D-TOPO vector between the *NcoI* and *HindIII* sites after subsequent restriction digestion of the inserts and the vector. The additional CACC sequence at the 5` end of the inserts and the

vector facilitated the unidirectional insertion of the ferredoxin genes into the vector, thereby enhancing cloning efficiency. The ligation mixtures of the inserts and the vector were then used to transform competent *E. coli* DH5α cells for further amplification. The chimeric vector was then isolated from the cells and the fidelity of the clone was checked by sequencing. The ferredoxin gene was then separated by *NcoI* and *HindIII* restriction digestion and re-cloned into expression vector pET24d (+). The resulting clone was then transformed into competent BL21-(DE3) cells.

Protein production and purification. A single colony of the recombinant *E. coli* strain was inoculated in Luria Bertani medium supplemented with 20 µg ml^{-1} of kanamycin and cultivated overnight aerobically at 310 K and 200 rev min^{-1}. This pre-culture was transformed in Terrific Broth medium [24] in a 1:20 ratio and grown for 2 h (until it reaches an OD600 value of 0.5 or higher) and then induced with 0.25 mM IPTG. Cells were then harvested by centrifugation after an additional 20 h of growth and stored at -80ºC or used immediately. The resultant *E. coli* cell pellet was thawed on ice and re-suspended in lysis buffer (50 mM Tris-HCl, pH 8, 100 mM NaCl, 2 mM sodium dithionite and 2 mM DTT, 10 mM phenylmethylsulfonyl fluoride (PMSF)) at room temperature and at 3 ml of buffer per gram of cell weight. The cells in suspension were then disrupted using a cell disruption system (Constant System) in single shoot mode using 1 kBar pressure. The cell extract was collected in a bottle, and RNase (5 µg/g of cells) and DNase (10 µg/g of cells) were added. The extract was degassed and incubated first at room temperature for 30 min and then at 90ºC for 60 min to denature the *E. coli* proteins. After cooling at 4°C at least for an hour cell-free extract was obtained by centrifugation (45 min at 48,000 x g and 4°C), the supernatant was either immediately used for column chromatography or stored at -80°C. The rest of the purification was similar to the protocol described previously [11]. Though the whole purification was carried out under strict anaerobic condition, some [3Fe-4S] form of ferredoxin was formed

presumably due to oxygen leakage. The [4Fe-4S] form of ferredoxin was purified from the [3Fe-4S] form using the protocol stated in reference [31], but using a POROS HQ/L column (Amersham Bioscience) instead of a MONO Q column. Purification of native *Pfu*Fd, SDS gel analysis, and gel filtration experiments were carried out as previously stated [30], except that tris(2-carboxyethyl) phosphine hydrochloride (TCEP) was used as the reductant instead of sodium dithionite (Na-DT) in addition to DTT.

Determination of free SH group(s). Quantification of free thiol content of the native, wild type and mutant varieties was carried out using Molecular Probes' Thiol and Sulphide quantification kit (Invitrogen) following the protocol stated by Sing *et al* [23]. Freshly prepared protein samples were separated from the reductants (TCEP and Na-DT) by gel filtration under anaerobic condition. One set of the reductant-free protein samples was then air oxidized for 30 minutes.

Thermal denaturation. Ferredoxin samples of sub-millimolar concentration were prepared in crimp- neck anaerobic bottles and incubated at 95ºC under a slight overpressure of argon. Thermally induced denaturation of ferredoxin varieties was monitored by visible absorption at 390 nm at various time intervals. UV/vis spectra were recorded with an HP8453 diode-array spectrophotometer.

Other methods. Concentration of the purified Fds was estimated from the absorbance at 390 nm, using an extinction coefficient of 17,000 $M^{-1}cm^{-1}$ and was cross-checked using the Bicinchoninc acid (BCA) method (Pierce). Cyclic voltammetry experiments were carried out as described earlier [24]. EPR measurements were carried out as described earlier [25]. Activity assay was performed as stated elsewhere [26].

RESULTS

Site directed mutagenesis. The production of the recombinant wild type ferredoxin and some of its mutant varieties has been reported previously, [27, 28] using different expression systems and host cells. Zhou *et al* demonstrated an improvement of the yield of the target protein as an effect of long induction time of cells with sub-mM IPTG concentration [28]. We have re-investigated the improvement of the yield using a different expression vector, host system and also a rich medium. We also find that long induction time of cells with similar concentration of IPTG, in combination with the aforementioned factors significantly improved yield of the target protein in case of both the wild type and single mutant varieties. Except for the case of double mutant, circa 6 to 8 mg of ferredoxin protein was obtained form a liter of overnight induced culture, with only trace amount of apoprotein produced. A higher amount of the apoprotein was obtained in the case of C21S compared to the wild type and the C48S mutant, which indicates a lower stability of the holoprotein for this mutant variety. The iron sulfur cluster in the wild type and the C21S and C48S mutants was intact and was obtained mainly in the [4Fe-4S] form when the purification was done anaerobically. The initial cell disruption and centrifugation steps were carried out under aerobic conditions which gave rise to a minor portion of the protein with the [3Fe-4S] form. The [4Fe-4S] form of the protein was then separated from the [3Fe-4S] form using a POROS HQ/L column. The addition of the reductant TCEP resulted in protein with free thiol groups, which can be directly chemisorbed on a polycrystalline gold electrode via gold-sulfur bond formation [29]. The double mutant was found to be relatively unstable even at ambient temperature. It readily looses the cluster and forms aggregates.

UV-visible spectroscopy. The UV-visible spectra of the reduced forms of the ferredoxin varieties are shown in Fig.1. The absorption ratios and the molar extinction coefficients of all four ferredoxins are similar. The ratios of A_{390} to A_{280} for the native, recombinant wild type

and C48S mutant were 0.579, 0.570 and 0.591, respectively. In case of the mutant C21S, this ratio was somewhat lower, 0.478. We attribute this to the loss of the cluster in a portion of this variant to decreased stability of the protein. In general, the similarity of the spectra suggests that mutation of either one of the additional cysteines is not sensed by the oxidized [4Fe-4S] cluster. The high amount of apoprotein in the preparation of the double mutant made it unsuitable for comparison with the UV-vis spectra of the other varieties.
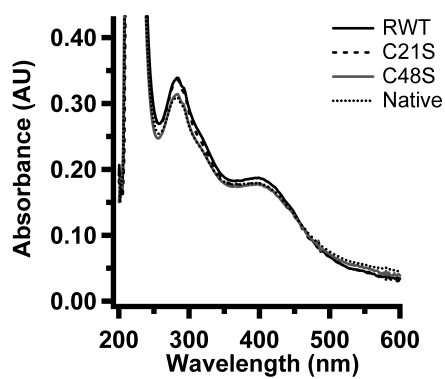
Fig. 1: UV-visible spectra of anaerobically purified variants of *Pfu*Fd. The protein samples were prepared in 50 mM Tris-HCl, pH 8.0, and 2 mM TCEP and were 12 µM of RWT and C21S, and 10.5 µM of native and C48S. The spectra were recorded at room temperature (25ºC).

Determination of free SH group. Two sets of samples have been used in thiol determination experiments. The first set was prepared by removing the reductants from the freshly prepared samples by gel filtration under anaerobic condition. A second set was prepared by exposing part of the reductant-free samples to air for 30 minutes. Both the anaerobic and aerobic samples were then allowed to react with the disulfide inhibited derivative of papain, resulting in stoichiometric amount of active papain-enzyme. The activated enzyme reacted with the chromogenic substrate, N-benzoyl-L-arginine-p-nitroanilide (L-BAPNA). The increase of the absorbance was then recorded at 410 nm. The absorption increase corresponded to ca.

2.17±0.10 mole of free thiol per mole of wild type protein and ca. 1.25±0.10 moles of free thiol per mole of mutants irrespective of the history of the samples. Thiols in a disulfide bond are not a substrate for the inactivated papain enzyme. Therefore, detection of the free thiols rules out the occurrence of inter (mutants) or intra-protein (native and wild type) disulfide bridge, either in the anaerobically isolated form or in the air exposed form of the ferredoxins.
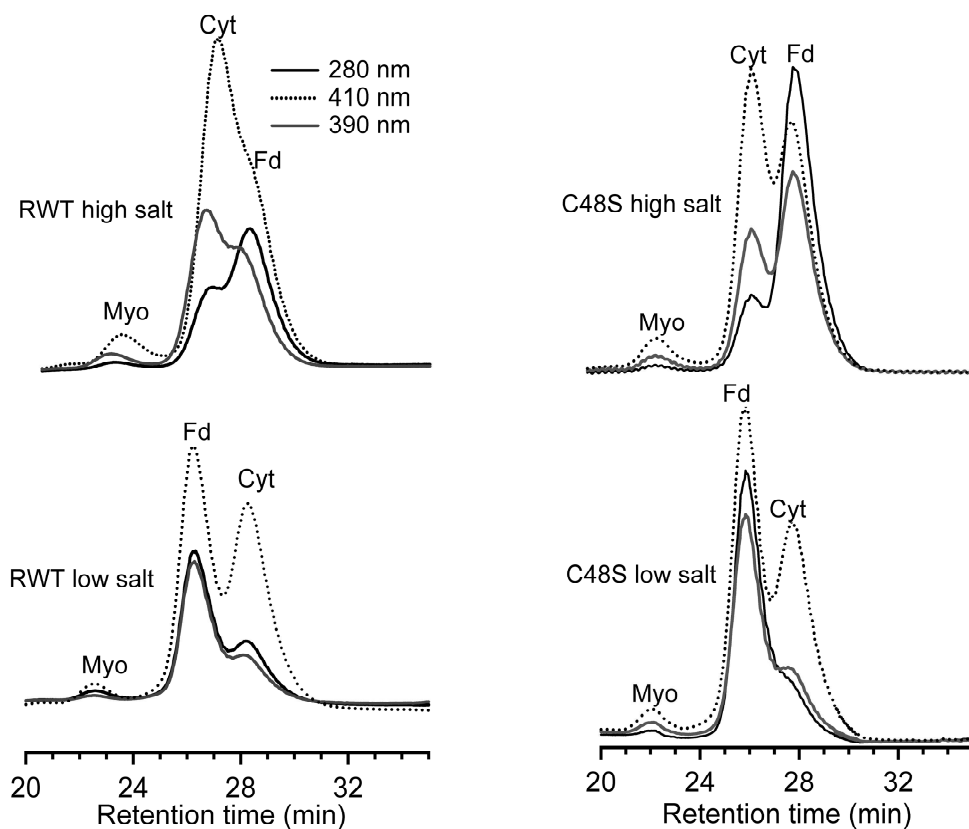
Fig. 2. Gel filtration of anaerobically purified Fds, horse heart cytochrome c, and horse myoglobin on a Superdex-75 column (10 mm x 30 cm). The buffer was 50 mM Tris-HCl (pH 7.4), and 2 mM TCEP. The experiment was carried out with a flow rate of 0.5 ml/min, at room temperature (~25°C) and anaerobic condition. Amounts of proteins loaded were Pfu Fd ~80 μg, cytochrome c ~40 μg and myoglobin ~30 μg.

Size exclusion chromatography. The molecular size of the recombinant ferredoxins and the native ferredoxin was studied by a chromatographic method. Two different salt

concentrations, 0.15 M (below the physiological ionic strength of ca. 0.5 M) and 3.5 M NaCl

(above the physiological condition) were chosen to carry out size exclusion chromatography
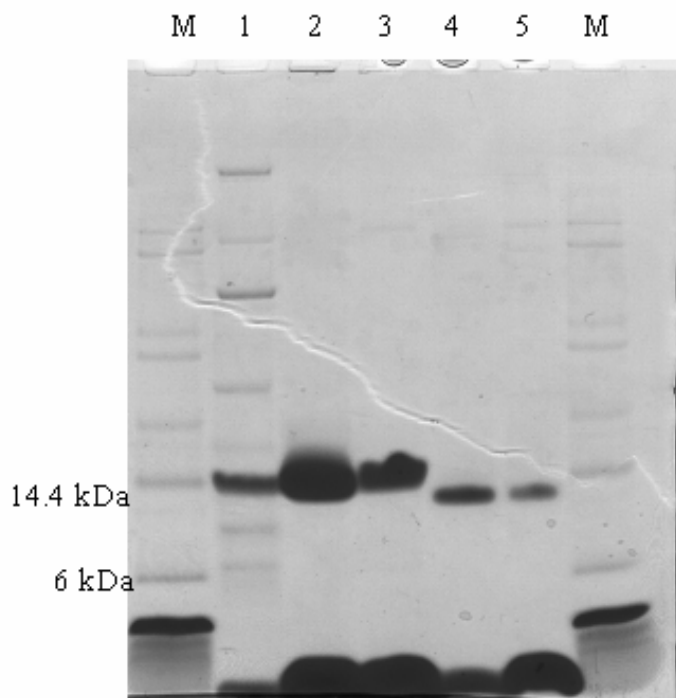
Fig. 3. SDS-PAGE of pure ferredoxins. Conditions: Bis-Tris buffered 10% polyacrylamide gel, 50 mM MES

running buffer with antioxidant, Lithium dodecyl sulfate sample buffer with 50 mM DTT. Lanes- M, Mark 12

Mw standards (Invitrogen); sizes are from top to bottom 66, 55, 36.5, 31, 21.5, 14.4, 6, 3.5 kDa; Lane 1-

C21S/48S Fd; Lane 2 - C48S Fd; Lane 3- C21S Fd; Lane 4- RWT Fd and Lane-5- native Fd.

experiments. At 0.15 M salt concentration the retention time for both the recombinant wild

type (RWT) and the mutants C21S and C48S was longer than that of myoglobin (Mw = 17

kDa) and shorter than that of cytochrome *c* (Mw = 13.7 kDa) (Fig. 2, lower panels). At an

increased salt concentration of 3.5 M NaCl all the recombinant Fds (Fig. 2, upper panels)

eluted later than cytochrome *c* indicating a similar shift from dimer to monomer as was

observed in case of the native ferredoxin [30]. A similar pattern of elution was obtained (data

not shown) in a control experiment using native *Pfu*Fd. Experiments were also carried out in

the presence and in the absence of 2 mM DTT plus 2 mM TECP. No difference was observed between the two conditions, which rules out the occurrence of dimers held by disulfide bridge. Therefore, the possibility of inter-protein disulfide bond formation, in particular in case of the mutant Fds an also be excluded. Due to its unstable nature, the double mutant was not subjected to SH group determination nor to the gel filtration experiments.
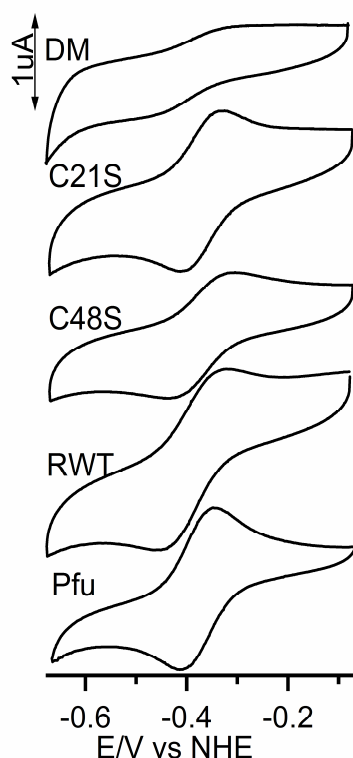
Fig. 4. Cyclic voltammograms of different variants of *Pfu*Fd. Experimental conditions: scan rate 20 mV/s, at room temperature, hydrophobic carbon electrode surface, in 25 mM MOPS (pH 7.2) with 7 mM neomycin and 1 mM TCEP.

Gel electrophoresis. *Pfu*Fd and the recombinant Fds as isolated appeared as a 12-13 kDa protein in denaturing polyacrylamide gel electrophoresis (Fig. 3). Heating at 95°C for one hour is one of the steps in the purification protocol of the recombinant Fds. As previously

reported for the native *Pfu*Fd [30] no change was observed in the molecular oligomeric state of the purified recombinant ferredoxins. We also did not observe a band corresponding to the monomeric weight of the ferredoxin neither in case of RWT nor for the mutants. The double mutant shows weak bonds corresponding to higher molecular weights (Fig. 3) which we attribute to oligomerization of the unfolded peptide. Furthermore, gel electrophoresis experiments were carried out under denaturing condition in the presence of 100 mM DTT plus 2 mM TCEP and an additional anti-oxidant (provided by the manufacturer of the gel, NuPage, Invitrogen). Therefore, the formation of dimer through inter-protein disulfide bond can be excluded. This confirms that the physiological oligomeric form of the protein is formed by other mechanisms, e.g., by ionic interactions between the monomeric Fds, as previously reported by us [30] and also as suggested recently from the crystal structure of the [3Fe-4S] form of recombinant ferredoxin [13].
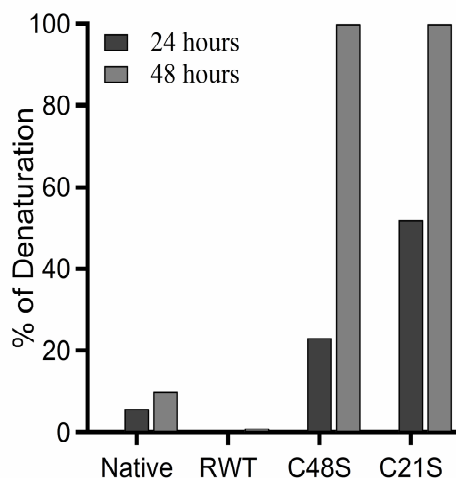

Fig. 5. Comparison of the extents of thermal denaturation of native, WT and mutants Fds as function of incubation time.Protein samples were prepared in 50 mM Tris-HCl, pH 8.0, 100 mM NaCl, 2 mM TCEP, 2 mM sodium dithionite and incubated anaerobically at 95ºC.

Cyclic voltammetry. Native, recombinant wild type, and the mutant varieties of *Pfu*Fd were subjected to direct electrochemistry on activated glassy carbon at pH 7.2, at room temperature (approximately 22°C), and with 150 mM NaCl. Well defined, reversible and reproducible voltammograms were obtained at a low potential scan rate of v = 20 mV/s for all the ferredoxin varieties (Fig. 4). The derived midpoint potentials and peak separations of all five variants of *Pfu*Fd on glassy carbon in the presence of neomycin as facilitator have been collected in Table 1. Native Fd gives a reversible response (61 mV peak separation), with a midpoint potential of -351 mV, which is close to the value reported previously [30, 31]. The midpoint potentials of the RWT ferredoxin and the mutants are similar to that of the native protein. The electron transfer kinetics of the C48S and C21S mutants and the double mutant are reproducibly slower compared to native ferredoxin. The double mutant is very unstable which is reflected in a rapidly decreasing peak intensity with time. Moreover, the peak shape is somewhat sigmoidal, which suggests partial blocking of the electrode with denatured protein, leading to a radial diffusion profile. [32].

Thermal denaturation. Native, wild type and mutant varieties of *Pfu*Fd were subjected to thermal denaturation at 95°C for 48 hours. The unfolding of the Fd varieties were monitored by absorption spectroscopy at 390 nm. The extents of the thermal denaturation upon anaerobic incubation are shown in Figure 5. Loss of absorbance at 390 nm which is caused by the decomposition of the Fe-S cluster was taken as the measure of denaturation. Native ferredoxin showed up to circa 10% denaturation after 48 hours of incubation while the recombinant wild type remained unaffected. We have no explanation for this difference. Both the mutant varieties were denatured totally after 48 hours of incubation, and C21S denatured more readily, due to the lower resistance of this mutant variety to high temperature. Upon decomposition of both mutants, black precipitations were observed indicating that none of the denaturations was reversible. Hence no refolding has been attempted.

Table 1. Redox potentials and cathodic to anodic peak separations of different ferredoxin forms obtained from cyclic voltammetric experiments.

Ferredoxin type	E_m (mV)	ΔE_p (mV)
Native	-351	61
RWT	-358	62
C48S	-352	100
C21S	-359	113
DM	-398	153

Experimental conditions: 50 µM protein and 7 mM neomycin in 25 mM MOPS, pH 7.4 on glassy carbon, scan rate 20 mV/s, *T*=295 K

EPR spectroscopy. Concentrated samples (circa 1 mM) of wild type recombinant protein and mutants in 150 mM NaCl were anaerobically reduced with sodium dithionite, and were studied with EPR spectroscopy (Fig. 6). The spectrum of recombinant wild type protein is identical to that previously reported for native *Pfu*Fd in 150 mM NaCl [30]; it consists of a high-spin, S = 3/2 spectrum whose characteristics are a double absorption peak around circa 1500 Gauss and a very broad derivative feature around circa 2500 Gauss, and a low-spin, S = 1/2 spectrum around the free electron value with unusually broad and asymmetric peaks. Both spectra have been assigned to the single $[4Fe-4S]^{1+}$ cubane in a physical mixture of spin states. It has previously been found for the native *Pfu*Fd that the high-spin over low-spin concentration ratio (i.e. the intensity ratio of the S = 3/2 and S = 1/2 spectra) is a function of ionic strength with relatively more S = 3/2 form at higher NaCl concentration, and a possible correlation with the extent of protein dimer dissociation has been suggested [30]. The spectra

from the single and double mutants also exhibit the S = 3/2 and S = 1/2 spectra, and no other new signals were found not only in Fig. 6 but also over a wide range of microwave power values and temperature values (not shown). The only difference with the spectra from native
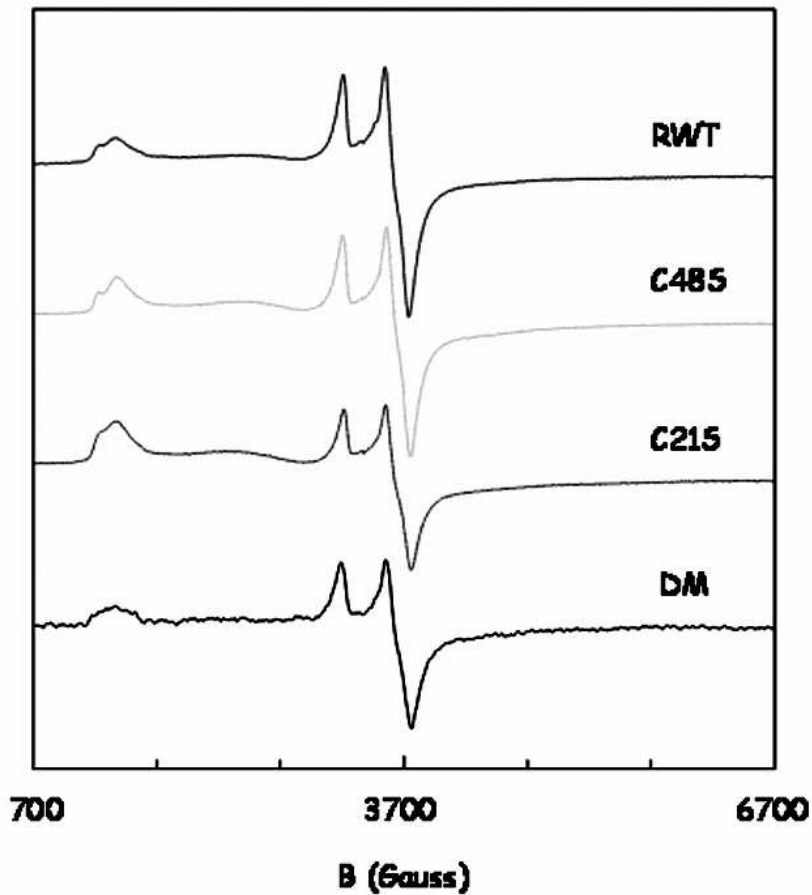
Fig. 6. EPR spectra of wild type and mutant varieties of *Pfu*Fd purified under anaerobic and reducing condition. Traces from top to bottom are RWT, C48S, C21S and C21S/C48S mutants, respectively. Protein concentrations for all the traces are circa 1 mM in 50 mM Tris-HCl, pH 8, 150 mM NaCl, 2 mM DTT and 2 mM Na-DT. EPR conditions: Microwave frequency, 9.44 GHz, microwave power, 80 mW; modulation frequency, 100 kHz, modulation amplitude, 80 Gauss, temperature, 11 K. For the double mutant the microwave power was 126 mW, the temperature was 9 K, and the electronic amplification was increased.

or wild type recombinant protein is an apparent increase in the S = 3/2 to S = 1/2 ratio, which is especially pronounced for the C21S mutant, although both single mutants were found to be essentially completely dimerized at an ionic strength of 150 mM NaCl (see above). The

spectrum of the double mutant has a poorer signal-to-noise ratio due to instability of this protein; the spectrum appears to be slightly broadened compared to the spectra of the other varieties. All in all the EPR spectral changes upon mutation of C21 and/or C48 are very subtle: the two surface cysteines appear to be only remote contributors to the structure of the reduced cubane.

Functional studies. The role of *Pfu*Fd as electron acceptor in the oxidation of various aliphatic aldehydes including crotonaldehyde by aldehyde oxidoreductase (AOR) from *Pfu* and from *Pyrobaculum aerophilum* has been demonstrated earlier [26, 33]. Here, all the four varieties of ferredoxin were subjected to functional analysis using *Pfu*AOR as the redox enzyme and crotonaldehdye as the electron donor. Analysis of data obtained by using 200 µM ferrdoxin, i.e., at the K_M value of the enzyme for ferredoxin [26], 200 µM crotonaldehyde and at 90ºC gave apparent rates of 72, 60, 51 and 49 units/mg of AOR respectively for *Pfu*Fd, RWT, C48S and C21S.

DISCUSSION

Thermal stability studies of proteins. With the advancement of bioinformatics recent years have witnessed an explosion of sequence and structural information for thermophilic and hyperthermophilic proteins. The availability of the complete genome sequences for many hyperthermophilic archaea facilitated studies elucidating the unique features of hyperthermophilic proteins and the similarities or dissimilarities with their mesophilic homologues. The very first high-resolution crystal structure of a thermophilic protein, thermolysin by Mathews et al [34], motivated continued efforts to understand the mechanism(s) of adaptation of these proteins at elevated temperature [35-38]. The stereochemical basis of the thermostability of ferredoxins and hemoglobin A2 has been described by Perutz and Raidt [2] 30 years ago. Among the range of factors hypothesized to

be involved in the thermal stability of hyperthermophilic proteins are cumulative or individual contribution of electrostatic interactions, compactness and quarternary structure [7], greater hydrophobicity, better atom packing, deletion or shortening of loops [39], smaller and fewer cavities, an increased surface area buried upon oligomerization [40, 41], residue substitution within and outside the secondary structures [42, 39], increased occurrence of proline residues in loops [47,48], decreased occurrence of thermolabile residues [39, 46], increased helical content, increased polar surface area, more hydrogen bonds, and increased salt bridge formation [43, 44, 46, 45]. It must be emphasized that until now studies predicting the factors contributing to the thermal stability of proteins all have limitations in some ways. Poor understanding of the relation between the protein sequence and structure, analysis of small sets of samples, bundling up proteins from different domains of life to increase the size of the sample data set, comparison of predicted and resolved structures of proteins, are a few of the notable limiting factors. Therefore, at this time no general rule can be drawn yet as to how the (hyper)thermophilic proteins attain their stability. In-depth analysis of specific protein families would perhaps provide better insight into mechanisms governing protein stability.

Site directed mutagenesis in combination with structure-functional analysis is a powerful technique to investigate the role of particular amino acid residue in rendering the stability or function of a protein. In the current study on *Pfu*Fd we have used this approach to elucidate the specific contribution of the cluster non-ligating cysteines at position 21 and 48. Alteration of either of these two residues at one time has not given rise to an altered quaternary structure. The UV-vis spectra of all varieties confirm the formation of the Fe-S cluster in the protein. The electrochemical data and EPR analysis further attest to the intact nature of the [4Fe-4S] cluster. These findings rule out any significant contribution of these residues in the formation of the cluster and also in the dimerization of the protein.

Disulfide bond formation is not physiological. Several studies involving *Pfu*Fd and some of its homologues from hyperthermophiles and mesophiles have suggested a disulfide bond formation between two cysteines under prolonged aerobic condition [11, 21, 6]. Sham *et al* [12] proposed a solution NMR molecular model for *Pfu*Fd in which the [4Fe-4S] cluster is oxidized and a disulfide bond is formed upon exposure of the protein to 100% oxygen for 24 hours. The authors proposed that the ease of reducibility of the disulfide bond suggests it to function as a redox active group of physiological relevance. From the crystal structure of the air oxidized [3Fe-4S] form of *Pfu*Fd, Nielsen et al [13] also described the existence of a disulfide bond with both left and right handed conformations. However, both procedures require exposure of the protein to air for days which is not of physiological relevance for the host organism. The existence of a disulfide bond between two additional cysteines at position 18 and 42 has also been described for *D.gigas* Ferredoxin II from a crystal obtained under aerobic condition [6]. In a latter study the crystal structure of *Dg*FdII obtained under anaerobic condition showed significant structural variations and opening up of the disulfide bond [49].

Purification of the *Pfu*Fd under anaerobic and reducing conditions resulted in a ferredoxin preparation with intact [4Fe-4S] cluster and with no disulfide bond (this work and [11]). In our hands exposure of the protein to air for thirty minutes in the absence of chemical reductant has not resulted in the formation of a disulfide bond. Furthermore, ferredoxins with only four cluster coordinating cysteines from both mesophilic (*D. africanus* FdI) and thermophilic (*B. thermoproteolyticus* Fd) sources exhibit similar stability and functionality under comparable conditions.

Cysteine 21 contributes to overall protein stability. From the analysis of the crystal structure in which C21 is bridged to C48 it is evident that the C21 is well buried in the structure while C48 is surface exposed (cf supplementary information). Hence, any possible disulfide bond

between these two residues will be at least partly surface exposed and thus would be accessible for reduction in the reducing cytosolic environment. Alteration of C21 and, to a lesser extent, of C48 decreased the stability of the protein. We propose that it is the buried, momomeric C21, not the disulfide bond, which contributes significantly toward the thermostability of the protein.

Concluding remarks. Based on experimental data and comparison to studies on other ferredoxins it can be concluded that the additional cysteines at position 21 and 48 of *P. furiosus* ferredoxin are not involved in disulfide bond formation under physiological condition nor do they participate in the dimerization of the protein. Apart from a diffusive but significant contribution towards the (thermo)stability of the protein, no clear role of these residues has been identified. Perhaps these two cysteines are remnants in the course of evolution of single cluster ferredoxins from two cluster ferredoxins.

REFERENCES

1. Kumar S an Nussinov R (2001) Cell Mol. Life Sci. 58, 1216–1233

2. Perutz, M. and Raidt, H. (1975) Nature. 255, 256–259

3. Otaka E and Ooi T (1987) J. Mol. Evol. 26, 257–267

4. Wächtershauser G. (1992) Prog. Biophys. Mol. Biol. 58, 85–201

5. Alexander F, Tsafi D, Itzhak O, Rachel N, and Oded L (2005) J. Mol. Biol. 350, 599–608

6. Kissinger CR, Sieker LC, Adman ET and Jensen LH (1991) J. Mol. Biol. 219, 693-715

7. Robinson-Rechavi M, Alibes A, and Godzik A, (2006) J. Mol. Biol. 356, 547–557

8. Moczygemba C, Guidry J, Jones KL, Gomes CM, Teixeira M and Wittung-Stafshede P (2001) Protein Sci. 10, 1539-1548

9. Fukuyama K, Matsubara H, Tsukihara T and Katsube Y (1989) J. Mol. Biol. 210, 383-398

10. Higgins CL, Meyer J and Wittung-Stafshede P (2002) Biochimica Biophysica Acta 1599, 82-89

11. Kim CH, Brereton PS, Verhagen MFJM and Adams MWW (2001) 334, 30-40

12. Sham S, Luigi C, Wang PL, Bren K, Haarklau H, Brereton PS, Adams MWW and La Mar GN (2002) Biochemistry 41, 12498-12508

13. Nielsen MS, Harris P, Ooi BL and Christensen HEM Biochemistry 43, 5188-5194 , 2004

14. Gorst CM, Yeh YH, Teng Q, Calzolai L, Zhou ZH, Adams MWW and La Mar G (1995) Biochemistry 34, 600-611

15. Gorst CM, Zhou ZH, Ma K, Teng Q, Howard JB, Adams MWW and La Mar G (1995) Biochemistry 34, 8788-8795

16. Telser J, Davydov R, Kim C-H, Adams MWW and Hoffman BM (1999) Inorg. Chem. 38, 3550-3553

17. Brereton PS, Verhagen FJM, Zhou ZH and Adams MWW (1998) Biochemistry 37, 7351-7362

18. Brereton PS, Duderstadt RE, Staples CR, Johnson MK and Adams MWW (1999) Biochemistry 38, 10594-10605

19. Beeby M, O'Connor BD, Ryttersgaard C, Boutz DR, Perry LJ and Yeates TO (2005) PLoS Biol 3(9), e309.

20. Meyer J, Clay MD, Johnson MK, Stubna A, Münck E, Higgins C and Wittung-Stafshede P (2002) Biochemistry 41, 3096-3108

21. Sticht H, Wildegger G, Bentrop D, Darimont B, Sterner R and Rösch P (1996) Eur. J. Biochem. 237, 726-735

22. Kissinger CR, Adman ET, Sieker LC, Jensen LH and Le Gall L (1989) FEBS Lett 244, 447-450

23. Singh R, Blattler WA and Collison AR (1993) Anal. Biochem. 213, 49-56

24. Hagen WR (1989) Eur. J. Biochem.182, 523-530

25. Pierik AJ and Hagen WR (1991) Eur. J. Biochem.195, 505-516

26. Mukund S and Adams MWW (1991) J. Biol. Chem. 266,14208-14216

27. Zhou ZH and Adams MWW (1997) Biochemistry 36,10892-10900

28. Zhang JD, Christensen HEM, Ooi BL, Ulstrup J (2004) Langmuir 20,10200-10207

29. Hasan MN, Kwakernaak C, Sloof WG, Hagen WR and Heering HA (2006) J. Biol. Inorg. Chem. 11, 651-662

30. Hasan MN, Hagedoorn PL and Hagen WR (2001) FEBS Lett 531, 335-338

31. Fawcett SEJ, Davis D, Breton JL, Thomson AJ and Armstrong FA. (1998) Biochem. J. 335, 357-368

32. Armstrong FA, Bond AM, Hill HA, Oliver BN and Psalti ISM (1998) J. Am. Chem. Soc. 111, 9185-9189.

33. Hagedoorn PL, Chen T, Schröder I, Piersma SR, de Vries S and Hagen WR (2005) J. Biol. Inorg. Chem. 10, 259-269

34. Matthews BW, Jansonius JN, Colman PM, Schoenborn BP, Dupourque D (1972) Structure of thermolysin. Nature 238, 37-41

35. Vihinen, M. and Mantsala, P. (1989) Crit. Rev. Biochem. Mol. Biol. 24, 329–418

36. Adams MWW and Kelly RM (1995) Chem. Eng. News 73, 32–42

37. Persidis A (1998) Nature Biotechnol 16, 593–594

38. Lehmann M, Pasamontes L, Lassen SF and Wyss M (2000) Biochim. Biophys. Acta. 1543, 408–415

39. Russell RJM, Ferguson JMC, Haugh DW, Danson MJ and Taylor GL (1997) Biochemistry 36, 9983-9994

40. Salminen T, Teplyakov A, Kankare J, Cooperman BS, Lahti R and Goldman A (1996) Pro. Sci. 5,1014-1025

41. Karshikoff A and Landestien R (1998) Protein Eng. 11, 867-872

42. Zuber H (1998) Biophys. Chem. 29,171-179

43. Querol E, Perezs-Pons JA and Mozon-Villarias A (1996) Protein Eng. 9:256-271

44. Vogt G, Woell S and Argos P (1997) J Mol Biol 269, 631-643

45. Szilagyi A and Zavodszky P (2000) Structure 8, 493-504

46. Kumar S, Tsai CJ and Nushinov R (2000) Protein Eng. 3, 179-191

47. Haney P, Konisky J, Koretke KK, Luthey-Schulten Z and Wolynes PG (1997) Proteins 28, 117-130

48. Watanabe K, Hata Y, Kizaki H, Katsube Y and Suzuki Y (1997) J. Mol. Biol. 269, 142-153

49. Hsieh YC, Liu MY, LeGall J and Chen CJ (2005) Acta Crystallography D 61, 780-783

Supplementary material

Atom		X	Y	Z	Acc	B	VdW	AtOK
N	A	6.4	-4.9	8.7	0.0	15.8	1.7	+
CA	A	6.9	-4.0	7.6	0.0	15.4	1.8	+
C	A	8.2	-4.6	7.1	0.0	15.3	1.8	+
O	A	9.2	-3.9	7.2	0.0	14.1	1.4	+
CB	A	7.1	-2.6	8.1	0.0	15.3	1.8	+
SG	A	6.9	-1.2	6.9	0.0	15.6	2.0	+

CYS(21)A Bridged with CYS(48)A

Atom		X	Y	Z	Acc	B	VdW	AtOK
N	A	3.2	1.7	7.4	0.3	15.2	1.7	+
CA	A	3.6	0.5	8.1	0.5	14.1	1.8	+
C	A	4.9	0.7	8.9	0.0	12.7	1.8	+
O	A	5.1	-0.1	9.8	0.0	12.5	1.4	+
CB	A	3.7	-0.8	7.3	4.0	15.6	1.8	+
SG	A	5.0	-1.2	6.1	5.0	17.4	2.0	+

CYS(48)A Bridged with CYS(21)A

Fig 1: Analysis of surface exposure of cysteines at position 21 and 48 in *Pyrococcus furiosus* Ferredoxin using the "What If" program (http://swift.cmbi.kun.nl/WIWWWI/) based on 1SJ1.PDB. Column 'Acc' depicts the surface accessibility of a particular atom of the residue in the 3-D structure of the protein. None of the atoms in residue C21 are surface accessible while in the case of C48 the β-carbon and γ-sulfur are well exposed to the surface. The value (<60) of the crystallographic factor 'B' confirms the exact positioning of the particular atom within the structure. 'VdW' is the van der Waals' radius of the atom. Positive signs in column 'AtOk' confirm that the atom was correctly interpreted.

Chapter four

Pyrococcus furiosus 4Fe-ferredoxin, chemisorbed on gold, exhibits gated reduction and ionic strength dependent dimerization.

ABSTRACT

Pyrococcus furiosus ferredoxin is a small metalloprotein that shuttles electrons between redox enzymes. In its native 4Fe-4S form the protein is highly thermostable. In addition to three cluster-ligating cysteines, two free cysteine residues (C21 and C48) are present. We used the reactivity of these thiols to directly immobilize ferredoxin on a bare gold electrode, with an orientation in which the cluster is exposed to solution. Voltammetry, XPS and AFM studies establish the immobilization of the 4Fe form. Native and recombinant wild-type ferredoxins are compared to the C48S, C21S, and C21S/C48S mutants. The variants with one and two free cysteines can be directly chemisorbed on bare gold. Cyclic voltammetry demonstrates that the reduction potentials are similar to those in solution. The interfacial electron transfer kinetics reveals that the reduction is gated by the interconversion between two oxidized species. AFM images show that dimers are chemisorbed at low ionic strength, while monomers are present at high ionic strength. XPS spectra reveal the presence of S, Fe, C, N, and O at the surface, which are assigned to the corresponding atoms in the peptide and the cofactor. Analysis of the sulfur spectrum corroborates that both C21 and C48 form gold-thiolate bonds. Moreover, two inorganic sulfide and two iron species are identified, suggesting inhomogeneous charge distribution in the 4Fe-4S cluster. In conclusion, *P. furiosus* ferredoxin can be directly and vectorially chemisorbed on gold with retention of its properties. This may provide a biocompatible electrode surface with docking sites for redox enzymes.

INTRODUCTION

Pyrococcus furiosus ferredoxin (*Pfu*Fd) is one of the most thermostable ferredoxins. It is a small electron-transfer protein of 66 amino acids, containing a cubane type 4Fe-4S cluster bound by a CxxDxxC….CP sequence motif (similar to the CxxCxxC….CP consensus) and possesses several unique features. *Pfu*Fd can undergo reversible cluster conversion between the 4Fe-4S and 3Fe-4S forms under aerobic condition [1,2]. In addition to the cluster-coordinating cysteines, two free cysteines are present at position 21 and 48, which have been shown to form an intra-molecular disulfide bond under aerobic condition [3]. Adams and co-workers have studied the native, recombinant wild type and several mutant varieties of *Pfu*Fd (mainly altering the cluster coordinating amino acids) and explored the redox states under different conditions, their structural and functional relevance, and the role of the disulfide bridge in the stability and redox properties of the protein [3-6]. The authors reported the existence of four formal redox states of *Pfu*Fd, where the cluster is either reduced ($[4Fe-4S]^{1+}$) or oxidized ($[4Fe-4S]^{2+}$) and Cys21 and Cys48 either form a disulfide bond or exist as free thiols [3]. A solution NMR molecular model for the oxidized 4Fe-form has been reported [7], and the X-ray crystallographic structure of the 3Fe-form of the protein has been determined by Christinsen et al. [8]. We have demonstrated the functional dimeric state of the protein [9], and are investigating the role of the two free cysteines in the thermostability, structural integrity, and reduction potentials of the protein in solution by mutagenesis (data to be published).

Direct electrochemistry of redox proteins provides detailed kinetic information of the electron transfer reactions and coupled chemical reactions, in addition to the thermodynamic parameters. Enzyme electrochemistry is also applied in the development of biosensor devices. Armstrong and co-workers [10] have significantly contributed to the direct electrochemistry on the iron-depleted 3Fe-form of *Pfu*Fd in solution and in the physisorbed state, as well as the

forms reconstituted with iron (4Fe-4S) and other metal ions (M-3Fe-4S). In addition, Zhang et al. [11] have recently reported the analysis of the 3Fe-form of *Pfu*Fd on an adlayer of mercaptopropionic acid or cysteine on single-crystal gold (Au111) by scanning tunneling microscopy and voltammetry.

Voltammetry of adsorbed protein, termed as Protein Film Voltammetry (PFV) by Armstrong et al., does not rely on slow protein diffusion, thus allowing for direct control of the redox state of the whole protein population. PFV is therefore a powerful tool to probe the potential dependence of enzymatic activity and the role of cofactors in relaying electrons, and to study chemical reactions coupled to electron transfer [12]. A variety of electrode materials and surface modifications have been used, such as pyrolytic graphite (both basal and edge plane), surfactant films on graphite, conducting metal oxides, gold surfaces with a variety of self-assembled organo-thiolate monolayers, as well as a bare gold surface [12-16]

PFV has been successfully applied to study a variety of enzymes, but other redox enzymes do not directly exchange electrons with the electrode. In the latter case, one solution is to modify the surface with the natural electron donor/acceptor protein [16, 17]. Small blue copper proteins (e.g., azurin), heme proteins (cytochromes), and FeS proteins (e.g., ferredoxins) are metalloproteins that shuttle electrons between redox enzymes, and can be used as mediators between the electrode and redox enzymes. For PFV on such a system, with the mediator protein and the enzyme co-adsorbed, the orientation of the mediator protein must allow for electron exchange with both the electrode and the associated enzyme. This can be achieved by tethering the mediator protein to a gold electrode by direct chemisorption through a surface Cys thiolate [13,14]. Ulstrup and co-workers reported the direct, vectorial chemisorption of azurin in this way [18]. Heering et al. have demonstrated fast and reversible electron transfer between a gold electrode modified with vectorially chemisorbed yeast iso-1-cytochrome *c*, and redox enzymes such as nitrite reductase [14]. The third major class of small electron-

transferring metalloproteins is that of FeS proteins such as ferredoxin. Until now, however, no electrode is available on which ferredoxin is immobilized with a well-defined orientation suitable for interaction with redox enzymes.

Pyrococcus furiosus ferredoxin has been shown to mediate electrons to and from its redox partner enzymes; e.g., aldehyde oxidoreductase, glyceraldehyde-3 phosphate oxidoreductase, ferredoxin: NADP oxidoreductase, pyruvate oxidoreductase, the fifth tungsten-containing aldehyde oxidoreductase found in *Pyrococcus furiosus* ("WOR5"), and membrane bound hydrogenase [5, 19, 20] It is therefore of particular interest as a candidate to obtain a ferredoxin-modified electrode. The two native free cysteines may act as the tethers to hold the protein on the gold surface. The crystal structure reveals that Cys21 is slightly buried in the structure, while Cys48 is exposed to the surface [8]. Anaerobic purification under reducing condition results in the reduced 4Fe-4S form of the protein with free thiols, appropriate for chemisorption on bare gold. With the thiolates bound to the electrode, the aspartate-coordinated edge of the cofactor faces solution (the line between the surface-bound thiol and the center of the cluster is at a ~45º angle to the gold surface), while the distance between the gold surface and the nearest atom in the cluster is approximately 1.5 nm [8]. This allows for efficient electron relay by *Pfu*Fd between the electrode and co-adsorbed partner enzymes, as has been demonstrated for yeast cytochrome *c* on gold [14]. Moreover, the site predicted to be involved in dimerization also faces solution. Dimers of *Pfu*Fd are formed through β-sheet interactions, as deduced from crystal packing, and are predicted to be of physiological relevance [8, 9]. The structure predicts that when the dimer is chemisorbed via Cys21 or Cys48 of one monomer, the cofactor of the other monomer is fully accessible from solution.

In this paper we show for the first time that the as-isolated 4Fe-form of *Pyrococcus furiosus* ferredoxin and the C48S and C21S mutants can be directly chemisorbed on a bare gold electrode via either of the two free cysteines, with retention of the native properties. The

electron transfer kinetics, integrity, and topography of the immobilized ferredoxin are studied by voltammetry, X-ray photoelectron emission spectroscopy (XPS), and atomic force microcopy (AFM).

EXPERIMENTAL

Materials. Native *Pyrococcus furiosus* ferredoxin was purified as described elsewhere [1,9]. The recombinant wild-type (RWT) ferredoxin, the C48S and C21S single mutants, and the C21S/C48S double mutant were produced as described in chapter three. In brief: the double mutant was raised by two consecutive rounds of PCR reactions (SOE PCR), and by subsequent cloning (shuttle vector pENTR^{TM}/SD/D-TOPO, expression vector pET24d(+)). The resultant chimeric vector was used to transform *E.coli* BL21(DE3) cells. Terrific broth was used as culture medium, and protein purification was carried out as for native ferredoxin. Deionized water (18 MΩ.cm milli-Q, Millipore) was used to prepare all solutions and to rinse the electrodes. All the buffers and solutions were freshly prepared and made anaerobic by flushing with wetted argon or nitrogen.

Electrochemistry. For protein film voltammetry of the ferredoxin variants, a gold disk electrode (Bioanalytical Systems, BAS) with diameters of 1.6 mm (2.0 mm^2) was used as working electrode. The reference electrode was an Ag/AgCl/3 M NaCl electrode (BAS RE-5B, +215 mV versus the Normal Hydrogen Electrode, NHE), and a Pt wire was used as counter electrode. Prior to immobilization of *Pfu*Fd, the gold surface was polished with a water-based diamond suspension (Buehler, 1 µm particles), thoroughly rinsed and dried. A 25 µL droplet composed of 3 µM reduced ferredoxin, 2 mM tris[2-carboxyethyl] phosphine (TCEP, Pierce), and 1.5 M NaCl in 25 mM N-(2-hydroxyethyl) piperazine-N-(2-

ethanesulfonate) (Hepes, Merck) at pH 7.2 was applied between the electrodes, mounted in an anaerobic setup as described by Hagen [21]. The cell was flushed with wetted argon and connected to an EcoChemie Autolab 10 potentiostat. We noticed that, in order to obtain a stable ferredoxin film on the gold electrode, the protein has to be reduced with freshly prepared TCEP shortly before the measurement. TCEP was added from an anaerobic 20 mM stock solution to a strictly anaerobic droplet of the buffered protein solution. The droplet was hanging on the reference electrode, and brought into contact with the working electrode only after 5-10 min. of incubation. Equal results were obtained with protein that was pre-reduced with TCEP, desalted under strictly anaerobic conditions (superdex 75, Amersham Bioscience), and immediately applied to the electrode without added TCEP. Cyclic voltammograms were recorded between +0.215 V and -0.585 V versus NHE at 100 mV/s scan rate until a stable response was obtained. Bakers yeast invertase (Fluka) was used as an inert protein to record background voltammmograms. A gold electrode covered with invertase yields a pattern of background peaks that is similar to that of the gold surface covered with ferredoxin, and a comparable blocking of the hydrogen evolution due to adsorbed protein.

Atomic Force Microscopy. AFM samples were prepared using electrodes made of 250±50 nm gold on borosilicate glass with a 2.5±1.5 nm chromium sticking layer (purchased from Arrandee[TM], Germany). To obtain atomically flat gold (111) terraces, the gold was annealed in a blue butane flame. AFM inspection shows that this yields typical grain sizes of 1.5 x 1.5 μm, with Au (111) terraces of more than 200 x 200 nm. These chips could also be mounted as gold working electrode in the electrochemistry setup, yielding voltammograms that are similar to those recorded with BAS gold disk electrodes. *Pfu*Fd samples were either prepared in the electrochemical setup as described above, or a freshly annealed gold chip was incubated for 10 min. with a 25 μL droplet containing 10-100 nM ferredoxin and 0.2-2 mM TCEP in 25

mM Hepes at pH 7.2. The electrode was rinsed, dried under a stream of nitrogen, and mounted in the AFM (Nanoscope IV, Digital Instruments). Images were recorded under ambient conditions, in tapping mode at minimal force and amplitude, using silica cantilevers (Olympus), with a typical tip size of 10 nm. The smallest observed lateral sizes of isolated features were ~10 nm, confirming the specified tip size. The error in the z-direction is less than 10%, as judged form the measured height of atomic gold crystal steps.

X-ray photoelectron spectroscopy. For X-ray photoelectron spectroscopy (XPS), samples were prepared as described for AFM, but using 3 µM *Pfu*Fd and 1.5 M NaCl to obtain full monolayer coverage. A monolayer of 3-mercaptopropionic acid (>98%, Merck) on flame-annealed gold was used as reference. Spectra of the photoelectron lines of the respective elements were recorded with a PHI 5400 ESCA instrument using non-monochromatized incident Mg X-ray radiation (Mg K$\alpha_{1,2}$ = 1253.6 eV). The X-ray source was operated at 15 kV, and at low power (200 W) to minimize degradation. The emitted photo-electrons were detected at a take-off angle of 45º with respect to the sample surface. The photoelectron spectra were recorded with a step size of 0.2 eV and the Spherical Capacitor Analyzer set at constant pass energy of 35.75 eV. The energy scale of the SCA was calibrated according to a procedure described by the American Society for Testing and Materials [22]. The base pressure of the analysis chamber was less than 2×10^{-7} Pa during these measurements. The MultiPak 6.1 (PHI) analysis software was used to analyze the photoelectron spectra. After subtracting the background intensity using the Shirley-method [23], the chemical states of the elements were resolved by linear least square fitting of the spectra to mixed 90% Gaussian / 10% Lorentzian functions. In the case of the S *2p* spectra, a constrained curve-fitting procedure was applied. For the peak separation of the S *2p$_{3/2}$-2p$_{1/2}$* doublet, a constant value of 1.18 eV was used, and the intensity ratio of the S *2p$_{1/2}$* to *2p$_{3/2}$* was kept constant at 0.5 [24].

In addition, the full width at half maximum (FWHM) of each function was kept constant at 1.10 eV, a value close to the 1.06 ± 0.01 eV obtained for the FWHM of the Au *4f$_{7/2}$* peak. The Fe *2p$_{3/2}$* spectrum was fitted to three peaks with a FWHM of 2.50 eV. To exclude any effects on the values of binding energies due to charging of the sample during the measurement, all data were corrected by a linear shift such that the Au *4f$_{7/2}$* peak maximum corresponds with a binding energy of 84.00 eV.

RESULTS

Electrochemistry. When a bare, clean gold electrode is brought into contact with a low concentration (3 µM) of either of the ferredoxin variants containing one or two surface Cys residues, reduced with TCEP, a clear, quasi-reversible response is observed (Figure 1). The derived $[4Fe-4S]^{2+/1+}$ midpoint potentials of these four variants of *Pfu*Fd are collected in Table 1. The double mutant C21S/C48S, in which both free cysteines are absent, does not yield a significant ferredoxin response but only the common decrease of the hydrogen evolution background. This is indicative of non-specific physisorption of protein on the surface with loss of the cofactor, yielding a current similar to the background observed with invertase (Figure 1, dotted trace).

Within 2-5 scan cycles at a scan rate of 100 mV/s, the response reaches a stable maximum intensity. When the electrode is subsequently rinsed and brought into contact with the same buffer at pH 7.2 without protein, most of the response is still present, indicating that the protein is firmly adsorbed on the surface. In the presence of 1.5 M NaCl (added either prior to, or after the initial adsorption process) the response persists, demonstrating that the adsorption is not electrostatic in nature. In fact, the response increases with salt, because shielding of the protein charges allows for a more tightly packed layer (cf. Discussion section). The apparent midpoint potentials at low scan rate (cf. below) are close to those
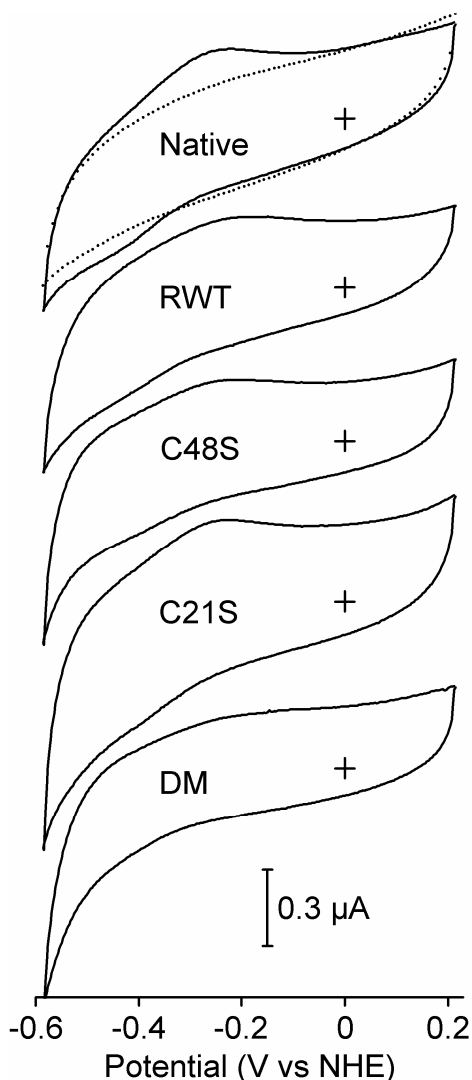

Figure 1. Voltammograms of the *P. furiosus* ferredoxin variants adsorbed on a bare gold electrode surface (2 mm^2), in 25 mM Hepes pH 7.2 with 1.5 M NaCl and 2 mM TCEP. The scan rate is 100 mV/s for all traces. The dotted line is the blank voltammogram, recorded with inert protein (invertase) on the gold electrode. DM is the double mutant C21S/C48S.

measured with the proteins in solution by diffusion-controlled voltammetry (our unpublished results, E_m values collected in Table 1).

At low scan rates, we routinely scanned down to -485 mV (for long-term stability at ≤50 mV/s) or -585 mV versus NHE. When the vertex point is lowered to < -0.7 V (only used at scan rates >2 V/s) we found that the 4Fe-4S response is rapidly decreasing. A small peak is observed around -0.54 V, which we assign to the reduction of the gold-thiolate bond. However, the reductive loss of the 4Fe-4S redox couple is not accompanied by the large, capacitive response, often associated with the reductive desorption of thiolates from gold [13]. Moreover, we did not observe an increase of the reductive current at low potential due to hydrogen evolution at bare gold, expected when protein is desorbing. These observations indicate that upon breaking the gold-thiolate bond at low potential, the protein remains bound to the electrode, but tends to denature (or at least lose the FeS cluster), analogous to the double mutant lacking both surfaces thiols. To minimize the reductive loss of the ferredoxin film, we start cycling from high potential. Although it is known that the oxidized 4Fe-4S cluster can be converted to the 3Fe-4S form [1,2], we did not observe the typical redox response of the 3Fe-4S cluster, expected around -160 mV. However, we did observe the responses for both 4Fe-4S and 3Fe-4S ferredoxin when a mixture of both forms was used as the starting material for the immobilization process. This demonstrates the stability of the chemisorbed *Pfu*Fd.

Scan rate dependence. To resolve the interfacial electron transfer kinetics of the chemisorbed ferredoxin variants, we monitored the peak potentials as function of scan rate (*v*). To avoid systematic errors (e.g., gold-thiolate bond reduction at the low vertex potential required at high scan rates) the scans were started after 5 sec. equilibration at +0.215 V, and the scan rates were varied per decade (0.01, 0.1, 1, and 10 V/s, then 0.02 to 20 V/s, then 0.05 to 50 V/s). The measurements were done in the presence of 1.5 M NaCl to prevent the formation of
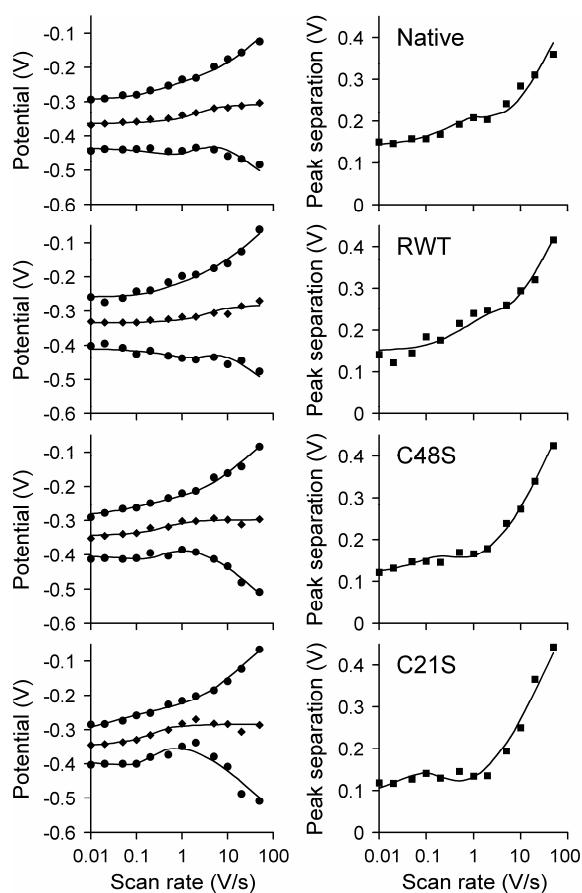
Figure 2. Scan rate dependent peak potentials (circles), midpoint potentials (diamonds) and peak separations (squares) of the *P. furiosus* ferredoxin variants on gold, in 25 mM Hepes pH 7.2 with 1.5 M NaCl and 2 mM TCEP (see Figures S1 and S2). The solid lines are the fitted potentials derived from the simulated voltammograms according to Eqns 1-3 (see Figure S3). The parameters are listed in Table 1.

multi-layers of protein with slow electron transfer kinetics, since at low ionic strength *Pfu*Fd is know to form dimers [9]. Moreover, the addition of salt lowers the ohmic resistance of the solution, which is important at high scan rates. The peak positions were determined by first subtracting the background voltammogram (with invertase) measured at each scan rate. Linear baselines were then subtracted from each peak to determine the maximum.The results, plotted in Figure 2 (circles), clearly show that the peak positions do not follow the symmetrical "trumpet" plot expected for pure redox kinetics [25,26], and the peak heights normalized to scan rate decrease reversibly with scan rate. In addition we noticed a rather large difference in potentials between the cathodic and anodic peaks, a non-monotonic increase of this difference with scan rate (Figure 2, squares), and relatively broad and low cathodic peaks at intermediate scan rates (see Figure 1). Moreover, the apparent midpoint potentials shift markedly to a less negative value at high scan rate (Figure 2, diamonds). These

observations are indicative for the existence of a second oxidized species (X) that cannot be directly reduced at the electrode. The conversion of X to the reducible oxidized form (Ox) is thus gating the electron transfer reaction to form reduced ferredoxin (Red):

$$X \xrightleftharpoons[k_{ox}]{k_{xo}} Ox \xrightleftharpoons[k_{ro}]{k_{or}} Red \qquad (1)$$

To obtain the kinetic parameters, the data were fitted to the peak potentials as function of scan rate, as derived from simulated staircase voltammograms for this gating mechanism. The Butler-Volmer equations are used to calculate the interfacial electron transfer rate constants for reduction and oxidation:

$$k_{or} = k_0 \exp\left\{-\alpha n F\left(E - E^{0'}\right)/RT\right\} \qquad (2)$$

$$k_{ro} = k_0 \exp\left\{(1-\alpha)nF\left(E - E^{0'}\right)/RT\right\} \qquad (3)$$

where k_0 is the standard rate constant, E is the applied potential, $E^{0'}$ is the reduction potential of the Ox to Red reaction, α is the transfer coefficient, n is the number of electrons, F is the Faraday constant, R is the gas constant, and T is the temperature [27]. At high scan rates, the peaks separate symmetrically around a shifted but constant midpoint potential ($E_m = E^{0'}$ at high scan rates) which implies that α is close to 0.5. Unfortunately, the value of n cannot be directly obtained from the peak shapes due to the complex kinetics. However, linear analysis of the peak potentials versus log(scan rate) at the highest scan rates where electron transfer becomes kinetically irreversible [27] yields $n=1.0\pm0.1$ and $\alpha=0.56\pm0.09$ (at $v \geq 10$ V/s for C48S and C21S; $v \geq 20$ V/s for RWT; native *Pfu*Fd is not fully irreversible at highest

available scan rates). Moreover, the measured midpoint potentials at low scan rates are close to the equilibrium one-electron 4Fe-4S cluster reduction potentials of the *Pfu*Fd variant in solution.

In the simulations the current at each potential step was derived analytically, analogous to the method described previously for the non-gated mechanism [28]. The time-dependent fractional surface concentrations of X, Ox and Red at given applied potential were obtained by solving the matrix of linear differential equations at each potential step. Equilibrium was assumed before the first step, and the surface concentrations at the start of each step of 2 mV were set equal to the final concentrations of the previous step. A spreadsheet was set up, implementing this scheme to simultaneously calculate the voltammograms at all scan rates and to derive the full set of peak potentials at each actual set of parameter values.

As apparent from the data plotted in Figure 2, additional, constant hysteresis is present at low scan rates (e.g., for native ferredoxin the observed peak splitting for scan rates 1, 10, and 20 mV/s are 146, 150, and 147 mV, respectively). Such a non-zero peak separation (coined "unusual quasi-reversibility", or UQR, by Feldberg and Rubinstein [29]) is commonly observed for redox proteins adsorbed on electrodes [25,26,30-32]. UQR is not due to interfacial electron transfer kinetics [25,29,32], and also cannot be obtained by introducing additional species in the mechanism (cf. Discussion section). Therefore, we included the finite peak splitting $\Delta E_\mathrm{p}(v\rightarrow0)$ as a fit parameter in addition to the rate constants k_{xo}, k_{ox}, and k_0 and the reduction potential $E^{0\prime}$. The data were fitted by minimizing the sum of squared differences between the peak potentials obtained from the data and those from the simulations. The resulting fits at fixed T=295 K, α=0.5, and n=1 (n=2 yields very poor fits) are plotted in Figure 2 (solid lines), and the parameters are collected in Table 1.

Table 1. Parameters obtained from fitting the peak potentials (Figure 2) to the three-species model (Eqn 1)[a].

	Ox⇔Red		X⇔Ox			(X+Ox)⇔Red			in solution [d]
	k_0	$E^{0'}$	k_{xo}	k_{ox}	K_x [b]	$\Delta E_p(0)$	$E_m(0)$ [c]	ΔE_m [c]	E_m
	(s^{-1})	(mV)	(s^{-1})	(s^{-1})		(mV)	(mV)	(mV)	(mV)
Native	94	-306	5.1	44	8.7	139	-364	-58	-351
RWT	76	-280	9.6	72	7.5	147	-334	-54	-358
C48S	47	-297	1.6	8.1	5.0	115	-343	-45	-352
C21S	34	-284	0.44	4.8	10.8	82	-347	-63	-359

[a] α=0.5, n=1, T=295 K; [b] K_x=k_{ox}/k_{xo}; [c] $E_m(v\to0)$ and ΔE_m=$E_m(v\to0)$–$E^{0'}$ are calculated from eqn 4; [d] 50 µM protein and 7 mM neomycin in 25 mM Mops buffer, pH 7.4 on glassy carbon, scan rate 20 mV/s.

The general trends observed in the measured voltammograms can be fully understood from the mechanism and are accurately reproduced by the derived simulations. At low scan rates, interconversion between X and Ox is fast relative to the time allowed for the redox reaction. Therefore, both oxidized forms are effectively reduced and re-equilibrated between X and Ox upon re-oxidation, yielding reversible voltammetry (apart from UQR) with an apparent midpoint potential equal to:

$$E_m(v \to 0) = E^{0'} - \frac{RT}{nF}\ln\left(1 + \frac{k_{ox}}{k_{xo}}\right) \tag{4}$$

At very high scan rates (starting at $E > E_m$), however, the time allowed for the reduction is very short, giving no opportunity for X to be converted into Ox before the scan direction is

reversed and re-oxidation occurs. Part of the oxidized ferredoxin is now trapped in species X and only a fraction of the total population (the already present Ox and Red) participates in the redox reaction. Therefore, the area under the redox peaks is predicted to be much lower compared to that at low scan rates, as indeed is observed experimentally. Since species X does not participate in the overall reaction at high scan rates, the midpoint potential is equal to $E^{0'}$, and the peak separation has the symmetrical "trumpet" shape predicted from the Butler-Volmer equation. At intermediate scan rates the reduction peaks are predicted and observed to be low and broad because the reduction rate is limited by the potential-independent conversion of X to Ox. Since re-oxidation of the reduced form is not gated, the anodic peaks remain relatively narrow. Both the cathodic and anodic peak areas (and heights divided by scan rate) decrease with increasing scan rate because increasing amounts of the oxidized species remain trapped as X.

For native ferredoxin, the thermodynamic equilibrium midpoint potential (i.e., at low scan rate) is close to the midpoint potential measured by voltammetry with ferredoxin in solution (Table 1), while for all three the recombinant proteins, this midpoint potential is slightly lowered. The kinetic parameters of RWT ferredoxin are, however, very similar to those of the native protein, but are markedly lowered for both mutants. The interfacial electron transfer kinetics of the mutants are two-fold lower compared to native and RWT ferredoxin, suggesting a correlation between electron tunneling efficiency and the number of surface-bound thiolates. The observed UQR peak separations at low scan rates are the largest values reported for adsorbed redox proteins. However, we emphasize that this is a fully reproducible characteristic of the system, which does not interfere with the analysis nor with the application of the ferredoxin electrode to study redox enzymes (cf. Discussion section).

The inter-conversion rate constants between X and Ox are one order of magnitude lower for the mutants. However, the equilibrium constant K_x for the formation of X is similar in all four

variants: at equilibrium, around 90% of oxidized ferredoxin is present as species X. For native and RWT ferredoxin the rate constants are relatively high, leading to full trapping only at high scan rates (>1 V/s). The pronouncedly gated reduction of the mutants, with full trapping already observed at scan rates below 1 V/s, is due to the slower kinetics but not to a shifted equilibrium. Figure 1 shows that partial trapping, resulting in a low and broadened reduction peak, is already observed at 100 mV/s in all variants.
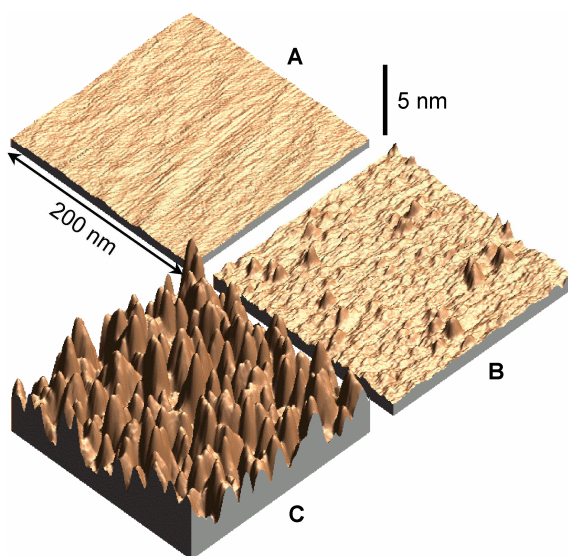

Figure 3. Tapping mode AFM images of flame-annealed gold (200 x 200 nm, 512 x 512 pixels, vertical scale bar 5 nm). **A:** Freshly flame-annealed surface. **B:** Incubated for 5 min. with 25 mM Hepes pH 7.2. **C:** Incubated for 5 min. with 100 nM reduced *P. furiosus* ferredoxin in 25 mM Hepes pH 7.2, then incubated for 10 min. with 20 mM TCEP in the same buffer.

Atomic force microscopy. AFM images were recorded under ambient conditions on the atomically flat Au(111) terraces obtained by flame-annealing. The surface was incubated with low concentrations (10-100 nM) of reduced *Pfu*Fd to obtain the sub-monolayer coverage required for accurate height-determination. The stability of the ferredoxin film on flame-annealed gold in air was verified by cyclic voltammetry before and after drying. The unaltered E_m values confirm the structural integrity of the protein on the surface as well as the independence of the surface environment (Au(111), polycrystalline gold) . This stability can

be explained by the hygroscopic nature of the protein, which ensures that the monolayer retains sufficient water to stabilize the *Pfu*Fd structure under ambient conditions.

Figure 3 shows AFM images of the flame annealed (panel A) and buffer treated flame annealed gold electrode (panel B), both washed with water and dried under nitrogen. The buffer-treated surface is slightly rougher (within one gold atom height), with additional ~0.5 nm high features. Figure 3C demonstrates the adsorption of pre-reduced *Pfu*Fd (with 20 mM TCEP, followed by gel-filtration to remove the reductant). The density of features increases with higher *Pfu*Fd concentration and upon longer incubation. The observed heights are mostly between 3 and 4 nm, but ~20% are between 1.5 and 2 nm high. The crystallographic height of monomeric ferredoxin is 2.2 nm, assuming that Cys48 and Cys21 are facing the surface [8]. This suggests that the majority of the protein is adsorbed as end-on dimers.
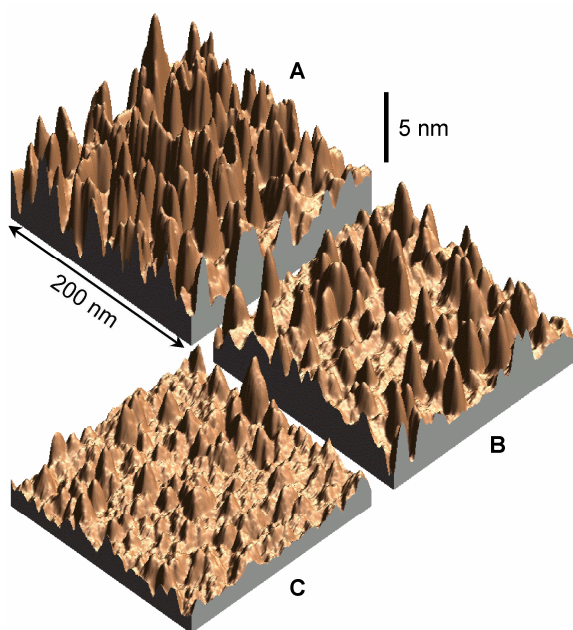

Figure 4. Tapping mode AFM images of flame-annealed gold, demonstrating the salt-dependent monomerization (200 x 200 nm, 512 x 512 pixels, vertical scale bar 5 nm). **A:** Incubated for 5 min. with 100 nM *P. furiosus* ferredoxin and 2 mM TCEP in 25 mM Hepes pH 7.2. **B:** Washed for 30 sec. with 3 M NaCl. **C:** Incubated for 15 min. with 3 M NaCl.

As we reported earlier [9], *Pfu*Fd forms electrostatic dimers in solution under physiological conditions (0.35 M ionic strength), and monomerizes in the presence of ≥1.5 M salt. With AFM, we here demonstrate a similar salt-dependent monomerization on the electrode (Figure

4). A gold surface was incubated with a low concentration (100 nM) of *Pfu*Fd at low ionic strength buffer. The obtained sub–monolayer coverage allows for accurate determination of the feature heights. Under these conditions, most of the features are around 4 nm high, with only a few 2 nm high features (panel A). Upon incubation with 3 M NaCl for 30 seconds, followed by rinsing with milli-Q water, the ratio of features with monomeric (2 nm) to dimeric (4 nm) height increases significantly (panel B). Incubation with the same salt concentration for a further 15 min. results in almost exclusively monomeric heights (Panel C). Because the lateral resolution is limited by the tip radius (~10 nm), we could not fully exclude that the 4 nm high features found in Figures 3 and 4 are stacked side-on dimers instead of end-on dimers. We therefore incubated the gold surface with a ten-fold lower ferredoxin concentration (10 nM) at low ionic strength. This resulted in a ten-fold lower coverage compared to Figures 3C and 4A with almost exclusively 4 nm high features (data not shown). Interestingly, we observed that at this low coverage, the isolated features tilt in the direction of the AFM scan. These observations strongly suggest that the 4 nm high features are indeed due to individual, isolated dimers, adsorbed "end-on" on the gold surface. Upon scanning with higher tapping force and amplitude we found that some of these features were reduced to 2 nm height in the consecutive image, suggesting that the dimers can be mechanically separated. This implies that the protein-protein interaction in the dimer is relatively weak, which is supported by the small number of interaction points observed in the crystal structure of the dimer [8]. As before, the monomer to dimer ratio increases after incubation with salt.

Most of the dimeric features, obtained at low ionic strength, persist after incubating with TCEP. In fact, the AFM image shown in Figure 3C was recorded after 10 min. incubation with a high concentration of TCEP (20 mM). The monomer-to-dimer ratio observed in this image is very similar to that before washing with reductant. This corroborates that the dimers are electrostatic in nature, rather than due to inter-protein disulfide bond formation.

X-ray Photoelectron Spectroscopy. The photoelectron spectra of *Pfu*Fd adsorbed on a flame annealed gold surface contained lines at binding energies of C, O, N, S, Fe, and Au atoms, as expected. No P or Cl lines were detected in any sample, and also no S line corresponding with sulfonate was found. This implies that neither TCEP nor salt nor Hepes buffer, present in the ferredoxin solution used to prepare the samples, was adsorbed at the gold surface. Photoelectron spectra of the gold surface incubated for 15 minutes with 3M NaCl (shown in Figure 4C), did not show the presence of Cl. Thus, no salt crystals are present at the surface after the treatment with 3 M NaCl, corroborating our assignment of the observed features to monomeric ferredoxin. The absence of Cr lines in the photoelectron spectra indicates that the gentle flame annealing of 250 nm Au on a Cr sticking layer does not affect the composition of the gold surface. The S *2p* spectrum is shown in Figure 5A. Analysis of the core level region encompassing 160-168 eV shows contributions from four different components. The values of the binding energies of the S $2p_{3/2}$ lines and the fractional contributions to the spectrum, as obtained by curve fitting, are listed in table 2.
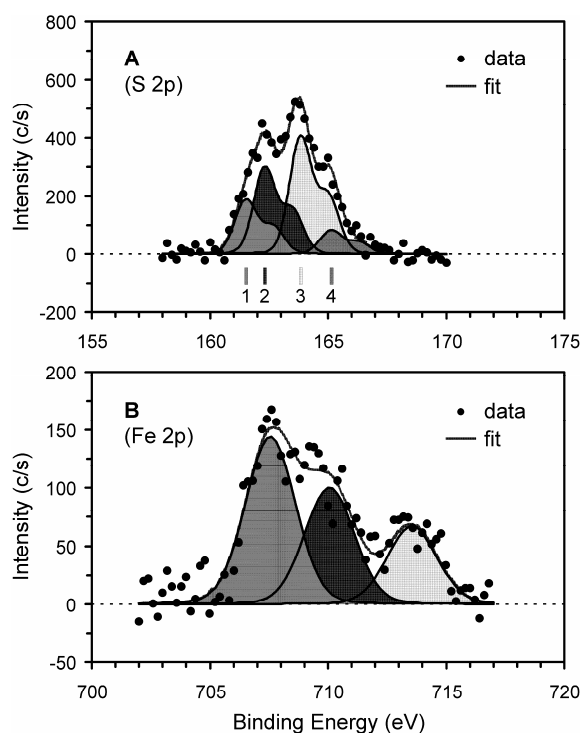
Figure 5. XPS spectra of *P. furiosus* ferredoxin on flame-annealed gold showing the core-level regions of S *2p* (**A**) and Fe *2p* (**B**). *Pfu*Fd was adsorbed from a 3 µM solution in 25 mM Hepes pH 7.2 with 1.5 M NaCl and 2 mM TCEP. The S *2p* spectrum comprises four components (see Table 2 for details). The Fe $2p_{3/2}$ spectrum was resolved into two components and a shake-up feature of Fe(II) (see text for details). Measurement conditions: Mg K$\alpha_{1,2}$ = 1253.6 eV, 15 kV, 200 W, take-off angle 45°, analyzer pass energy 35.75 eV, step size 0.2 eV and integration times 150 s/step.

The binding energy of component 1 (161.4 eV) corresponds to that of several compounds in which sulfide occurs in ionic bonds with metal ions, e.g., K_2S, chalcogenide (FeS), CuS, Cu_2S, and ZnS [33]. The fractional contribution of 19% is close to 2 out of the total of 11 sulfur atoms in *Pfu*Fd. Thus, component 1 can be assigned to two inorganic sulfur atoms in the 4Fe-4S cluster.

Component 2 (162.2eV) is assigned to sulfur bound to gold [13,18,34,35] and iron [33,36]. The fractional contribution of 31% corresponds to 3-4 sulfur atoms. In accordance with S *2p* electron binding energies reported for thiolates bound to gold, the Cys-CH_2-S-Au bonds contribute to this component. If both Cys21 and Cys48 are involved in chemisorption, they account for more than half of the intensity. Based on the binding energy reported for pyrite (FeS_2), the remaining intensity of component 2 can be assigned to inorganic sulfur atoms in the 4Fe-4S cluster.

78

Table 2. The S $2p_{3/2}$ binding energies and the relative intensities of the four components in the S $2p$ XPS spectrum of *Pfu*Fd, obtained by peak fitting (Figure 5).

Component	binding energy (eV)	fraction (%)	assigned species
1	161.4	19	4Fe-4S
2	162.2	31	Cys-S-Au, 4Fe-4S
3	163.8	41	Cys-S-Fe, Met
4	165.0	9	S

The fractional contribution of component 3 (163.8 eV) corresponds to 4-5 out of 11 sulfur atoms. Based on the binding energies of 163.5 eV, reported for iron complexes with thiolate ligands [37], the three cluster-coordinating Cys contribute to this component. The difference between the S $2p$ electron binding energies of the cysteines ligating the 4Fe-4S compared to those of the Cys bound to Au, can be attributed to the different chemical environments of the sulfur atoms (electrophillic mineral versus metal surface). Free thiols and dithiols are also expected to contribute to component 3 [33,35]. However, the two exclusively carbon-bound methionine sulfur atoms account for the remaining part of the intensity of this component [18, 37, 38]. Therefore, the observed fractions of components 1, 2, and 3 can only be accounted for if the cluster-coordinating cysteines, as well as the majorities of Cys21 and Cys48 in the sample are bound to a metal atom. This implies that *Pfu*Fd is chemisorbed to gold via both exposed cysteine thiolates.

A self-assembled monolayer of 3-mercaptopropionic acid on flame-annealed gold also yielded component 2 and 3 (data not shown), indicating the presence of not only gold-bound thiolates but also free thiols due to bilayer formation with hydrogen-bonded carboxylates and

exposed thiols [35]. Since the *Pfu*Fd XPS samples were prepared at high ionic strength, we can exclude the formation of a similar bilayer (i.e., dimeric layer) of ferredoxin (Figure 4C).

The occurrence of component 4 (165.0 eV) may be attributed to elemental S (164.8 eV), oxidized species, or a doubly bound S to a C atom (164.4 to 165.6 eV) [33]. These chemical states may be a result of a decomposition reaction during the measurement (e.g., radiation damage). Alternatively, the relatively high binding energy may be due to electron-depleted inorganic sulfur in the cluster.

The inorganic sulfur atoms in the 4Fe-4S cofactor are present in component 1, 2, and perhaps 4. This heterogeneity of the sulfur atoms in the cofactor can be explained by the inhomogeneous charge distribution, as has also been observed by other spectroscopic methods [39]. The presence of the different sulfur species, bound to iron, is supported by curve fitting of the Fe $2p_{3/2}$ spectrum of *Pfu*Fd (Figure 5B). The values of the binding energies of the three features observed in the Fe $2p_{3/2}$ spectrum (707.5, 709.9, and 713.3 eV) correspond to those of FeS_2, FeS, and the shake-up photoelectron line of Fe(II), respectively [33,36].

The integrated intensities of the core level regions of S, Fe, and the other elements present in the protein (C, N, O) give, within experimental errors, relative atomic ratios equal to those calculated from the crystal structure. This confirms the presence of *Pfu*Fd on the surface, and supports our assignment of the sulfur and iron components to ferredoxin. To our knowledge, this is the first time that XPS analysis of a 4Fe-4S protein is reported.

DISCUSSION

The results obtained with voltammetry, AFM and XPS clearly show that *Pfu*Fd can be chemisorbed directly on bare gold. Both the variants with two free cysteines as well as the single mutants C21S and C48S can be chemisorbed without major disruption of the conformation. The double mutant, lacking both surface Cys residues, does not yield a

voltammetric response on gold. The crystal structure reveals that Cys48 is exposed to the surface, and can directly interact with the electrode, while Cys21 is slightly buried. However, the chemisorption of the C48S mutant on bare gold demonstrates that enough flexibility is present in structure to allow for rotation of the Cys21 thiol towards the surface. In fact, two conformations of the cysteine dimer are observed in the crystal structure of the fully oxidized protein. The transition between these conformers requires only local rearrangement of the backbone [8]. Chemisorption on gold results in an orientation that allows for dimerization between the monomers on the surface and from solution, through the β-sheet interactions, as deduced from crystal packing (Figure 6). The dimer interactions are electrostatic in nature and relatively weak, as we demonstrated earlier in solution [9], and on surface by AFM in this work. Upon washing with salt or after applying relatively high tapping force, we observed that the initially 4 nm high features were converted to 2 nm high features, coinciding with the crystallographic dimensions of dimers (4.5 nm) and monomers (2.2 nm), respectively.

 The ferredoxin molecules are strongly bound to the gold surface. In all experiments, washing the samples with water did not result in loss of adsorbed protein. Moreover, we did not observe a depletion of the ferredoxin monomer film upon addition of salt. This demonstrates that the protein is not adsorbed on the electrode by electrostatic interactions. In fact, in the presence of 1.5 M NaCl, the electrochemical response is higher rather than lower.

The AFM data show that the protein film prepared at low ionic strength consists mostly of end-on chemisorbed dimers, while a monolayer of monomeric ferredoxin is present on the electrode at high ionic strength. At low ionic strength the maximum surface coverage is 7 pmol/cm^2, or an apparent area of 48 nm^2 per dimer, while at high ionic strength, the maximum coverage is 28 pmol/cm^2, or 6.0 nm^2 per monomer [40]. The crystallographic dimensions yield a footprint area of 6.1 nm^2 per monomer when Cys21 and Cys48 face the surface. This implies that at high ionic strength a close packing of the overall negatively charged protein

molecules can be obtained, while the coverage is limited by electrostatic repulsion at low ionic strength. The lateral repulsion between the dimers at low ionic strength is also suggested by the observed increased tendency to topple (i.e., display rotational mobility) under the AFM probing needle at lower coverage.

Initial trials of AFM and voltammetric experiments showed that the adsorption process requires reduced ferredoxin, probably because *Pfu*Fd is most stable in this form [3]. We used TCEP as reductant because it also efficiently reduces disulfide bonds. Initially, we speculated that TCEP would be required to prevent the formation of inter-protein disulfide dimers that interfere with the chemisorption on gold, as was clearly observed for yeast cytochrome *c* chemisorption [14]. However, the AFM results show that the dimerization does not involve a disulfide bond, confirming the earlier reports by La Mar and co-workers [3,41]. Instead, for the native and RWT proteins, the reduction of the intra-protein cysteine bond probably renders the thiols more mobile and thus more prone to interact with the electrode surface. The
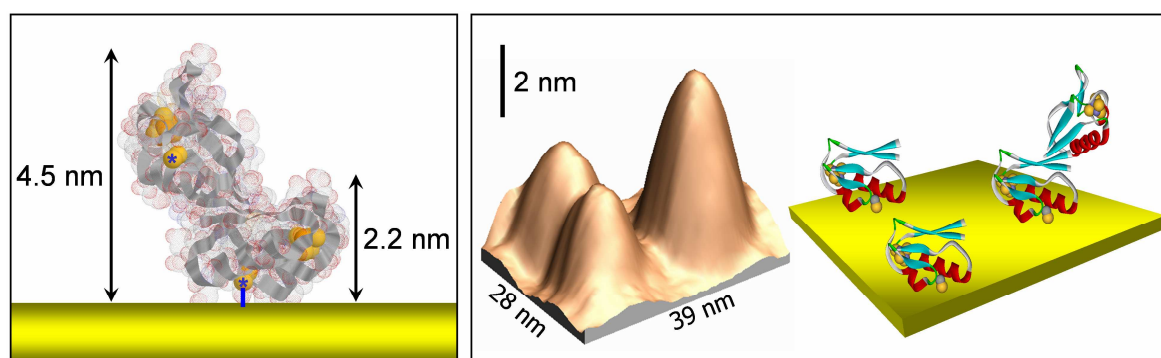

Figure 6. Left panel: Cartoon of dimeric *Pyrococcus furiosus* ferredoxin, chemisorbed on gold via Cys21 and Cys48 (based on 1SJ1.PDB and 1SIZ.PDB [8]). The asterisks indicate the Cys48 sulfur atoms. Right panel: Tapping mode AFM image of *Pfu*Fd on Au(111) after controlled salt treatment (for conditions, see Figure 4B), and the inferred molecular interpretation (z-dimensions drawn to scale).

reduction of the single cysteine mutants is probably important because the intrinsically lower stability of the oxidized form of the protein would favor denaturation rather than chemisorption. Gold incubated with ferredoxin in the presence of TCEP yields similar coverage compared to pre-reduced ferredoxin, gel-filtered to remove TCEP. Therefore, it can be concluded that TCEP does not directly promote chemisorption. In addition, the reduction potentials are not influenced by the presence of TCEP in solution, showing that TCEP does not significantly influence the properties of ferredoxin. Moreover, no phosphorus signal was observed in the XPS spectra. We can therefore exclude monolayer formation of TCEP on gold, on which ferredoxin might co-adsorb, as was reported for the 3Fe-form of *P. furiosus* ferredoxin on a layer of mercaptopropionate [11].

The midpoint potentials of the adsorbed ferredoxin variants are close to those measured in solution. Since the reduction potential is extremely sensitive to the environment of the cofactor, this implies that the immobilized proteins retain their global conformation. Moreover, the reduction potential of *Pfu*Fd is unaltered after drying and the heights observed with AFM are close to the crystallographic dimensions, demonstrating that the structural integrity is also preserved under ambient conditions. For native ferredoxin on gold, the midpoint potential at low scan rate is closest to that measured by diffusion-controlled voltammetry (Table 1), while for the recombinant proteins, the midpoint potentials are slightly lowered. This suggests a slightly larger conformational flexibility of the proteins expressed in *E. coli*.

From the scan-rate dependent asymmetrical shifts and heights of the reduction and oxidation peaks, we conclude that the oxidized protein exists in two forms, X and Ox, while only the reduction of species Ox is observed at the electrode. The nature of species X is unknown. It is most likely not a (de)protonated form of Ox, because the midpoint potential does not depend on pH [10]. Species X may instead be oxidized ferredoxin in a slightly different

conformation. However, this conformation is not directly related to the global stability of the protein because the mutants are unfolding more rapidly (to be published), while the interconversion between X and Ox is significantly slower in the mutants. Redox-dependent conformations have been observed in the crystal structures of the related 3Fe-4S ferredoxin from *Desulfovibrio gigas* [42]. A conformational difference between oxidized and reduced ferredoxin may facilitate preferential docking to the respective partner enzymes such as aldehyde oxidoreductase [19] and hydrogenase [43].

Finite, non-kinetic peak separations are regularly observed in protein film voltammetry (typically 50 mV or less) [14, 25]. Kasmi and co-workers propose that this hysteresis is due to a reversible, electron-transfer induced conformational change [30]. However, a redox reaction coupled to a reversible chemical reaction will appear as a single, reversible net reaction at low scan rates (see Eqns 1 and 4), with peak separations approaching zero [30,32]. Instead, Feldberg and Rubinstein [29] propose an N-shaped free energy (potential versus charge) curve that results in a time-independent hysteresis equal to the free energy difference between the maximum and minimum of the curve. Heering et al. [14] postulated that such an N-shaped curve can be due to vibrational relaxation associated with the redox reaction. The somewhat smaller UQR separation in the ferredoxin mutants coincides with slower trapping kinetics, lower global stability, possibly increased conformational flexibility, and weaker coupling between the redox cofactor and the electrode surface. This suggests that the exceptionally pronounced UQR of *Pfu*Fd on gold is, at least in part, related to redox-linked conformational or orientational states that are modulated by the electric field.

In chemisorbed ferredoxin, the surface-bound cysteine thiolates are at an estimated distance of 1.5 nm from the 4Fe-4S cluster [8]. According to Marcus theory for electron transfer this yields a maximum electron transfer rate sufficient to drive enzymatic turnover [44]. This is an important consideration for the application of the ferredoxin electrode to study redox

enzymes: the very low k_0 (rate at zero overpotential) for the 3Fe form of *Pfu*Fd on organo-thiolate monolayers, reported by Ulstrup et al [11], stipulate the importance of close proximity between ferredoxin and the gold surface. Yeast cytochrome *c* chemisorbed on gold has a k_0 of 1800 s^{-1} for an electron tunneling distance of 1.6 nm and an estimated reorganization energy of 0.6 eV [14]. Here we observe a k_0 of 34-94 s^{-1} for tunneling over a similar distance. This lower rate at zero overpotential is indicative for a significantly higher reorganization energy compared to cytochrome *c*. A high reorganization energy is predicted by the intrinsically high polarity of a 4Fe-4S cluster with an Asp ligand (as observed by the heterogeneity of both the iron and sulfur species in the XPS spectra), and by the relatively polar environment of FeS clusters in ferredoxins [45]. The interfacial electron transfer rate constant of native and RWT ferredoxin are similar, but are two-fold lower for the C48S and the C21S mutants. This implies that the electron transfer pathway is altered in the variants with one free cysteine instead of two. The lower k_0 might be due to a slightly different orientation with a larger distance between the electrode surface and the 4Fe-4S cluster in the mutants. Alternatively, in both native and RWT ferredoxin, the two thiolate bonds to gold provide two parallel electron entrance points, resulting in two-fold faster electron transfer compared to the mutants that are anchored by a single thiolate.

The results show that vectorially chemisorbed PfuFd retains its integrity and is able to transfer electrons and dimerize. As shown in Figure 6, the 4Fe-4S cluster access is not blocked by chemisorption. Although not fully opposite the thiols, the cluster presumably is sufficiently exposed to accommodate a partner redox protein. Moreover, the AFM results reveal some degree of rotational mobility, which may aid docking of the enzyme. Therefore, the chemisorbed ferredoxin electrode not only offers the possibility to characterize the immobilized electron-transfer protein itself, but also its complexes formed with redox partner proteins.

CONCLUSIONS

The as-isolated 4Fe-4S form of *Pyrococcus furiosus* ferredoxin can be directly chemisorbed on a bare gold electrode. Voltammetry, XPS and AFM data of native *Pfu*Fd on gold, and comparison of native and RWT to mutant ferredoxins show that both the C21 and C48 thiols are able to form a covalent bond to the surface. The protein retains its native properties, as the reduction potentials are similar to those in solution. Moreover, the characteristic ionic strength-dependent monomer-dimer equilibrium is also observed for the immobilized ferredoxin. Direct, quasi-reversible electron transfer between the cofactor and the electrode surface is observed. However, the reduction is gated due to the existence of two oxidized forms, most likely conformers. The XPS spectra confirm the formation of gold-thiolate bonds, and also indicate inhomogeneous charge distribution in the 4Fe-4S cluster.

With this new ferredoxin-modified electrode, and the existing azurin and cytochrome *c* electrodes, all three major types of small, electron transferring metalloproteins have a representative that can be vectorially chemisorbed on bare gold via naturally occurring free cysteines. This means that biocompatible electrodes are available for a wide range of redox enzymes by providing docking sites at the surface. This facilitates the study of the interactions and electron transfer between redox proteins, both by electrochemistry and by scanning probe methods, and is of potential interest in sensor applications. We are currently successfully applying the ferredoxin electrode to study its native redox partner enzymes.

REFERENCES

1. Conover RC, Kowal AT, Fu W, Park JB, Aono S, Adams MWW, Johnson MKJ (1990) Biol Chem 265:8533-8541

2. Park JB, Fan C, Hoffman BM, Adams MWW (1991) J Biol Chem 266:19351-19356

3. (a) Gorst CM, Yeh YH, Teng Q, Calzolai L, Zhou ZH, Adams MWW, La Mar G (1995) Biochemistry 34:600-611, (b) Gorst CM, Zhou ZH, Ma K, Teng Q, Howard JB, Adams MWW, La Mar GN (1995) Biochemistry 34:8788-8795

4. (a) Kim CH, Brereton PS, Verhagen MFJM, Adams MWW (2001) Methods Enzymol 334:30-40 (b) Telser J, Davydov R, Kim CH, Adams MWW, Hoffman BM (1999) Inorg Chem 38:3550-3553

5. Brereton PS, Verhagen MFJM, Zhou ZH, Adams MWW(1998) Biochemistry 37:7351-7362

6. Brereton PS, Duderstadt RE, Staples CR, Johnson MK, Adams MWW (1999) Biochemistry 38:10594-10605

7. Sham S, Luigi C, Wang PL, Bren K, Haarklau H, Brereton PS, Adams MWW, La Mar GN (2002) Biochemistry 41:12498-12508

8. Nielsen MS, Pernille H, Ooi BL, Christensen HEM (2004) Biochemistry 43:5188-5194

9. Hasan MN, Hagedoorn PL, Hagen WR (2002) FEBS Lett 531:335-338

10. Fawcett SEJ, Davis D, Breton JL, Thomson AJ, Armstrong FA (1998) Biochem J 335:357-368

11. Zhang JD, Christensen HEM, Ooi BL, Ulstrup J (2004) Langmuir 20:10200-10207

12. (a) Vincent K, Armstrong FA (2005) Inorg Chem 44:798-809 (b) Armstrong FA (2005) Curr Opin Chem Biol 9:110-117 (c) Armstrong FA, Wilson GS (2000)

Electrochim Acta 45:2623-2645 (d) Armstrong FA, Heering HA, Hirst J (1997) Chem Soc Rev 26:169-179

13. Hansen AG, Boisen A, Nielsen JU, Wackerbarth H, Chorkendorff I, Andersen JET, Zhang JD, Ulstrup J (2003) Langmuir 19:3419-3427

14. Heering HA, Wiertz FGM, Dekker C, de Vries S (2004) J Am Chem Soc 126:11103-11112

15. Tarlov MJ, Bowden EF (1991) J Am Chem Soc 113:1847-1849

16. (a) Wei JJ, Liu HY, Dick AR, Yamamoto H, He YF, Waldeck DH (2002) J Am Chem Soc 124:9591-9599 (b) Wei JJ, Liu H Y, Khoshtariya DE, Yamamoto H, Dick AR, Waldeck DH (2002) Angew Chem Intl ed 41:4700-4703

17. Willner I, Katz E (2000) Angew Chem Int Ed 39:1180-1218

18. Chi QJ, Zhang J, Nielsen JU, Fris WP, Chorkendorff IB, Canters GW, Andersen JET, Ulstrup J (2000) J Am Chem Soc 15:4669-4679

19. Mukund S, Adams MWW (1991) J Biol Chem 266:14208-14216

20. (a) Bevers LE, Bol E, Hagedoorn P-L, Hagen WR (2005) J Bacteriol 187:7056-7061 (b) Hagedoorn P-L, Freije JR, Hagen WR (1999) FEBS Lett 462:66-70 (c) Silva PJ, van den Ban ECD, Wassink H, Haaker H, de Castro B, Robb FT, Hagen WR (2000) Eur J Biochem 22:6541-6551

21. Hagen WR (1989) Eur J Biochem 182:523-530

22. ASTM standard E902-88 (1991) Surf Interface Anal 17:889-892

23. Shirley DA (1972) Phys Rev B 5:4709-4714

24. Chastain J (1992) Handbook of X-ray Photoelectron Spectroscopy, Perkin-Elmer Corporation, Eden Prairie USA

25. Armstrong FA, Camba R, Heering HA, Hirst J, Jeuken LJC, Jones AK, Léger C, McEvoy JP (2000) Faraday Discuss 116:191-203

26. Hirst J, Armstrong FA (1998) Anal Chem 70:5062-5071

27. Bard AJ, Faulkner LR (2001) Electrochemical methods: fundamentals and applications, 2nd ed, John Wiley & Sons

28. Heering HA, Mondal MS, Armstrong FA (1999) Anal Chem 71:174-182

29. Feldberg SW, Rubinstein I (1988) J Electroanal Chem 240:1-15

30. EL Kasmi A, Leopold MC, Galligan R, Robertson RT, Saavedra SS, EL Kacemi K, Bowden EF (2002) Electrochem Comm 4:177-181

31. Hirst J, Jameson GNL, Allen JWA, Armstrong FA (1998) J Am Chem Soc 120: 11994-11999

32. Jeuken LJC (2003) Biochim Biophys Acta 1604:67-76

33. Powell CJ (2003) NIST Standard Reference Database 20, Version 3.4 (Web Version), *http://srdata.nist.gov/xps/*

34. Cavalleri O, Gonella G, Terreni S, Vignolo M, Pelori P, Floreano L, Morgante A, Canepa M, Rolandi R (2004) J Phys-Condens Mat 16: S2477-S2482

35. (a) Cecchet F, Rudolf P, Rapino S, Margotti M, Paolucci F, Baggerman J, Brouer AM, Kay ER, Wong JKY, Leigh DA (2004) J Phys Chem B 108:15192-15199 (b) Arnold R, Azzam W, Terfort A, Wöll C (2002) Langmuir 18:3980-3992

36. Skinner WM, Nesbitt HW, Pratt AR (2004) Geochim & Cosmochim Acta 68:2259-2263

37. Best SA, Brant P, Feltham RD, Rauchfuss TB, Roundhill DM, Walton RA (1977) Inorg Chem 16:19776-1979

38. Kelemen SR, George GN, Gorbaty ML (1990) Fuel 69:939-944

39. Priem AH, Klaassen AAK, Reijerse EJ, Meyer TE, Luchinat C, Capozzi F, Dunham WR, Hagen WR (2005) J Biol Inorg Chem 10:417-424

40. The surface coverage was calculated from the areas under the voltammetric peaks of native ferredoxin at low scan rate and the geometric electrode area multiplied by a roughness factor of 1.5 (assuming that polishing with particles with radius r yield scratches of depth ~ r, thus a contour area that is $\pi r/2r$ ~ 1.5 times the macroscopic area).

41. La Mar GN (2001) Biochemistry 41:12498-12508

42. Hsieh YC, Liu MY, Gall LJ, Chen CJ (2005) Acta Crystallogr Sect D-Biol Crystallogr 61:780-783

43. Sapra R, Karine B, Adams Michael WW (2003) Proc Natl Acad Sci U.S.A. 100:7545-7550

44. Page CC, Moser CC, Chen X, Dutton PL (1999) Nature 402:47-51

45. (a) Heering HA, Bulsink YBM, Hagen WR, Meyer TE (1995) Biochemistry 34:14675-14686 and references cited therein, (b) Contera SA, Iwasaki H (2002) Ultramicroscopy 91:231-243

Supplementary Material

Voltammograms

In Figures S1 and S2, the voltammograms are plotted from which the peak parameters in Figure 2 are derived. These are obtained by subtracting the blank scans (gold coated with invertase) from the data scans (gold with immobilized ferredoxin). The blank scans are normalized to the capacitive current of the data scans to correct for differences in roughness after polishing. In addition, an exponential baseline is subtracted to compensate for most of the difference in hydrogen evolution background between the two electrodes:

$$baseline = p\,E + q + r\exp(-\,s\,E)$$

Additional linear baselines for each individual peak were used to determine the maxima (not implemented in Figures S1 and S2).

Simulations

The simulations were carried out at $T=295$ K, $\alpha=0.5$, and $n=1$, with free parameters k_{xo}, k_{ox}, k_0, $E^{0'}$, and $\Delta E_p(v\to 0)$ to fit to the observed peak positions, midpoint potentials and peak separations, as described in the main text, cycling from equilibrium at +0.2 V with a lower vertex of -0.8 V. UQR is implemented in the simulations by using $E^{0'}$(cathodic)$=E^{0'}-\Delta E_p(v\to 0)/2$ and $E^{0'}$(anodic)$=E^{0'}-\Delta E_p(v\to 0)/2$. The resulting cyclic voltammograms (normalized to the peak height of a fully reversible, non-gated voltammogram at the given scan rate) are plotted in Figure S3.
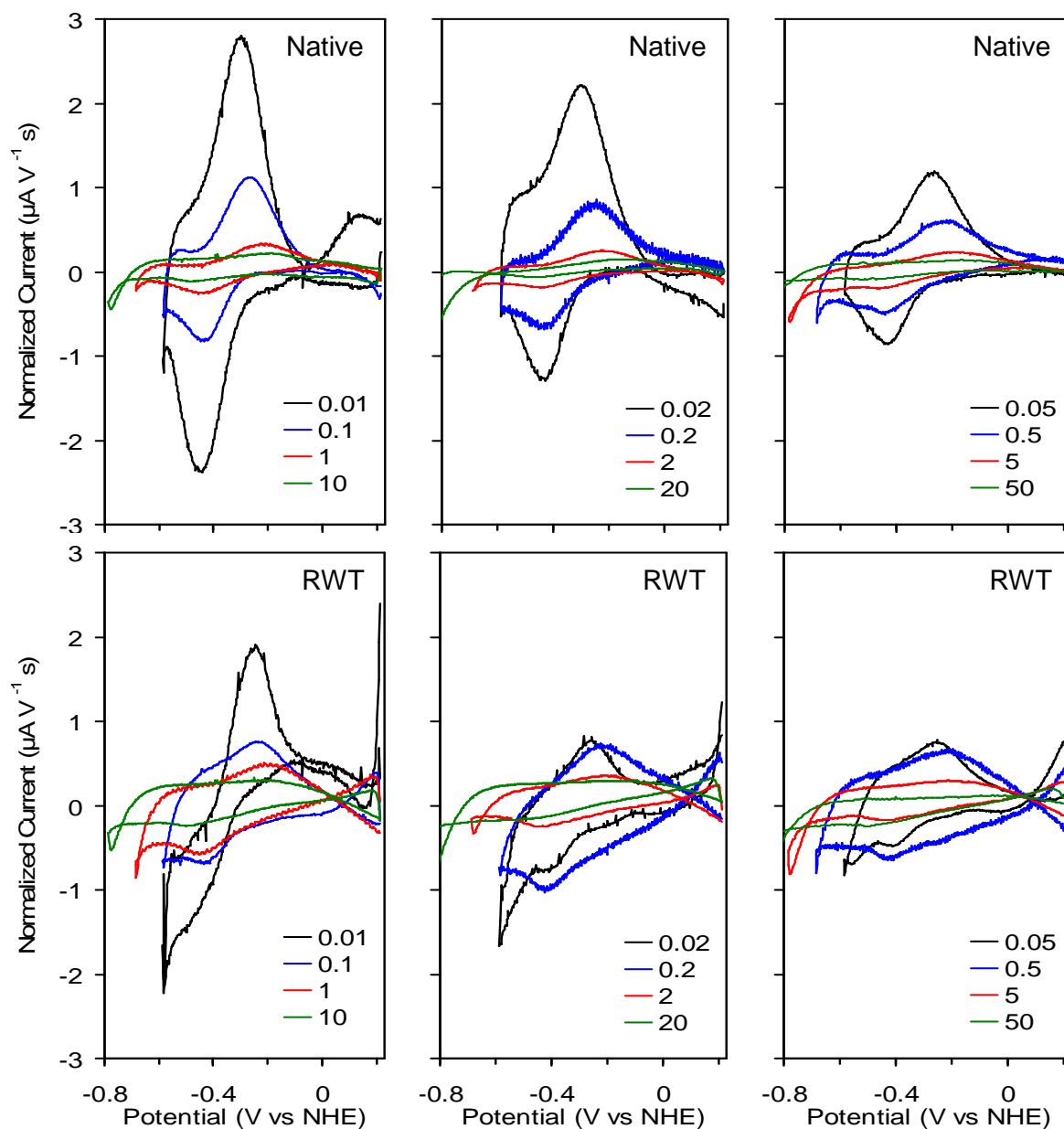
Figure S1. Voltammograms of native (top) and RWT (bottom) *Pfu*Fd. The inverase blank and baseline are subtracted, and the scans are normalized to scan rate. The panels are in order of measurement (from left to right, and from low scan rate to high scan rate). The legends are the scan rates in V/s.

Figure S2. Voltammograms of C48S (top) and C21S (bootom) *Pfu*Fd. The inverase blank and baseline are subtracted, and the scans are normalized to scan rate. The panels are in order of measurement (from left to right, and from low scan rate to high scan rate). The legends are the scan rates in V/s.
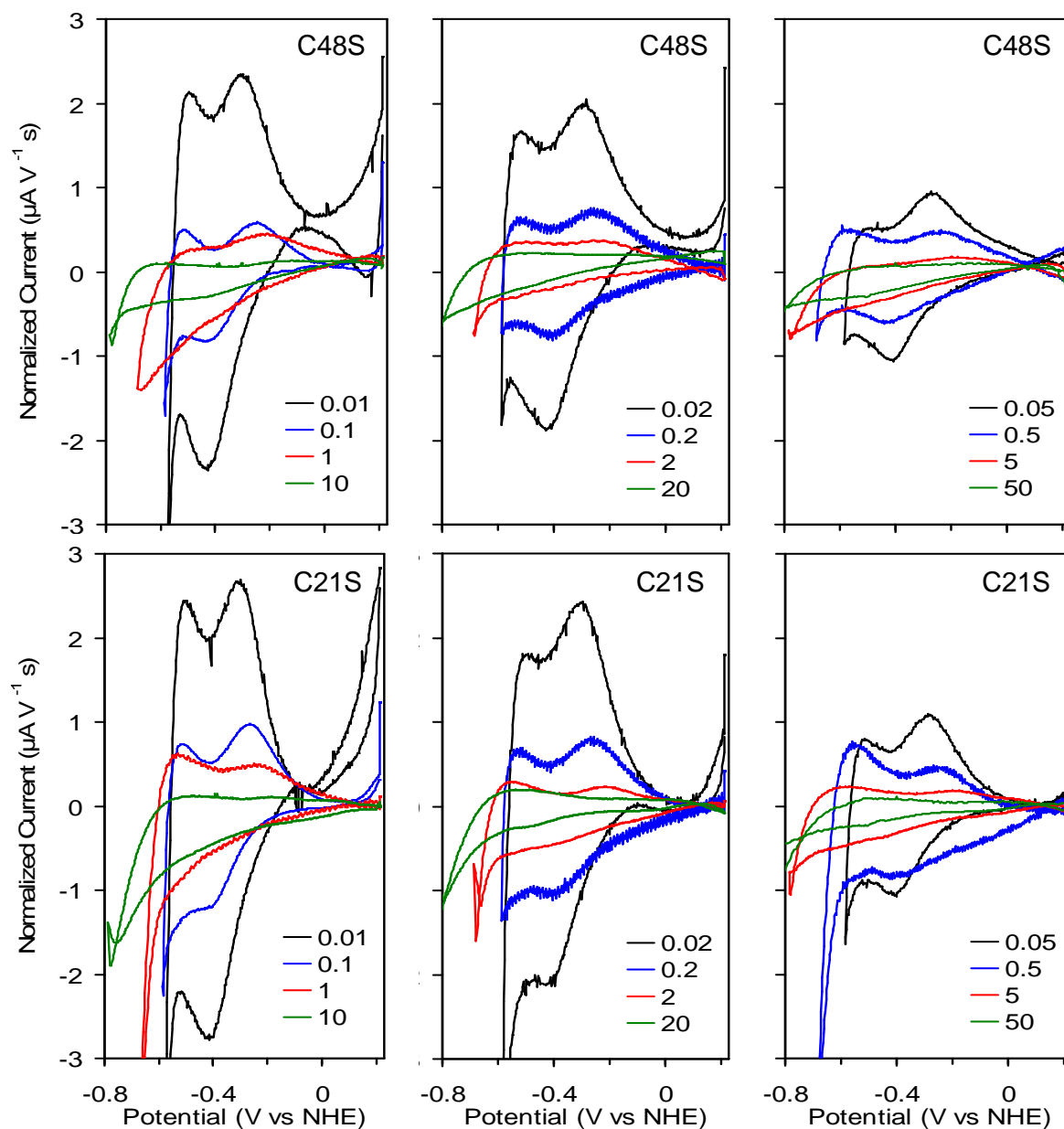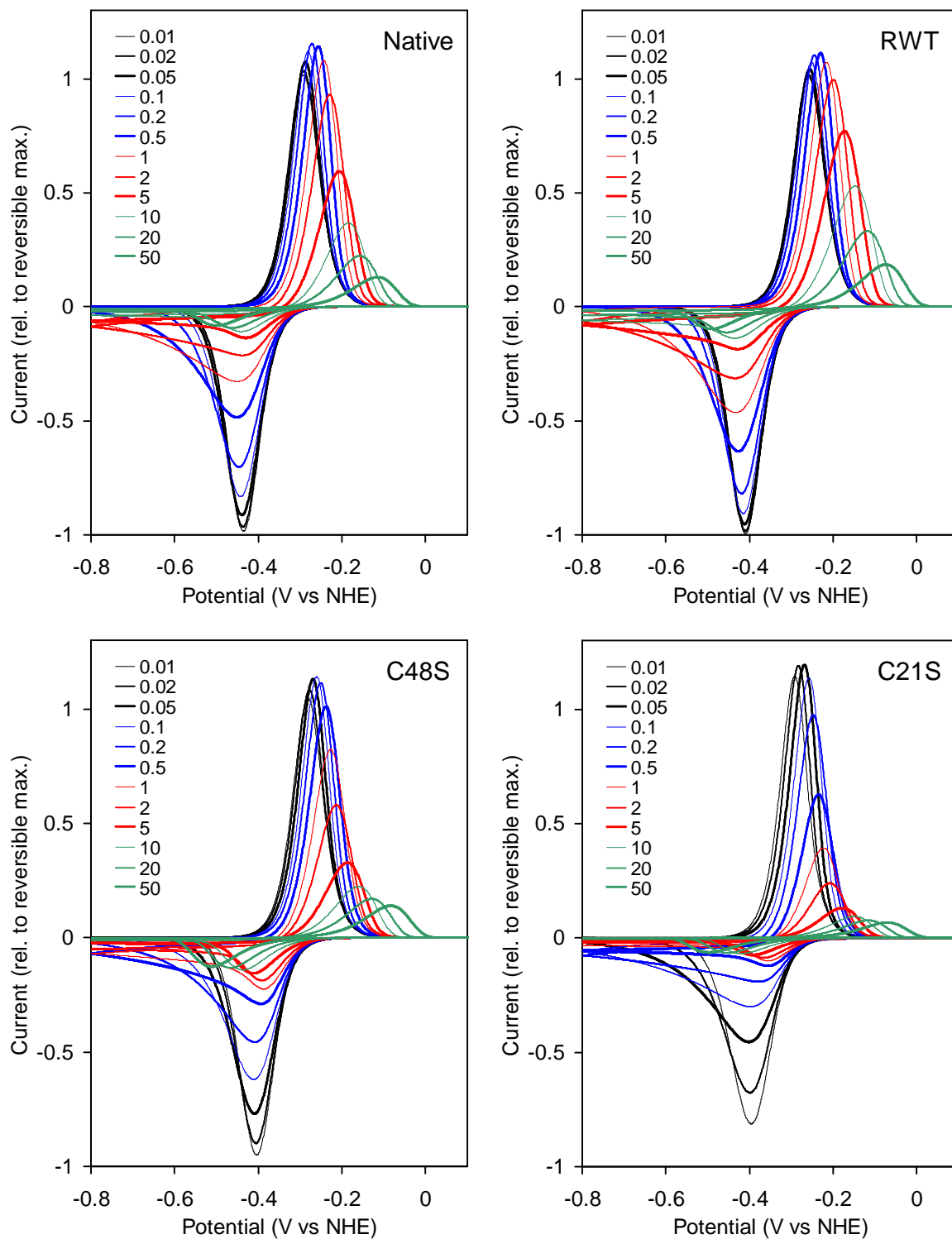
Figure S3. Cyclic voltammetry simulations according to Eqns 1-3, and the parameters listed in Table 1. The legends are the scan rates in V/s.

Chapter five

Electrocatalytic aldehyde oxidation by *Pyrococcus furiosus* hyperthermophilic tungsten-containing oxidoreductases on ferredoxin-modified gold electrode.

This chapter is to be submitted.

ABSTRACT

The hyperthermophilic aldehyde:ferredoxin oxidoreductase (AOR) and glyceraldehyde-3-phosphate (GAP) oxidoreductase (GAPOR) from *Pyrococcus furiosus* form complexes with their native redox partner ferredoxin (Fd), chemisorbed on gold. At room temperature, voltammetry of the immobilized complexes reveals the non-turnover responses both in the absence and in the presence of respective substrates crotonaldehyde and GAP. At high temperature and in the presence of substrate, electrocatalytic turnover current is observed. With GAPOR, a well-developed response is observed at room temperature and pH 7.4, consisting of the [4Fe-4S] clusters of the enzyme and Fd, at -368mV and -383 mV, respectively. At 60ºC a clear catalytic wave is observed upon addition of the substrate GAP, which is not inhibited by the product 3-phosphoglycerate. With AOR, a broad, reversible voltammetric response is observed due to overlapping potentials of the Fd and AOR [4Fe4S] clusters in addition to several W species. The AOR / Fd complex formation on the electrode is corroborated by elipsometric analysis. At 80ºC and in the presence of crotonaldehyde, three catalytic peaks are observed. Remarkably, these three aldehyde oxidation peaks are followed by the electrocatalytic reduction of the produced acid. The averages of the oxidation and reduction peaks are found at -380 mV, -270 mV and -102 mV. The bi-directional and peak-shaped electrocatalytic responses are indicative of a rapid switch-off of the enzymatic

activities at high overpotentials. Colorimetric analysis and dye mediated optical assays confirm the reversibility and switching of AOR activity. A minimal mechanism is proposed, involving a switch between an aldehyde oxidizing form and an acid reducing form of the enzyme. The present work opens the way for the application of Fd electrodes in achieving controlled reduction of carboxylic acids at preparative scale.

INTRODUCTION

Pyrococcus furiosus is a hyperthermophilic, heterotrophic and strictly anaerobic organism and it utilizes peptide as main carbon source. Numerous studies have shown that several oxidoreductases in combination with the small electron transport protein, ferredoxin play important role in the metabolic activity of the organism. Among the five thus far purified tungsten-containing oxidoreductases, only glyceraldehyde-3-phosphate oxidoreductase (GAPOR) has been shown to be involved in glycolysis (1). Aldehyde oxidoreductase (AOR), formaldehyde oxidoreductase (FOR) and recently purified WOR5 (2) have been showed to have a broad substrate specificity for aliphatic and aromatic aldehydes. Though the physiological roles for these enzymes are not known, it has been suggested that they are involved in amino acid catabolism. One other tungsten-containing putative oxidoreductase (WOR4) has been purified but no activity has been determined yet (3). In addition to these tungsten enzymes a few other enzymes like pyruvate ferredoxin oxidoreductase (POR), indolepyruvate oxidoreductase (IOR) (4), 2-ketoglutarate oxidoreductase (KGOR) (5), 2-ketoisovalerate oxidoreductse (VOR) (6), ferredoxin:NAD(P)$^+$ oxidoreductase and membrane-bound hydrogenase have been described to play an important role in the metabolism of the organism. All these enzymes use ferredoxin as a redox partner.

Usually, redox enzymes require a natural redox partner (here: ferredoxin) to sustain catalysis, more precisely to balance the substrate-product half reaction. The detailed mechanism of single or multi-electron redox reactions mediated by these enzymes can be studied in great detail by the use of direct or mediated electrochemistry. In this method the natural redox partner can be replaced either by a bare electrochemical working electrode or by a modified working electrode (by immobilizing the redox partner on the working electrode). However, the use of electrochemical methods to study protein electron-transfer kinetics, thermodynamics, and reaction mechanisms has only slowly gained acceptance over the last

three decades. The pioneering work by the groups of Hill and of Kuwana in 1977 triggered the use of direct electrochemistry for both electron-transfer proteins and redox enzymes (7, 8). Denaturation of the protein on electrode surfaces, slow diffusion, and complicated organization of the cofactors are the major reasons of a limited use of this approach in enzyme studies in the past. However, in recent days these problems have mostly been overcome by the modification of the electrode (by DNA, spacer groups etc) and / or the proteins (mutational approach) (9, 10, 11). Electrochemistry has been successfully applied in studying the intricate properties of some electron-transfer proteins like ferredoxin, cytochrome *c* etc. due to the smaller size and simple cofactor. (11-15).

Redox enzymes with a molecular mass of typically 50 kDa and above and with complex metal clusters, such as tungsto-enzymes, pose significant problems in terms of achieving understandable responses in electrochemistry, and voltammetric investigations of such enzymes are scarce. However, Anderson *et al* first described the rate limiting events in the electrocatalytic activity of the Mo-enzyme nitrate reductase (16). Using protein film voltammetry this and other groups demonstrated that the activity follows a pattern of inactivation and activation steps, revealing oxidation-state dependent substrate affinity. (17-18). Kerensa *et al* first described direct electrochemical investigation of the catalytic activity of *E.coli* dimethyl sulfoxide reductase (DMSOR) on a graphite electrode (19), revealing a maximum activity at intermediate potentials, associated with Mo(V). However, the first non-turnover Mo $^{VI/V}$ and Mo $^{V/IV}$ responses in the direct electrochemistry of *Rhodobacter capsulatus* DMSOR in the absence of substrate were described by Aguey-Zinsou *et al* (20). The same group has also reported non-turnover responses from the molybdenum and heme cofactors of sulfite oxidoreductase (21) and from all the cofactors of xanthine oxidoreductase of *R. capsulatus* (22). No non-turnover or catalytic voltammetric investigation has been reported yet for tungsten containing redox enzymes. Recently, we have successfully

developed and characterized a *Pfu*Fd modified polycrystalline gold electrode (23). Here we describe direct electrochemical investigations on this electrode that reveal non-turnover and catalytic responses from both the Fe-S clusters and tungsten centers from two associated redox enzymes from *P. furiosus* namely AOR and GAPOR.

AOR is a homodimeric protein containing one [4Fe-4S] cubane and a tungsten cofactor in each subunit and a single tetrahedral iron atom at the interface of the subunits. AOR has been subjected to extensive EPR studies by Adams *et al* and Hagen *et al* (24, 25). Adams *et al* demonstrated that the spectrum of oxidized AOR exhibits an EPR signal typical for W (V). Interestingly, the redox titration revealed three major species of the W center, labeled as the "low", "mid" and "high" potential forms (24).

At temperature above 60°C pure AOR catalyzes the oxidation of a variety of aliphatic aldehydes using methyl viologen or *Pyrococcus furiosus* ferredoxin (*Pfu*Fd) as the electron acceptor. The highest specific activity for oxidation of crotonaldehyde was obtained at 80°C using either methyl vilogen or *Pfu*Fd as the electron acceptor. The enzyme also exhibits sensitivity towards oxygen, temperature, pH and substrate concentration (26). However, a detailed mechanism elaborating the redox activity of the enzyme at its different potential forms (low, mid and high-potential), in particular a possible switching among the different potential forms and the activity at these potentials under a given set of condition, has be not elucidated.

GAPOR from *P. furiosus* is another tungsten-containing enzyme and has been well studied by Mukund *et al* (1) and Hagedoorn *et al* (27). Studies revealed that the tungsten centre cycles among the redox states VI, V and IV and the midpoint potentials range from *ca.* -600 mV to *ca.* -400 mV. In solution voltammetry Hagedoorn *et al* also demonstrated the appearance of a catalytic wave upon addition of the substrate, glyceraldehyde-3-phosphate and the physiological electron acceptor, *Pfu*Fd to the enzyme in solution (27). However, direct

evidence for the formation of an Fd-GAPOR complex and its characterization has not been reported yet. The catalytic activity of another enzyme, WOR5 using hexanal as the substrate has also been observed in a similar setup for solution voltammetry (2). However, due to the fast denaturing of the enzyme on the electrode this enzyme has not been applied to the *Pfu*Fd electrode.

In this paper we report the application of the *Pfu*Fd modified electrode towards the elucidation of the functional details of GAPOR and AOR from *P. furiosus*. While GAPOR displays an uncomplicated sigmoidal catalytic voltammogram on the *Pfu*Fd electrode, AOR reveals multiple catalytic species and potential-dependent switching. The three major forms of AOR identified by Adams and co-workers (24) at low-, mid- and high potentials are observed in the catalytic voltammograms. Notably, these forms of AOR show reversible oxidation and reduction of aldehyde and acid, respectively, and display a maximum activity at low overpotential. A minimal model is proposed that incorporates both the voltammetric and cuvette assay results.

METHODS AND MATERIALS

Purification of proteins. [4Fe-4S] *Pfu*Fd has been purified anaerobically by the protocol described earlier (28). With the same protocol a mixture of [3Fe-4S] *Pfu*Fd and [4Fe-4S] *Pfu*Fd was obtained when the purification was carried out under aerobic condition. *Pfu* AOR and GAPOR enzymes were a kind donation from Dr. P.-L. Hagedoorn, purified according to the protocols described by Mukund and van der Oost (26, 29).

Electrochemistry.

*a) Setup***.** An anaerobic, isothermic setup was used, as described previously (30), and modified with a thermostatted water jacket. A 1.6 mm diameter gold disk electrode (Bioanalytical Systems) was used as working electrode. The gold surface was polished with a water-based aluminum oxide suspension (Buehler, 1 µm particles), thoroughly rinsed, and dried. An Ag/AgCl/saturated KCl electrode (Radiometer REF201, +202 mV at 22 ^{0}C, 164 mV at 60 ^{0}C, and 144 mV at 80 ^{0}C, all versus NHE) was used as reference electrode, and a Pt wire was used as counter electrode. All the potentials are reported versus NHE. The three electrodes were connected to a digital potentiostat (EcoChemie µAutolab type II, or Autolab Pstat 10) and staircase cyclic voltammograms were recorded.

*b) Preparation of the ferredoxin electrode***.** Immobilization of ferredoxin was accomplished via the thiol groups of the free cysteines at position 21 or 48, as previously reported [23]. In short: prior to immobilization *Pfu*Fd was reduced by freshly prepared tris[2-carboxyethyl] phosphine (TCEP, Pierce). A droplet of 25 µl was subsequently applied to the gold electrode, containing 3 µM reduced ferredoxin, 2 mM TCEP, 1.5 M NaCl and 25 mM N-(2-hydroxyethyl) piperazine-N-(2-ethanesulfonate) (Hepes, Merck) at pH 7.2, and voltammograms were recorded until a stable response was obtained.

c) GAPOR electrochemistry. Fd voltammograms were recorded at 60°C until a stable signal for [4Fe-4S] was obtained. The droplet was then replaced by a new droplet of 25 µl volume containing 25 mM Hepes, pH 7.2 and ca. 5 µM GAPOR. Cyclic voltammograms were recorded until a stable response from GAPOR was obtained. The substrate GAP was then added to a final concentration of 7.5 mM, and cyclic voltammograms were recorded between +0.150 V and -0.650 V vs NHE. Although a temperature of 60°C is sub-physiological, at higher temperature the substrate becomes increasingly unstable (27). In another set of

experiments an excess of 3-PG (~25 mM) as an inhibitor was added prior to the addition of GAP.

d) AOR electrochemistry. In this case cyclic voltammograms were recorded between +0.2 V and -0.65 V vs NHE until a stable response for the [4Fe-4S] cluster of ferredoxin was obtained at room temperature (22 ^{0}C). The droplet was then replaced by a new droplet of 25 µl volume containing 25 mM Hepes, pH 7.2 and ca. 3.5 µM *Pfu*AOR. Cyclic voltammograms were then recorded at room temperature between +0.35 V and -0.7 V vs NHE. In case the ferredoxin electrode was prepared from a mixture of [4Fe-4S] and [3Fe-4S] forms, the voltammograms of co-adsorbed AOR were recorded between +0.50 V and -0.7 V vs NHE. Once the stable response from AOR was attained, 2 µl 7 mM crotonaldehyde was added to the droplet and voltammetry was continued. Then the temperature was gradually increased to 80°C.

Colorimetric analysis for crotonaldehyde. Purpald$^®$, 4-amino-3-hydrazino-5-mercapto-1,2,4-trizole (Aldrich) was used to detect the amount of crotonaldehyde remaining or formed after enzymatic conversion of crotonaldehyde or crotonic acid, according to the protocol described by Dickinson and Jacobs (31). After allowing the enzymatic conversion for 15 min., the anaerobic reaction vial was cooled to 22°C, and 34 mM Purpald was added to form an amin-al intermediate, followed by 36 mM H_2O_2 to obtain the colored product. The reaction mix was then incubated for 30 minutes at room temperature. A characteristic purple color was obtained in the presence of crotonaldehyde.

Elipsometry. Gold nanoparticles of ca. 14 nm were prepared by the sodium citrate reduction method (32). The nanoparticles obtained were then coated with purified *P. furiosus* ferredoxin via the thiol group of free cysteines by adding 10 nM ferredoxin to a 2 nM colloidal solution of gold nanopaticles. This solution was then concentrated by 50 fold over a 100 kDa filter according to the protocol described by Matyushin et al (33). Using a Mirco-arrayer (GMS

417, Genetic Microsystems) *Pfu*AOR (from an 88 nM stock solution in 50 mM EPPS buffer pH 8.4) or chicken serum albumin (CSA) (from a 100 µg/ml solution in water) were spotted on the activated gold chips by following the procedure described by Matyushin et al (34). In short, gold chips were prepared by sputtering multi-layers of thin metal films of 10 to 100 nm thickness on a glass surface, followed by drying and cleaning steps. A clean chip surface was then coated with 0.1% cystamine (Cystamine dihydrogen chloride, Sigma) in Milli Q water for 15 minutes followed by a washing step and a drying step by a vacuum centrifuge. A 0.5% solution of divinylsulfone (Aldrich) in 100 mM Na_2CO_3, pH 9 was then applied to the chip for the activation of surface-bound cystamine, i.e. for the activation of the chip surface. A ferredoxin coated gold nanoparticle preparation was then applied on the AOR- or CSA-containing chip and incubated at room temperature for 60 minutes. To remove non-specifically bound ferredoxin-coated gold nanoparticles the chip was then subject to multiple washing steps, first with Milli Q, then with a mixture of 300 mM NaCl plus 0.5% detergent (triton) in 50 mM Tris buffer of pH 7.4, then two times with 100 mM NaCl, and finally with Milli Q . Imaging Ellipsometry (I-Elli2000, Nanofilm Technology, Germany) was used to visualize the ferredoxin-coated nanoparticles bound to immobilized AOR or CSA on the chip.

RESULTS

Uncomplicated electrochemistry of GAPOR demonstrates functionality of Fd electrode.

Co-adsorption of GAPOR. Fd monomers were first chemisorbed on the gold electrode in the presence of 1 M NaCl and 2 mM TCEP and 25 mM Hepes, pH 7.2. After removing the original droplet the electrode was washed twice, and voltammograms were recorded at 22 and 60 °C. The determined midpoint potential of Fd is -368 mV at 22°C, and -372 mV at 60 °C indicating that the redox potential does not significantly differ with temperature, and is equal within the experimental error to the previously reported *Em* = -364 mV of chemisorbed *Pfu*Fd

[23]. The redox enzyme GAPOR was then applied to the droplet at a final concentration of 6 μM. An additional shoulder was observed in the voltammogram suggesting the appearance of an additional redox couple (Fig 1A). An Em = -383 mV was measured from the difference voltammogram obtained by subtracting the Fd-only voltammogram from the Fd+ GAPOR voltammogram (Fig 1B). This value is lower than the value (Em = - 335 mV) reported from EPR-monitored bulk titrations at 50°C and pH 8 for the [4Fe-4S] cluster in GAPOR (27). The peak width at half maximum current is around 100 mV which is equal to the expected value for a single-electron process at 60 °C (35). We therefore tentatively assign the -383 mV couple to the [4Fe-4S] cluster of the enzyme. The midpoint potential is down-shifted relative to the value in solution, possibly due to interaction with the negatively charged ferredoxin layer.

Surface coverage. The average area under the Fd peaks is 404 nC which equates to 4.2 pmol on a area of 7 mm^2 or 59.8 pmol/cm^2. Considering the footprint area of 6.1 nm^2 per Fd monomer, obtained from the crystallographic structure, and assuming a full layer of monomers (as expected at high ionic strength [23]) this yields an electrode surface roughness factor of 2.2. After subtracting the Fd voltammogram (Fig 1B) from the GAPOR plus Fd voltammogram, we obtained an average peak area of 96 nC on the 7 mm^2 electrode. Assuming that only the one-electron redox couple at -383 mV is due to the [4Fe-4S] cluster of GAPOR, this yields a surface coverage of 14.2 pmol/cm^2. With the surface roughness factor of 2.2, a projected area of 26 nm^2 per molecule or a diameter of 5.7 nm for GAPOR was obtained, which is close to the globular dimensions expected for a 73 kDa protein. This implies that a densely packed monolayer of GAPOR is co-adsorbed on top of a closely packed chemisorbed monolayer of Fd, with a coverage ratio of 4.2 Fd per GAPOR.
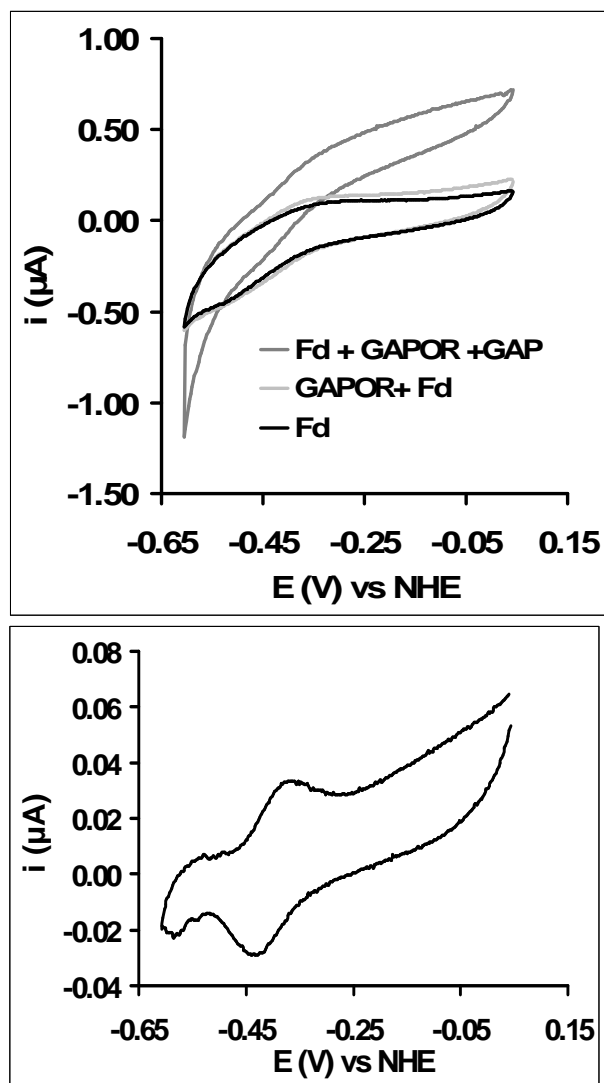
Figure 1 A: Cyclic voltammograms of *Pfu*Fd only, *Pfu*Fd + GAPOR and *Pfu*Fd + GAPOR + GAP at 60 °C. *Pfu*Fd was first chemisorbed on a polycrystalline gold electrode at 3 µM concentration in 25 mM Hepes pH 7.2 and 2 mM TCEP, thereafter 5 µM GAPOR and 7.5 mM GAP were added sequentially. The scan rate was 20 mV/S.

Figure 1 B: Difference cyclic voltammogram obtained by subtracting the *Pfu*Fd-only from the *Pfu*Fd + GAPOR voltamogram.

Electrocatalysis. Upon addition of the substrate GAP the anodic current inceases at 60°C, resulting in a characteristic catalytic wave, centered at a mid-wave potential of -384 mV, which is close to the observed non-catalytic GAPOR midpoint potential. No inhibition was

observed by the product 3-PG at a final concentration of 10 mM, added either at the beginning or at a later stage during catalysis. The derivative peaks have FWHM of ~100 mV suggesting a one-electron rate-limiting step in the two-electron oxidation reaction. These findings suggest that the rate-limiting step scales with the fraction of oxidized [4Fe-4S] cluster in GAPOR, thus that this cluster is involved in electron relay between the W active site and the electrode. The maximum current for the catalytic wave is 0.20 µA on the 2 mm^2 electrode, which together with the GAPOR coverage of 14.2 pmol/cm^2 yields an aldehyde turnover rate of 3.6 s^{-1}. This rate is significantly lower than the turnover rate of 96 s^{-1} obtained in a solution containing 150 µM Fd and 10 mM GAP (27).

Electrochemistry of AOR is complex but demonstrates functionality of the Fd electrode.

Co-adsorption of AOR. Voltammograms were recorded for [4Fe-4S] *Pfu*Fd chemisorbed on the gold electrode at room temperature and at pH 7.2. A typical response for chemisorbed [4Fe-4S] Fd was obtained at Em = -368 mV ±10 mV. Upon addition of AOR to the droplet, an additional broad but reversible redox couple appeared with a midpoint potential of -502 ±20 mV.
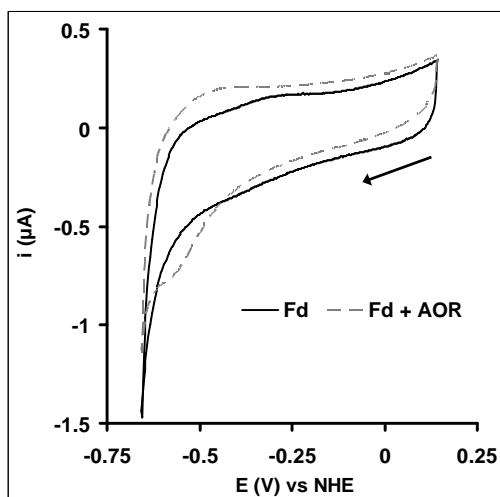

Figure 2: Cyclic voltammograms of a gold electrode with chemisorbed *Pfu*Fd, before and after addition of 3.5 µM AOR in 25 mM Hepes, pH 7.2 at 25 °C, with a scan rate of 100 mV/s.

Within 2-3 scans at 100 mV/s the peaks reached a maximal and stable intensity. The response persisted when the electrode was rinsed and a new buffer droplet was added. Premixed AOR and Fd, anaerobically incubated at room temperature for one minute, gave a similar response on bare gold. When only AOR was applied under the same conditions to the bare electrode, no response was obtained. These observations lead to the conclusion that the low-potential response is due to AOR, and that AOR co-adsorbs with Fd on the electrode.
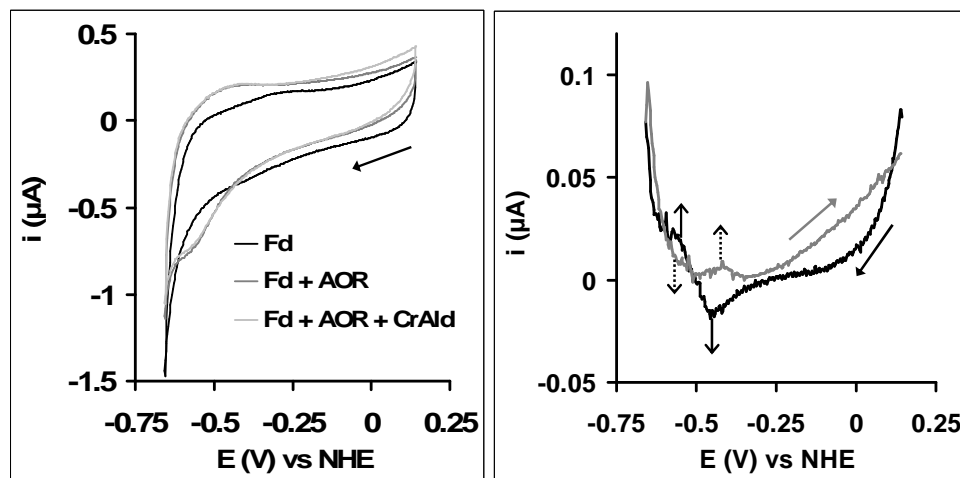

Figure 3: Left: Cyclic voltammograms of a gold electrode with chemisorbed *Pfu*Fd, and after subsequent additions of 3 µM AOR and 0.5 mM crotonaldehyde in 25 mM Hepes pH 7.2 at 25 °C, scan rate 100 mV/s. Right: The voltammogram in the presence of both AOR and crotonaldehyde minus the voltammogram with AOR only. The normal arrows indicate the scan direction; the bold arrows indicate the changes in the observed voltammetric peaks upon addition of crotonaldehyde (solid: appearing; dotted: disappearing).

The AOR reduction and oxidation peaks have a full-width-at-half-height of around 145 mV. This is significantly wider than the expected 90 mV for a single one-electron process at 22°C (35), which suggests that this broad response is formed by an envelope encompassing multiple redox couples. Adams *et al* have reported several redox couples of *Pfu*AOR (24), which may all contribute to this voltammetric response. The reduction potentials of "low

potential AOR" at -436 mV for W $^{IV/V}$ and -365 mV for W $^{V/VI}$, and those of "spin-coupled AOR" at <-550 mV for W $^{IV/V}$ and -443 mV for W $^{V/VI}$ are likely to contribute to the envelope. We also expect that the response from the [4Fe-4S] cluster of AOR is a component, because this is the primary electron donor/acceptor site for ferredoxin. However, in solution the midpoint potential is -350 mV, which would place the response on the edge of the observed envelope, overlapping with the Fd peaks. The difference between the voltammograms after and before adding crotonaldehyde to the droplet containing Fd and AOR at room temperature (at which temperature the enzyme is not active) reveals a new, reversible redox couple at Em = -422 mV. Concomitantly, part of the AOR envelope (Fig 3, Right, dotted arrows) decreases in intensity, revealing a reversible couple at -535 mV. This suggests that one of the W redox couples shifts from -535 mV to -422 mV upon binding of substrate.

After subtracting the Fd blank, we obtained an average AOR envelope area of 0.32 µC on the 7 mm^2 electrode, which yields a surface coverage of 16 pmol/cm^2, assuming 3e per AOR. With the surface roughness factor of 2.2 a projected area of 23 nm^2 per molecule or a diameter of 5.4 nm for AOR was obtained, which is close to the globular dimensions expected for a 67 kDa protein monomer. This implies that a densely packed monolayer of AOR is co-adsorbed on the Fd electrode.

At room temperature, the AOR-Fd complex is very stable, even persisting after washing. However, at 80ºC the non-catalytic response from AOR fluctuates over time, suggesting that at physiological temperature the AOR / Fd interaction is dynamic, as expected. The stability of the Fd electrode was extensively investigated at different temperatures starting from 25ºC up to 80ºC. As observed in the case of GAPOR plus Fd at 60ºC (see above), the chemisorbed ferredoxin retains its structural integrity and functional activity at 80ºC. Therefore, the

fluctuating AOR response at 80ºC is not due to the collapse of the ferredoxin, but is a characteristic of the AOR/Fd interaction.

The apparent midpoint potential of the envelope only displayed a small shift with pH, decreasing 20 mV upon changing the pH from 7.2 to 8.4, in agreement with the work of Mukund *et al* (26). Attempts to measure the potentials at pH 9 were unsuccessful due to instability of the Fd layer.

***Visualisation of Fd-AOR complex by Elipsometry*.** To verify the formation of AOR-Fd complexes, we have carried out binding experiments in an aerobic setup followed by elipsometric visualisation. Gold nanoparticles, coated with *Pfu*Fd, were applied to a gold chip on which spots of AOR were immobilized. Elipsometric analysis revealed the immobilization of the Fd-modified gold nanoparticles on the AOR spots (Figure 4A, green pixels). The nanoparticles response (observed layer height) persisted through repeated washing and drying
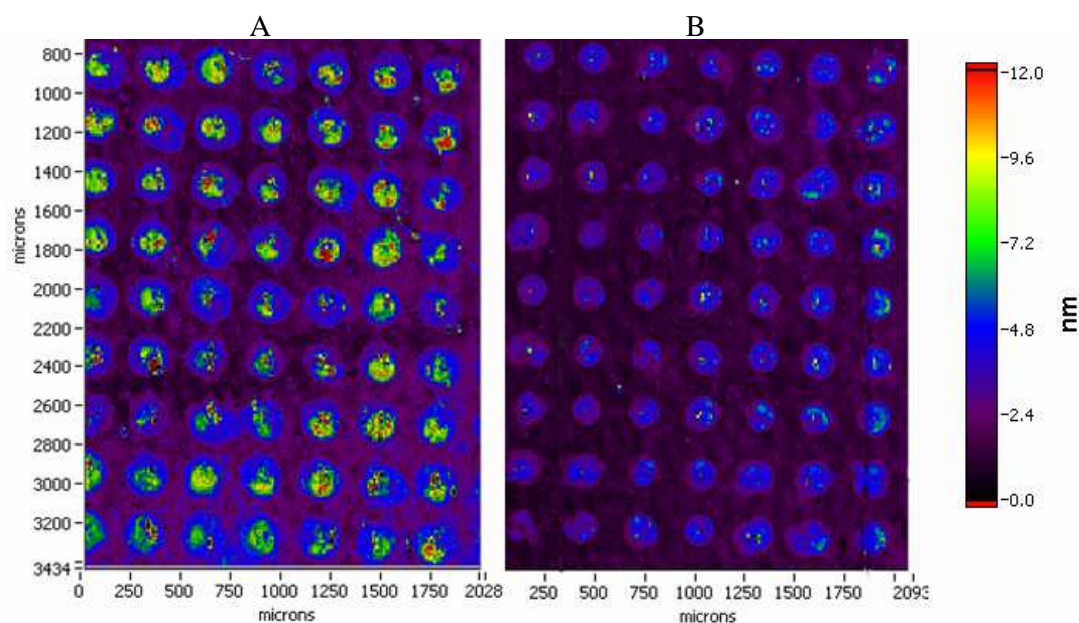

Figure 4: Elipsometric thickness map of AOR and chicken serum albumin (CSA) immobilized on a gold surface, and incubated with Fd-coated gold nanoparticles. Chip A: Spots of immobilized AOR; Chip B: Spots of immobilized CSA. Visualization area ~2 x 3 mm; layer thickness (due to adsorbed protein and nanoparticles) along the Z axis in nm.

steps and also did not collapse during the incubation at 4ºC for several days. In another set of experiments chicken serum albumin (CSA) was immobilised on the chip instead of AOR, and Fd coated gold nanoparticles were applied as above. No immobilized nanoparticles were observed when analysed by elipsometry (Figure 4B). This implies that the nanoparticles observed in Figure 4A were immobilized via the formation of AOR-Fd complexes.

Reversible electrocatalysis. At high temperature (80ºC) and in the presence of crotonaldehyde, a clear catalytic oxidation current is observed (figure 5). Remarkably, at high potential, the catalysis shuts off very rapidly, yielding a "half-peak" like shape, and appears to switch off faster when the current is higher (compare the oxidation peaks in Figure 5 in the order B, A, and C). In addition, the reverse scan reveals a catalytic reduction current, which also shows a switch-off at high driving force (low potential) when the activity is high (Figure 5B). Moreover, not a single pair of peaks, but in fact three distinct catalytic redox couples are observed, located around the average potentials -380 mV, -270 mV, and -102 mV. We propose that these correspond to "low potential AOR", "mid-potential AOR" and "high potential AOR", reported by Adams et al (24). In fact, the "mid-potential AOR" is visible as a minor trace of activity (the peaks indicated by purple broken lines in Figure 5), in agreement with the <3% EPR intensity (24), while the other two forms are dominant in both the catalytic voltammograms and the reported EPR spectra. Therefore, all three forms are catalytically active, and display reversible catalysis.

Colorimetric assay shows that the product of acid reduction by AOR is aldehyde. It has been established that AOR can oxidize crotonaldehyde using ferredoxin or methyl viologen as the electron acceptor (26). In the electrochemistry experiments we also observed the reversal of the catalytic current upon addition of crotonic acid during crotonaldehyde oxidation by AOR, or by accumulation of crotonic acid after prolonged oxidation of crotonaldehyde by AOR. This reverse reaction, i.e. the re-reduction of the product, has not been reported yet. Also, the

actual product of the aldehyde oxidation reaction has not been proven to be acid. We used a colorimetric assay to trace the consumption or the formation of aldehyde when using
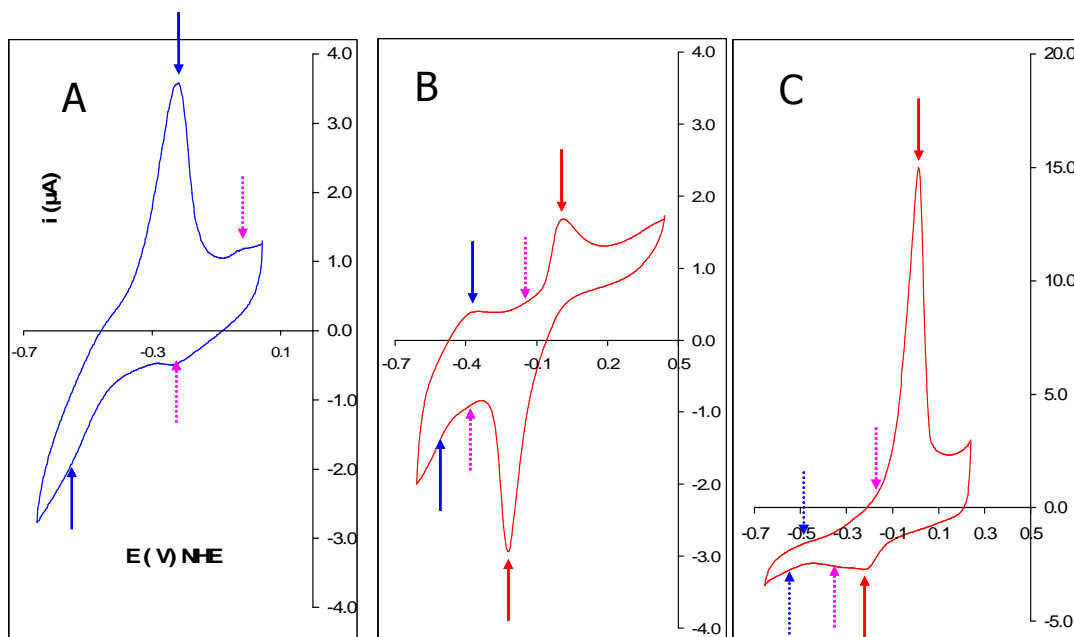

Figure 5: Catalytic cyclic voltammograms of *Pfu*AOR at 80ºC, on gold with chemisorbed *Pfu*Fd. Scan rate: 20 mV/s. **A:** 2.5 mM crotonaldehyde, 3µM 4Fe-Fd and 3µM AOR, 25 mM EPPS pH 8.4. **B**: 10 mM crotonaldehyde, 10 mM crotonic acid, 10 µM Fd, 15 µM mM AOR, 25 mM Hepes pH 7.2. **C:** 2.5 mM crotonaldehyde, 3µM 4Fe-Fd and 3µM AOR, 25 mM Hepes pH 7.2. The blue lines indicate the catalytic peaks of "low potential AOR"; the purple lines indicate the catalytic peaks of "mid-potential AOR"; the red lines indicate the catalytic peaks of "high potential AOR".

crotonaldehyde as substrate for oxidised AOR, or crotonic acid as the substrate for reduced AOR. The results of the assays are presented in figure 6. In assay B, the addition of 155 µM crotonaldehyde to 50 µM *Pfu* Fd and 200 nM AOR, at pH 8.4 and at 80°C, resulted in 77% oxidation of the added crotonaldehyde over a period of 15 minutes. In assay C, under the same conditions, oxidation of crotonaldehyde was significantly hindered (only 47% conversion after 15 min.) when Purpald (but not hydrogen peroxide) was added prior to the

addition of AOR. This is to be expected because the amin-al precursor of the colored adduct is already formed without peroxide, thus competing with the enzymatic reaction. In assays D and E, 155 µM crotonic acid was added to a reaction mixture containing reduced AOR–Fd complex. This reduced complex was obtained by incubating oxidized AOR and Fd with excess crotonaldehyde at 80°C for 15 min. and purifying the reduced proteins (AOR and Fd). AOR and Fd could also be reduced with dithionite, but this does not yield enzyme with
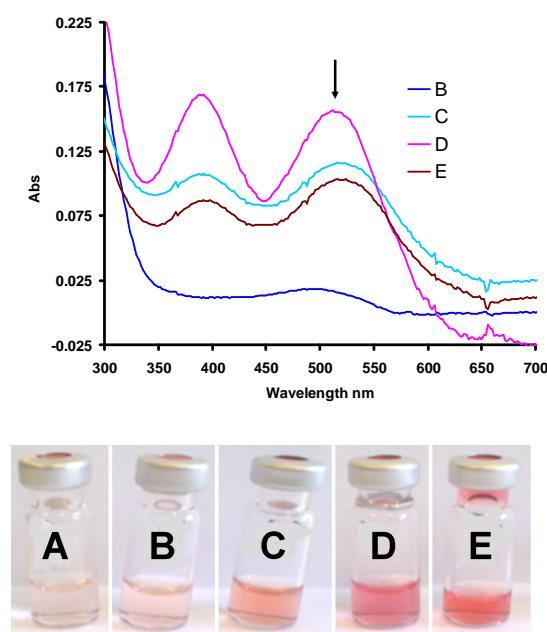

Figure 6: Colorimetric analysis of aldehyde formation or utilization; Bottom Panel: (A) control without AOR and aldehyde, (B) crotonaldehyde oxidation by AOR, (C) same as B except Purpald (not peroxide) was already added from the beginning of the assay, (D) crotonic acid reduction "spiked" with 15 µM crotonaldehyde, (E) crotonic acid reduction without "spiking" with crotonaldehyde. The reaction mixtures contained 50 mM EPPS pH 8.4 and 50 µM *Pfu* Fd (A-E), 200 nM AOR (B-E), and 155 µM crotonaldehyde (B, C) or 155 µM crotonic acid (D, E). The colorimetric end-point determination of aldehyde was done by quenching the enzymatic reaction after 15 min. by cooling, followed by the addition of 34 mM Purpald and 36 mM hydrogen peroxide. Top Panel: blank (reaction A) subtracted spectra of reaction B, C, D and E. The arrow indicates the absorbance at 540 nm from which the conversion rates are deduced.

acid reductase activity. No crotonaldehyde was added to assay E, while assay D was initiated by the addition of a small amount, 15 µM, of crotonaldehyde. Formation of aldehyde was evident from both D and E, but spiking with aldehyde significantly enhanced the conversion rate of acid (75% in 15 min. in D, compared to 48% in 15 min. in E). The control assays

Table: 1: Specific activity of AOR-mediated oxidation of crotonaldehyde and reduction of crotonic acid in the presence of different redox mediators, calculated from the initial rate. Assay composition: 1ml of 10-200 µM redox medaitor in 50 mM EPPS + 100 mM NaCl, pH 8.5 at 60ºC; 0.26 µM AOR, and 10 mM crotonaldehyde were consecutively added to the assays.

Mediator	$E^{0'}$(pH 7) mV	N	Concentration µM	Specific activity mU/mg
Phenazine ethosulfate	+55 mV	2	200	421 686 (maximum)*
Methylene blue	+11 mV	2	20	409 (maximum)*
Resorufin	-51 mV	2	10	39
2-hydroxy-1,4-naphthoquinone	-145 mV	2	50	<1
Antraquinone-1,5-disulfonate	-170 mV	2	25	<1
Riboflavin	-219 mV	2	37	<1
Neutral red	-329 mV	2	100	<1
Benzyl viologen	-358 mV	1	25	4

* maximum activity is higher than initial activity due to activation

containing only Fd, or Fd plus AOR, or Fd plus crotonic acid (assay A) did not show any colour formation upon addition of Purpald. These controls confirm the specificity of both the colorimetric reaction and the enzymatic conversion of aldehyde to acid and *vice versa*. The results prove that AOR not only catalyses the oxidation of croton aldehyde, but also the reduction of crotonic acid to aldehyde.
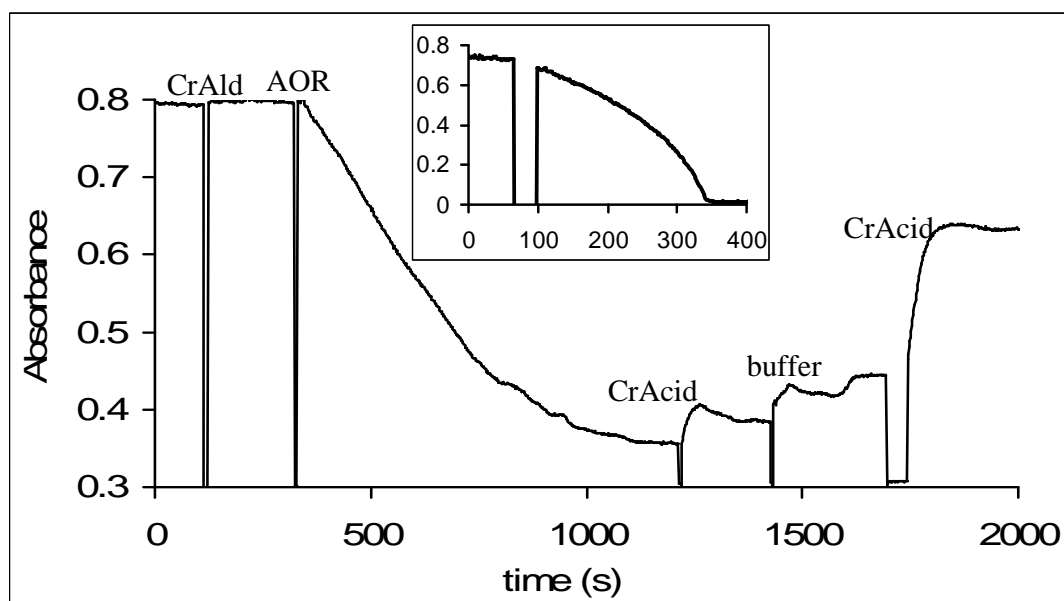

Figure 7: Absorbance-versus-time trace for 1 ml of 10 µM resorufin in 50 mM EPPS + 100 mM NaCl, pH 8.5 at 60ºC., measured at 571 nm. Consecutive additions: 1 µl 700 mM crotonaldehyde (=0.7mM); 1 µl 0.26 mM AOR (=0.26 µM); 10 µl 50 mM crotonic acid (=0.5 mM); 10 µl anaerobic buffer; 25 µl 50 mM crotonic acid (=3 mM). Inset: Absorbance-versus-time trace for 1 ml of 20 µM methylene blue and 0.5 µM AOR in 50 mM EPPS + 100 mM NaCl, pH 8.5 at 60ºC, measured at 664 nm, upon addition of 140 µM croton aldehyde (at t=96 s).

Figure 7: Absorbance-versus-time trace for 1 ml of 10 µM resorufin in 50 mM EPPS + 100 mM NaCl, pH 8.5 at 60ºC., measured at 571 nm. Consecutive additions: 1 µl 700 mM crotonaldehyde (=0.7mM); 1 µl 0.26 mM AOR (=0.26 µM); 10 µl 50 mM crotonic acid (=0.5 mM); 10 µl anaerobic buffer; 25 µl 50 mM crotonic acid (=3 mM). Inset: Absorbance-versus-time trace for 1 ml of 20 µM methylene blue and 0.5 µM AOR in 50 mM EPPS + 100 mM NaCl, pH 8.5 at 60ºC, measured at 664 nm, upon addition of 140 µM croton aldehyde (at t=96 s).

Redox mediators assisted assays. To support the proposal of reversibility, AOR-catalyzed oxidation of crotonaldehyde and reduction of crotonic acid have been carried out using redox

mediators as electron donors or acceptors in cuvettes. The results of these assays are collected in table 1. The highest potential two-electron mediators PES, methylene blue, and resorufin, as well as the low potentials one-electron mediator benzyl viologen are suitable as electron acceptors from AOR. However, AOR shows little or no activity with the intermediate and low potential mediators. Only with the one-electron mediator benzyl viologen some activity is observed, which might be due to compatibility with the one-electron [4Fe4S] cofactor at similarly low potential.

As demonstrated in Figure 7, the AOR-catalyzed reduction of the mediator resorufin ($E^{0'}$=-51 mV) by crotonaldehyde was reversed by the addition of acid in excess of aldehyde. Although the addition of 0.5 mM acid did not result in the re-oxidation of mediator, further addition of 3 mM acid did initiate this reversed reaction. From the plots of the initial slopes versus absorbance, a net aldehyde oxidation activity of 39 mU/mg, and a net acid reduction activity of 198 mU/mg can be calculated. This clearly demonstrates that AOR also catalyses the reduction of crotonic acid at a high rate. The crotonic acid / crotonaldehyde reduction potential is -123 mV, as calculated from the ratio's of acid to aldehyde and reduced to oxidized mediator at equilibrium (t=1200 sec).

DISCUSSION

GAPOR. Although the voltammetric response of the [4Fe-4S] cluster of GAPOR is clearly observed at E_m=-383 mV, the voltammogram in Figure 1B shows a seizable peak separation of 54 mV. This is indicative of sluggish electron transfer, either mediated by ferredoxin, or directly from GAPOR to the electrode. However, the electrode surface is fully covered by ferredoxin monomers, which renders ferredoxin as the most plausible route of electron transfer. For chemisorbed ferredoxin, we have previously reported that the reduction is gated

by a slow conformational change. The observed hysteresis in the GAPOR voltammogram is probably due to this gating, because both GAPOR oxidation and GAPOR reduction involve a ferredoxin reduction step. With GAP and at 60°C, the turnover rate of 3.6 s^{-1} is significantly lower than the turnover rate of 96 s^{-1} obtained in a solution containing 150 µM Fd and 10 mM GAP (27), but is comparable to the rate of the gating step of chemisorbed ferredoxin (5.1 s^{-1}) (23).

AOR. The combined results of voltammetry, purpald colorimetry, and cuvette assays prove that AOR catalyses the reversible aldehyde to acid interconversion. However, AOR is not a classical reversible oxidoreductase, because it needs to switch between two states with either "oxidase" or "reductase" activity (state O and state R). In an attempt to draw a minimal mechanism to encompass all our observations, as well as those reported by others, the following results are pivotal:

- A remarkably rapid switch-off is observed when the catalytic current for crotonaldehyde oxidation on the stationary electrode is high. The resulting unusual "half-peak" shape indicates that the switch-off occurs at relatively low overpotential, before the maximum turnover rate is reached.

- When the enzyme activity is low, the switch-off is also less rapid, eventually becoming indistinguishable from the $t^{-\frac{1}{2}}$ decay at high potential expected for turnover limited by linear diffusion.

- For crotonic acid reduction, a similar (point reflected) behaviour is observed at low potential. While the acid reduction current increases with time and displays increasingly abrupt switch-off behavior, the aldehyde oxidation current decreases, and displays slower switch-off.

- With the high potential mediators PES and methylene blue, a characteristic activation in solution is observed as a result of depletion of oxidized mediator and accumulation of reduced mediator, thus decreasing the driving force, as predicted by the voltammetric data.

- The "purpald" assay demonstrates that aldehyde is the product of acid reduction.

- The addition of a low concentration aldehyde to the solution of acid and reductant increases the acid reduction activity.

- With resorufin, reduction activity is also observed after fully reducing the mediator with aldehyde and then adding excess acid.

From these observations, the following mechanistic information can be deduced:

- On the electrode, when the activity (aldehyde turnover rate) per surface area is much greater than the mass transport rate (linear diffusion), aldehyde will be rapidly depleted and acid will be accumulated at the surface. This means that oxidized enzyme (high electrode potential) and high concentration of acid are present. A large acid to aldehyde ratio combined with enzyme being (partially) oxidized apparently alters the enzyme such that it does no longer oxidize aldehyde (form "O"), but instead is able to reduce acid (form "R") during the reductive sweep.

- The AOR "O" to "R" interconversion is reversible (both on the electrode and in solution), and occurs at relatively low overpotential.

These observations suggest that the "O" to "R" conversion is induced by acid bound to the $(W^V)_O$ or $(W^{VI})_O$ state, and that the "R" to "O" conversion is induced by aldehyde bound to the $(W^V)_R$ or $(W^{IV})_R$ state (but not necessarily coordinating W).

- The addition of a small amount of aldehyde increases the acid reduction rate. This suggests that the conversion from "O" to "R" occurs during turnover, thus involving a transient intermediate.

- The switch-off of the electrocatalysis requires a low overpotential and excess product.

- Form "R" can be induced also in the presence of reductant in solution.

These observations suggest the involvement of $[(W^V)_O.acid]$ and $[(W^V)_R.aldehyde]$ intermediate states. Although the switch is induced by product, it also explains the weak substrate inhibition observed by Adams and co-workers [26]: a higher concentration aldehyde will increase the rate of formation of W^{IV} and W^V intermediates with bound acid, thus shifting the steady-state distribution towards these intermediates:

This generic model is valid for the "low potential", mid-potential" and "high potential" forms of AOR, observed by EPR (24). However, no molecular model can be provided at this stage.

It is remarkable that many Mo-pterin and W-pterin enzymes display rich, non-classical redox and electrocatalytic behaviour, which appears to be linked to the stability of the intermediate W(V) or Mo(V) state [20-22] which is a unique feature of these metal centers.

Although the substrate specificity of AOR is not high, it displays a much higher activity with crotonaldehyde compared to saturated aliphatic aldehydes (26). Most likely, this is because crotonaldehyde is an activated aldehyde due to the conjugation with the 2,3 alkenyl group. The crotonic acid / crotonaldehyde reduction potential that we determined from the AOR-catalysed equilibrium with resurufin is -123 mV, which is higher than that of aliphatic acid/aldehyde [-560 mV (26)]. This renders the re-reduction more facile. At least with this substrate, all three forms of the enzyme are active both for the oxidation of aldehyde and reduction of acid in the presence of the appropriate mediator or electrode potential. In particular the two-electron reduction of an unsaturated acid to aldehyde is potentially interesting for application of AOR in organic synthesis.

$([4Fe4S]^{2+})(W^{VI})_O + aldehyde \rightarrow \rightarrow ([4Fe4S]^{2+})(W^{IV})_O . acid \rightarrow ([4Fe4S]^{+})(W^V)_O . acid.$

CONCLUSION

The *Pfu*Fd electrode provides a docking site for its redox partner enzymes GAPOR and AOR. The complexes are static at room temperature and dynamic at high (i.e. physiological) temperature. Uncomplicated classical electrocatalytic oxidation of GAP by GAPOR adsorbed on Fd-electrode was observed without product inhibition. Three forms of AOR; 'low-potential AOR', 'mid-potential AOR' and 'high-potential AOR' were observed in voltammetry which is in good agreement with finding in EPR studies. All of the forms are active, and catalyze the reversible two-electron aldehyde / acid interconversion, both in solution and on the Fd electrode. In addition, switching between O and R forms was observed, possibly involving a W(V) intermediate.
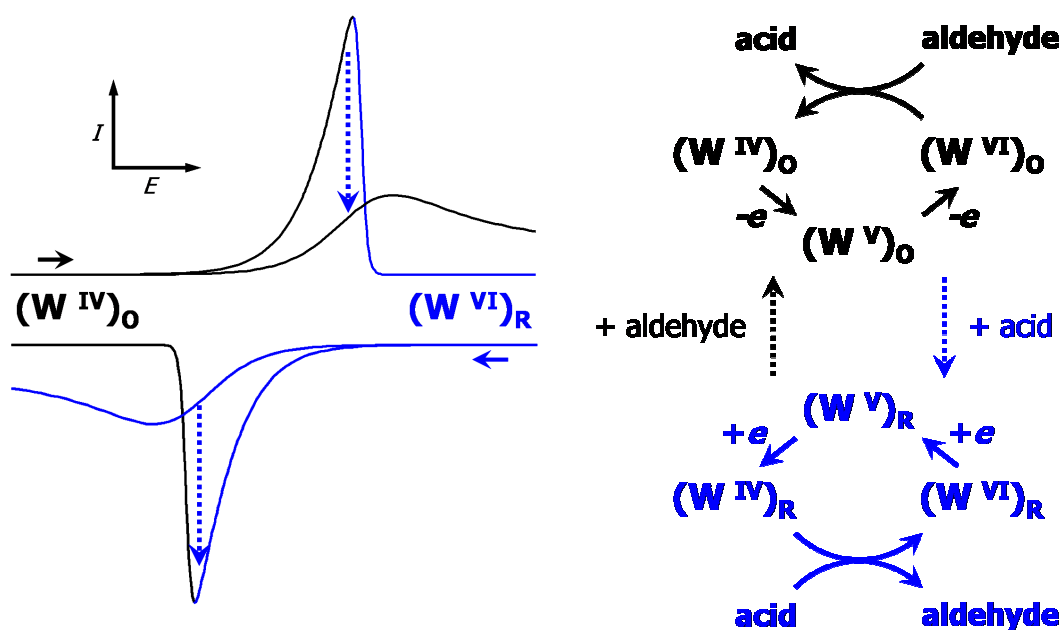

Figure 8: Left: schematic drawing of the observed Fd/AOR voltammograms with crotonaldehyde and crotonic acid. The dotted arrows indicate slow change from dominant oxidase activity to dominant reductase activity during repeated cycling. **Right:** Minimal mechanism deduced from the observations. The stepwize W oxidation/reduction by the electrode is mediated by the FeS clusters of AOR and ferredoxin. "O" and "R" indicate the forms of the enzyme with aldehyde oxidation and acid reduction activity, respectively. Acid-induced conversion to "R" involves W^V or W^{VI} intermediates. Aldehyde-induced conversion to "O" involves W^{IV} or W^V intermediates.

REFERENCES

1. Mukund S and Adams MWW (1995) J. Biol. Chem. 270, 8389-8392

2. Bevers LE, Bol E, Hagedoorn P-L, Hagen WR (2005) J. Bacteriol 187:7056-7061

3. Roy, R., and Adams. M. W. W. (2002) J. Bacteriol. 184:6952–6956

4. Mai, X. and Adams, M. W. W. (1994) J. Biol. Chem. 269, 16726-16732

5. Mai, X. and Adams, M. W. W. (1996) J. Bacteriol 178, 5890-5896

6. Heider, J., Mai, X. and Adams, M. W. W. (1996) J. Bacteriol. 178, 780-787

7. Eddowes, MJ and Hill HAO (1977) J. Chem. Soc. Chem. Commun, 771-772.

8. P Yeh and T Kuwana, Chem. Lett. (Jpn.) 1977, 1145 -1148.

9. Heering HA, Wiertz FGM, Dekker C, de Vries S (2004) J Am Chem Soc 126:11103-11112

10. Zhang JD, Christensen HEM, Ooi BL, Ulstrup J (2004) Langmuir 20:10200-10207

11. (a) Vincent K, Armstrong FA (2005) Inorg Chem 44:798-809 (b) Armstrong FA (2005) Curr Opin Chem Biol 9:110-117 (c) Armstrong FA, Wilson GS (2000) Electrochim Acta 45:2623-2645 (d) Armstrong FA, Heering HA, Hirst J (1997) Chem Soc Rev 26:169-179

12. Hansen AG, Boisen A, Nielsen JU, Wackerbarth H, Chorkendorff I, Andersen JET, Zhang JD, Ulstrup J (2003) Langmuir 19:3419-3427

13. Tarlov MJ, Bowden EF (1991) J Am Chem Soc 113:1847-1849

14. (a) Wei JJ, Liu HY, Dick AR, Yamamoto H, He YF, Waldeck DH (2002) J Am Chem Soc 124:9591-9599 (b) Wei JJ, Liu H Y, Khoshtariya DE, Yamamoto H, Dick AR, Waldeck DH (2002) Angew Chem Intl ed 41:4700-4703

15. Bernhardt PV (2006) Aust. J. Chem. 59, 233-256

16. Anderson LJ, Richardson, DJ and Butt, JN (2000) Faraday discuss. 116, 155-169

17. Elliott SJ, Hoke KR, Heffron K, Palak M, Rothery RA, Weiner JH, Armstrong FA (2004) Biochemistry 2004, 43, 799.

18. Anderson LJ, Richardson DJ, Butt JN (2001) Biochemistry, 40, 11294-11307.

19. Heffron K, Léger C, Rothery RA. Weiner JH, and Armstrong FA (2001) Biochemistry, 40 (10), 3117 -3126.

20. Aguey-Zinsou, K-F, Bernhardt PV, McEwan AG and Ridge JP (2002) J. Biol. Inorg. Chem. 7, 879–883.

21. Aguey-Zinsou K-F, Bernhardt, PV, Kappler U. and McEwan AG (2003) J. Am. Chem. Soc. 125, 530–535.

22. K. F.Aguey-Zinsou, P.V. Bernhardt, S. Leimkühler, J.Am. Chem. Soc. 2003, 125, 15352- 15358.

23. Hasan MN, Kwakernaak C, Sloof WG, Hagen WR and Heering HA (2006) J. Biol. Inorg. Chem. 11, 651-662.

24. Koehler BP, Mukund S, Conover RC, Dhawan I K, Roy R, Adams MWW and Johnson MK (1996) J. Am. Chem. Soc. 118, 12391-12405

25. Arendsen AF, de Vocht M, Bulsink YBM and Hagen WR (1996) J. Biol. Inorg. Chem. 1, 292-296

26. Mukund, S. and Adams, M. W. W. (1991) J. Biol. Chem. 266, 14208-14216

27. Hagedoorn P-L, Freije JR and Hagen WR (1999) FEBS Lett. 462, 66-70

28. Hasan MN, Hagedoorn PL and Hagen WR (2001) FEBS Lett 531, 335-338

29. Van der Oost J, Shuct G, Kengen SWM, Hagen WR, Thomm M and de Vos WM (1998) J. Biol. Chem. 273, 28149-28154.

30. Hagen WR (1989) Eur. J. Biochem.182, 523-530

31. Dickinson, R.G.; Jacobsen, N.W. Chem. Commun. 1970, 1719.

32. Frens G. Nature Phys. Sci. (1973) 241, 20-25

33. Stich N, Gandhum A, Matyushin V, Raats J, Mayer C, Alguel Y, and Schalkhammera T (2002) J. Nanosci. Nanotech., 2, 1-7

34. Matyushin V, Gandhum A, Stich N, Schalkhammer T, Hagen WR and Mayer C (2004) J Nanosci Nanotechnol. 4, 98-105

35. Bard, A. J.; Faulkner, L. R. Electrochemical methods: fundamentals and applications, 2nd ed.; John Wiley & Sons, 2001.

Summary

In *Pyrococcus furiosus* (*Pfu*) ferredoxin (Fd) replaces NAD$^+$ for carrying reducing equivalent to the oxidative phosphorylation machinery, and it also takes part in the regeneration of NADPH, which is necessary for biosynthetic pathways. Therefore, it plays a central role in various metabolic pathways of the organism. *Pfu*Fd is one of the most extensively studied ferredoxins, however, some fundamental aspects remain elusive. This thesis work focuses on some of the unresolved features of the protein.

Initially *Pfu*Fd was isolated as a dimer of 12-13 kDa, however, all the subsequent studies described the protein as a monomer without any experimental evidence. All (putative) natural electron-transfer partners of *Pfu*Fd are redox enzymes catalyzing two-electron reactions while ferredoxin is a one-electron carrier. It is possible that ferredoxin may interact with the redox partner enzymes in the dimeric form. Therefore, it is important to resolve the dilemma regarding the oligomeric state of the protein (chapter 2). The intra-cellular ionic strength of *P. furiosus* was determined to be ca. 350 mM, at which ferredoxin occurs predominantly in the dimeric form. Transition from the dimeric to monomeric form is observed at a salt concentration higher than 350 mM. We hypothesize that ferrdoxin is a dimer *in vivo*.

*Pfu*Fd demonstrates conservation of the minimal domain containing the cluster coordinating consensus sequence. However, the cluster is coordinated by three cysteines and one aspartate residue instead of by four cysteines. In addition, two additional cysteines are present which raises the possibility of a disulfide bond formation between them. In some earlier studies the formation of a disulfide bond was demonstrated under aerobic condition and a possible contribution of the disulfide bond to the redox chemistry of the protein has been described. However, formation of a disulfide bond under the strongly reducing intracellular condition of an anaerobic organism like *P. furiosus* is not understandable. We demonstrate (in chapter 3)

that these additional cysteines do not form a disulfide bond under intra-cellular mimicking conditions. Observing the effects of site directed mutagenesis, we attribute to the free cysteines an important structural role in the hyperthermostability of the protein.

Ferredoxin, cytochrome c, rubredoxin, etc. are small electron-transfer protein and they possess well characterised metal cofactors. Electrochemistry has been successfully applied in studying the intricate properties of these electron-transfer proteins mainly in solution. However, solution voltammetry suffers from various problems like mass transport / diffusion limitation, requirement of promoters, which can be avoided by immobilizing the protein on the electrode surface. A stable and functional *Pfu*Fd immobilized gold electrode has been developed, which shows a similar electrochemical response as in the solution voltammetry. The transition between the dimeric and monomeric state on the electrode is observed in an atomic force microscopic (AFM) setup. X-ray photoelectron spectrocopy (XPS) confirms the formation of gold-thiol bonds. We find the ferredoxin electrode to be a useful tool for studying the catalytic mechanisms of the associated redox enzymes from *P. furiosus*. We have thus studied two redox enzymes, glyceraldehyde-3-phosphate oxidoreductase (GAPOR) and aldehyde oxidoreductase (AOR), which are involved in ferredoxin-mediated redox processes in the organism. Addition of these enzymes at room temperature results in complex formation between the electrode-bound ferredoxin and the enzyme. At 60 ºC a catalytic wave appears upon addition of the substrate, glyceraldehyde-3-phosphate to the Fd-GAPOR complex. In the case of AOR at 80 ºC reversible oxidation of crotonadehyde to crotonic acid and *vice versa* was observed. This work opens the way for the application of Fd electrodes in achieving controlled reduction of carboxylic acids on a preparative scale.

Samenvatting

In *Pyrococcus furiosus* (*Pfu*) vervangt ferredoxine (Fd) NAD$^+$ voor de overdracht van reductie-equivalenten naar de oxidatieve fosforyleringsmachine, en het speelt bovendien een rol in de regeneratie van NADPH, dat nodig is in biosynthetische routes. Het speelt derhalve een centrale rol in verschillende metabole routes van het organisme. *Pfu*Fd is één van de meest intensief bestudeerde ferredoxines, maar toch blijven enige fundamentele aspecten onderbelicht. Dit promotieonderzoek richt zich op enkele van de onopgeloste aspecten van het eiwit.

Oorspronkelijk is *Pfu*Fd gezuiverd als een dimeer van 12-13 kDa, maar in alle volgende studies wordt het eiwit beschreven als een monomeer zonder enig experimenteel bewijs. Alle (mogelijke) natuurlijke electron-overdragende partners van *Pfu*Fd zijn redoxenzymen welke twee-electron reacties katalyseren terwijl ferredoxine een één-electrondrager is. Het is mogelijk dat ferredoxine misschien als dimeer reageert met de redoxpartner-enzymen. Het is daarom van belang om het dilemma wat betreft de oligomere vorm van het eiwit op te lossen (hoofdstuk 2). De intracellulaire ionensterkte van *P. furiosus* is bepaald op 350 mM, en bij deze concentratie is ferredoxine voornamelijk dimeer. Overgang van de dimere form naar de monomere vorm wordt waargenomen bij een zoutconcentratie hoger dan 350 mM. We maken de hypothese dat ferredoxine *in vivo* een dimeer is.

*Pfu*Fd is een voorbeeld waarin het minimumdomein dat de consensussequentie bevat voor clusterbinding is geconserveerd. Maar de cluster wordt gecoördineerd door drie cysteines en één aspartaat in plaats van door vier cysteines. Bovendien zijn er nog twee cysteines waartussen disulfidebinding mogelijk kan zijn. In eerdere studies is de vorming van disulfidebinding aangetoond onder aerobe omstandigheden, en een mogelijke bijdrage van de disulfidebinding aan de redoxchemie van het eiwit is beschreven. Vorming van een disulfidebinding is echter niet te begrijpen onder de sterk reducerende omstandigheden die

bestaan in een anaeroob organisme als *P. furiosus*. We laten zien (in hoofdstuk 3) dat deze extra cysteines geen disulfidebinding vormen onder intracellulair-nabootsende omstandigheden. Op grond van waarneming van effecten van plaats-gerichte mutagenese schrijven we aan de cysteines een belangrijke rol toe met betrekking tot de hyperthermostabiliteit van het eiwit.

Ferredoxine, cytochroom c, rubredoxine, enz., zijn kleine electron-overdragende eiwitten met goed gekarakteriseerde metaal-cofactoren. Electrochemie is met succes toegepast in de studie van de gedetailleerde eigenschappen van deze eiwitten voornamelijk in oplossing. Voltammetrie in oplossing kent echter een aantal problemen zoals limitatie door massa transport / diffusie, en de noodzaak van promotoren, welke vermeden kunnen worden door het eiwit te immobiliseren op het electrodeoppervlak. Een stabiele en werkende goudelectrode met geimmobiliseerd *Pfu*Fd is ontwikkeld, en deze vertoont een electrochemische respons vergelijkbaar met die in voltammetrie in oplossing. De overgang tussen de dimere en monomere vorm op de electrode is waargenomen in een atomic force microscopy (AFM) opzet. X-ray photoelectron spectroscopy (XPS) bevestigt de vorming van goud-thiol bindingen. De ferredoxine-electrode blijkt een handig gereedschap voor de bestudering van de katalytische mechanismen van de geassocieerde redoxenzymen van *P. furiosus*. We hebben aldus twee redoxenzymen bestudeerd: glyceraldehyde-3-fosfaat oxidoreductase (GAPOR) en aldehyde oxidoreductase (AOR), welke betrokken zijn bij ferredoxine-gemedieerde redoxprocessen in het organisme. Toevoegen van deze enzymen bij kamertemperatuur resulteert in de vorming van complexen tussen het electrode-gebonden ferredoxine en het enzym. Bij 60 ^{o}C verschijnt er een katalytische golf na toevoegen van het substraat glyceraldehyde-3-fosfaat aan het Fd-GAPOR complex. In het geval van AOR wordt bij 80 ^{o}C de reversibele oxidatie waargenomen van crotonaldehyde tot crotonzuur en *vice versa*. Dit

werk opent de weg naar toepassingen van Fd-electrodes voor gecontroleerde reductie van carbonzuren op preparatieve schaal.

Curriculum vitae

M. Nahid Hasan was born on the 30th December of 1973 in a small village of Laskmipur district in Bangladesh. He completed his secondary education from Lakshmipur Adarsha Samad High School in 1988. Afterwords he completed pre-university education from Dhaka College. Nahid has been awarded scholorships by Bangladesh government for outstanding results in the national examinations held at different levels. In 1995 he obtained his Bachelor in Science (BSc.) degree from the Department of Biochemistry and Molecular Biology, University of Dhaka. He then continued his Master of Science (MSc.) education in the same department. During this period he worked on a project involving "characterization of mRNAs related to salt tolerance in some rice varieties", funded by the Rockfeller Institute USA. He then aspired to continue higher studies in this field which brought him to London. There he completed his MSc. degree in Medical Molecular Biology from the School of Biological Sciences, University of Westminster. In addition to the taught courses he worked on a project entitled "comparative study of impact of *Fuserium* infection in resistant and susceptible wheat varieties." After completion of the MSc. degree from the UK he worked as a trainee research assistant in the Department of Molecular Cell Biology (MCB2) at Leiden University Medical Center, the Netherlands. In July 2001 he started his Phd study on the redox biochemistry of *Pyrococcus furiosus* ferredoxin under the supervison of Prof. W.R. Hagen. The results presented in this thesis have been conducted in the Enzymology Group of Department of Biotechnology, Delft University of Technology from July 2001 till October 2005. From October 2005 till Octber 2007 he continued as a postdoc researcher in the same group and successfully patented the results of one of his researches. Currently, he is continuing his scientific persuits as a postdoc researcher under the supervison of Prof. Simon de Vries in the same group. Also he is continuing the collaborations rose from his previous projects.

Acknowledgement

Though the journey towards a PhD degree is pretty long and sometimes seems exhausting, it is rewarding and exciting at the end. However, in the part of the world I was bron in it seemed as a "mission impossible" in the beginning. Actually it involved lots of real supports from people of various corners at different stages of my educational life. First and foremost, I would like to remember the endless support, motivation and inspiration provided by my father (who is in haven now, may Allah rest his soul in peace) in the persuit of my higher education. Probably he would have been the happiest person to see me as a Dr.

However, without the practical support of the people in the academic world it would not have been possible for me to come upto this point. It will be unfair to frame-up in few words the valauable contributions I enjoyd since the beginning of my PhD here. Yet I would like to pay my heartfelt gratitude and salutation to Prof. W.R. Hagen for giving me the opportunity to persuade my PhD work under his supervision. In addition to the wonderful guidance, critical review, valuable feedback, quick-easy and understandable suggestions, I would not forget the strong support and encouragement I enjoyed from him.

I gratefully remember the support Dr. Peter-Leon provided me in the beginning of my project and especially for teaching me the "abc" of electrochemistry.

Dr. H.A. Heering (Dirk), you were a rescuer at a crucial moment of my PhD project. The inhabitants of room 1.690 will not forget the usual 'shouting discussion' (mainly one-sided!) we had during our collaboration. Thank you very much for teaching me how to analyse the electrochemistry results in details. Now every small noise seems like a "peak" to me!! I hope to continue our collaboration further.

I would also like to thank Prof. Simon de Vries for his advice, suggestions and help in need. Cordial and yet enthesuastic support and tips from Dr. Jaap Jongejan during my difficult

times are unforgetable. His enthusiasm finally influenced me to learn 'Pymol' at least for some basic manipulation. Jaap, however, I still do not understand Ramachandra plot well!!!

Marc, being a "hard–ruler" you taught me a lot of laboratory discipline and of course a mass of chromatography techniques. Still I am trying to be your obedient disciple in learning how to destroy my finger tips in LN2!! Thank you very much for being such a good teacher.

Esengul, thank you very much for your efforts in bringing in the new PCR machines and help in the MB lab.

Loesje, your encouraging words in late evenings worked as a tonic for me at times. Of coruse valuable scientific discussions with you were also quite helpful.

Special thanks to Alidin, Ram, Daan, Slava, Emile, Yana, Frank, Marieke, Suharti, Barbara, Laura, Ana, Alexey, Elena, Angela, Aida, Inga and Sandra for your support, tolerance and sharing scientific and social views.

I would like to also thank Ing. Kees Kwakernaak and Dr. Cees van der Marel for their splendid supports for the XPS measurement.

My sincere thanks to all support staff particularly Sjak, Jos, Frieda, Astrid, Marleen and the people from the workshop.

I would also like to greatly acknowledge the valuable contributions from Prof. Anwar Hossain, Prof Haseena Khan and Prof. Pamela Greenwell in the persuit of my scientific career.

Outside the Kluyver laboratory, I am grateful to my friends from Bangladesh living here in the Netherlands for providing wonderful social and moral supports. I owe special thanks to all of them particularly Meer vai, Runa vabi, Tanzir, Heera, Puspok da, Lipi vabi, Amin vai, Sumi, Moshi and Saikat.

My sincere gratitude to my mother, brothers and sisters and the members of my in-law's family for their love and affection and endless supports. Lipi, thank you very much for being

such a wonderful wife, friend and partner. Without your continuous help, support, endurance

it would not have been possible for me to come upto this point of life.